AD NUMBER

AD068767

NEW LIMITATION CHANGE

TO

Approved for public release, distribution unlimited

FROM

Distribution authorized to U.S. Gov't. agencies and their contractors; Administrative/Operational Use; JUL 1955. Other requests shall be referred to Office of Naval Research, Arlington, VA.

AUTHORITY

ONR ltr, 9 Nov 1977

FC

Dielectric Spectroscopy of Ferromagnetic Semiconductors

Technical Report 97
Laboratory for Insulation Research
Massachusetts Institute of Technology

July, 1955

Dielectric Spectroscopy of Ferromagnetic Semiconductors

by

A. von Hippel, W. B. Westphal and P. A. Miles

Laboratory for Insulation Research
Massachusetts Institute of Technology
Cambridge, Massachusetts

Contracts: O.N.R. N5ori-07801 and
A.F. 33(616)-2191

July, 1955

Table of Contents

DIELECTRIC SPECTROSCOPY OF FERROMAGNETIC SEMICONDUCTORS

by

A. von Hippel, W. B. Westphal and P. A. Miles
Laboratory for Insulation Research
Massachusetts Institute of Technology
Cambridge, Massachusetts

Abstract: A broad-band dielectric spectroscopy of the ferrites is attempted. The objective of such a research is defined, the language of dielectric spectroscopy is formulated and the experimental techniques from d.c. to the ultraviolet are described. Sections 3-11 discuss the physics of the situation, outlining the existing information on the frequency dependence of ferromagnetic response, and reformulating in our language the gyroscopic effects in magnetization phenomena, the behavior of domain walls, and the possible resonance and relaxation-type responses that may be expected in polarization and magnetization processes. The criteria for distinguishing between these responses are considered.

Measurements in the optical and infrared ranges show the contributions to the low-frequency dielectric constant of the electronic and atomic polarizabilities, the latter showing sensitivity to cation distribution in ferrites. Conductivity measurements at microwave frequencies indicate a loss mechanism differing from the normal semiconducting behavior observed at lower frequencies. Boundary-layer effects predominate in the kilocycle range. The magnetization, in contrast, varies with frequency only in the electrical range. Two main dispersion regions can be distinguished and the uncertainty of their interpretation as domain-wall or spin-orientation processes is partly resolved by evidence from the nickel-zinc ferrite system and from temperature and time effects.

Dielectric spectroscopy, as a mode of thinking, can obviously contribute much to the perception of ferromagnetic effects and of their appraisal in proper perspective.

Introduction

The stirring sequence of spectral lines, shown by individual atoms and molecules and described by the Rydberg-Ritz combination principle, led to an understanding of the quantum states of electronic excitation, vibration and rotation. These resonance spectra of individual particles extend from the X-ray into the microwave region. By condensing gases to liquids and solids, the frequency range of the electrical engineer from microwaves to d.c. fills up with absorption spectra, and drastic changes occur in the optical spectral range. The characteristic response of the individual particles to the electromagnetic field becomes submerged in effects of mutual interaction.

In consequence, the original sharpness of the resonance response of atoms and molecules with its revealing detail is supplanted in liquids and solids by broad resonance and relaxation spectra with much more scrambled information. Only the nuclear and paramagnetic resonance spectra may still transmit fine structure and hyperfine structure intelligence, because the magnetic spins are loosely coupled to their surroundings.

The spectroscopist has always considered the optical range from infrared to ultraviolet as his domain and has added in recent years microwave and magnetic spectroscopy as far as they are concerned with resonance lines and therefore amenable to his old language. The electrical engineer, by necessity, has measured the dispersion and absorption of materials from d.c. to microwaves, but essentially from the empirical standpoint of knowing these characteristics for applications. Only the relaxation spectra caused by the orientation of permanent electrical dipole moments, first interpreted by Debye, have become an important and widely used source of molecular information, especially for chemical problems.

Obviously, for a true understanding of liquids and solids a much broader

approach is needed, encompassing the total range from d.c. to X rays as a unified stage on which the interplay between electromagnetic fields and matter is enacted. This we call "dielectric spectroscopy."

Background information for this broad-band approach has been obtained in the laboratory for Insulation Research over a number of years. In the range from d.c. to microwaves, the "Tables of Dielectric Materials"[1] summarize at intervals our measurements of frequency and temperature characteristics for important dielectrics. Electrical and optical studies are undertaken of the pressure broadening of spectral lines and the transition from the gaseous to the liquid state. Electric, magnetic, optical and X-ray methods are combined to learn about the position of ions and the motion of electrons in crystal structures. All of these measurements provide data for dielectric spectroscopy.

In selecting here for a first overall study a case of great complexity, the ferrites, where polarization, conduction and ferromagnetism enter simultaneously and in intimate interaction, we cannot hope in this report to make more than a start. We are furthermore well aware that the most important contributions on the ferrites have been made in other laboratories. But by placing them, together with our own observations, in a larger framework we will try to show the value of dielectric spectroscopy in providing a contour map of the areas of knowledge and ignorance.

1. The Language of Dielectric Spectroscopy[2]

The name "dielectric," in our sense of the word, refers to any material when viewed from the standpoint of electric or magnetic response. In their reaction to sinusoidal electric and magnetic fields dielectrics are characterized

1) Cf. A. von Hippel, "Dielectric Materials and Applications," Technology Press, Cambridge, Mass., and John Wiley and Sons, New York, 1954.

2) See A. von Hippel, "Dielectrics and Waves," John Wiley and Sons, New York, N.Y., 1954.

by complex permittivity and complex permeability,

$$\epsilon^* = \epsilon' - j\epsilon'' \qquad (1.1)$$
$$\mu^* = \mu' - j\mu'' \quad .$$

These parameters, the real permittivity (dielectric constant) ϵ' and permeability μ', describing the storage of electric and magnetic energy and the loss factors ϵ'' and μ'' its dissipation, are measured in reference to vacuum as the relative complex permittivity and permeability

$$\frac{\epsilon^*}{\epsilon_o} \equiv \kappa^* = \kappa' - j\kappa'' \qquad (1.2)$$
$$\frac{\mu^*}{\mu_o} \equiv \kappa_m^* = \kappa_m' - j\kappa_m'' \quad .$$

In the rationalized mks system, used here, the dielectric constant and permeability of free space are

$$\epsilon_o = \frac{1}{36\pi} \times 10^{-9} \simeq 8.854 \times 10^{-12} \quad [\text{farad/m}] \qquad (1.3)$$
$$\mu_o = 4\pi \times 10^{-7} \simeq 1.257 \times 10^{-6} \quad [\text{henry/m}] \quad .$$

Their product determines the velocity of light and their ratio the impedance of free space as

$$c \equiv \frac{1}{\sqrt{\epsilon_o \mu_o}} \simeq 3 \times 10^8 \quad [\text{m/sec}] \qquad (1.4)$$
$$Z \equiv \sqrt{\frac{\mu_o}{\epsilon_o}} = 120\pi \simeq 376.6 \quad [\text{ohm}] \quad .$$

Permittivity and permeability, as defined, refer to isotropic, linear dielectrics; that is, an electric field $\underset{\rightarrow}{E}$ creates a polarization $\underset{\rightarrow}{P}$ and a magnetic field $\underset{\rightarrow}{H}$ a magnetization $\underset{\rightarrow}{M}$ parallel and proportional to such field. The electric flux density $\underset{\rightarrow}{D}$ and the magnetic flux density $\underset{\rightarrow}{B}$ are the arithmetic sum of field lines and dipole chains,

$$\vec{D} = \epsilon_o \vec{E} + \vec{P} = \epsilon \vec{E}$$
$$\vec{B} = \mu_o \vec{H} + \mu_o \vec{M} = \mu \vec{H} \quad , \tag{1.5}$$

and the parameters ϵ and μ simply multiplication factors. If they are complex, this indicates a temporal phase shift between the acting field, $\vec{E}$ or $\vec{H}$, and the dipole moment per unit volume, $\vec{P}$ or $\vec{M}$, created by such field. The product of angular frequency and electric-loss factor represents a <u>dielectric conductivity</u>

$$\sigma = \omega\epsilon'' \left[\text{ohm}^{-1}\,\text{m}^{-1}\right] \quad , \tag{1.6}$$

which may correspond to a true conductivity created by migrating charge carriers.

Frequently, alternative sets of parameters are used in science and engineering, which can be converted to ϵ^* and μ^* in short order. The propagation of electromagnetic waves is described by the complex propagation factor

$$\gamma \equiv \alpha + j\beta = j\omega \sqrt{\epsilon^* \mu^*} \quad , \tag{1.7}$$

with α designating the attenuation factor and β the phase factor of the wave. The intrinsic impedance

$$Z_i \equiv \frac{E}{H} = \sqrt{\frac{\mu^*}{\epsilon^*}} \tag{1.8}$$

of the dielectric represents the ratio of the coupled electric and magnetic field components as to amplitude and temporal phase for an infinitely extended material. Wavelength λ and phase velocity v in the dielectric are

$$\lambda = \frac{2\pi}{\beta}$$
$$v = \nu\lambda = \frac{\omega}{\beta} \quad . \tag{1.9}$$

The ratio of wavelength or phase velocity in vacuum to that in the dielectric material is the index of refraction

$$n \equiv \frac{\lambda_o}{\lambda} = \frac{c}{v} = \frac{\lambda_o}{2\pi}\,\beta \quad , \tag{1.10}$$

and the attenuation per radian, the index of absorption,

$$k \equiv \frac{a\lambda}{2\pi} = \frac{a}{\beta} \quad . \tag{1.11}$$

The indices of refraction and absorption together define the complex index of refraction

$$n^* \equiv n(1 - jk) \quad , \tag{1.12}$$

which the physicist uses for the characterization of his materials in place of the propagation factor of the engineer

$$\gamma = j \frac{2\pi}{\lambda_o} n^* \quad . \tag{1.13}$$

In place of the relations between flux densities and fields, measured by permittivity and permeability (cf. Eq. 5), it is frequently convenient to refer to the dipole response of the material alone by introducing the electric and magnetic susceptibilities χ and χ_m :

$$\begin{aligned} \underset{\rightarrow}{P} &= (\epsilon' - \epsilon_o)\underset{\rightarrow}{E} \equiv \chi \epsilon_o \underset{\rightarrow}{E} \\ \chi &= \frac{\underset{\rightarrow}{P}}{\epsilon_o \underset{\rightarrow}{E}} = \kappa' - 1 \\ \underset{\rightarrow}{M} &= \left(\frac{\mu' - \mu_o}{\mu_o} \right) \underset{\rightarrow}{H} \equiv \chi_m \underset{\rightarrow}{H} \\ \chi_m &= \frac{\underset{\rightarrow}{M}}{\underset{\rightarrow}{H}} = \kappa'_m - 1 \quad . \end{aligned} \tag{1.14}$$

In anisotropic, linear dielectrics, $\underset{\rightarrow}{P}$ and $\underset{\rightarrow}{M}$ do not point, in general, parallel to the generating fields; hence each component of $\underset{\rightarrow}{D}$ or $\underset{\rightarrow}{B}$ is a linear function of the three space components of $\underset{\rightarrow}{E}$ or $\underset{\rightarrow}{H}$ as

$$\begin{aligned} D_1 &= \epsilon_{11}E_1 + \epsilon_{12}E_2 + \epsilon_{13}E_3 \quad , \\ D_2 &= \epsilon_{21}E_1 + \epsilon_{22}E_2 + \epsilon_{23}E_3 \, , \\ D_3 &= \epsilon_{31}E_1 + \epsilon_{32}E_2 + \epsilon_{33}E_3 \, , \end{aligned} \tag{1.15}$$

and

$$B_1 = \mu_{11}H_1 + \mu_{12}H_2 + \mu_{13}H_3 \ ,$$

$$B_2 = \mu_{21}H_1 + \mu_{22}H_2 + \mu_{23}H_3 \ ,$$

$$B_3 = \mu_{31}H_1 + \mu_{32}H_2 + \mu_{33}H_3 \ .$$

The matrices of permittivity and permeability characterizing an anisotropic material have the symmetry:

$$\begin{aligned} \epsilon_{ij} &= \epsilon_{ji} \\ \mu_{ij} &= -\mu_{ji} \ , \ i \neq j \ . \end{aligned} \tag{1.16}$$

The ϵ^* tensor is symmetric because of the purely displacive nature of the polarization process; the skew symmetry of the off-diagonal elements of the μ^* tensor derives from the rotative nature of the magnetization process (see Sec. 4). A possible maximum of six independent coefficients of permittivity and of permeability therefore exists. How many are actually not zero and different from each other, depends on the macroscopic crystal symmetry. Frequently more useful for the molecular analysis are the corresponding susceptibility matrices.

$$\chi = \begin{vmatrix} \chi_{11} & \chi_{12} & \chi_{13} \\ \chi_{21} & \chi_{22} & \chi_{23} \\ \chi_{31} & \chi_{32} & \chi_{33} \end{vmatrix} \ . \tag{1.17}$$

This description by permittivity, permeability and susceptibility coefficients suffices for materials in which each dipole moment acts on its own. For ferroelectrics and ferromagnetics the situation becomes more involved because the moments line up spontaneously forming electric or magnetic axes. Changes in position cause, in general, a crystal deformation, hence a coupling exists to the elastic coefficients of the crystal structure (piezoeffect and magnetostriction). Furthermore, the reponse to external fields is nonlinear and depends on the prehistory of the sample because the axes form domain arrays minimizing the field energy.

Ferroelectrics and ferromagnetics are therefore characterized by polarization and magnetization curves depending on field strength, and the permittivity and permeability coefficients here used designate certain slopes of these characteristics (Fig. 1.1). In evaluating these "normal" curves and hysteresis loops, corrections are required to transform from the applied field strength $\underset{\rightarrow}{E}$ or $\underset{\rightarrow}{H}$ to the internally acting field strength $\underset{\rightarrow i}{E}$ and $\underset{\rightarrow i}{H}$. The shape of the sample enters because the free poles at the sample boundaries produce depolarizing and demagnetizing fields. For ellipsoids of rotation the internal field is homogeneous and derived from the applied field as

$$\begin{aligned} \epsilon_o \underset{\rightarrow i}{E} &= \epsilon_o \underset{\rightarrow}{E} - w\underset{\rightarrow}{P} \\ \underset{\rightarrow i}{H} &= \underset{\rightarrow}{H} - w\underset{\rightarrow}{M} \end{aligned} \qquad (1.18)$$

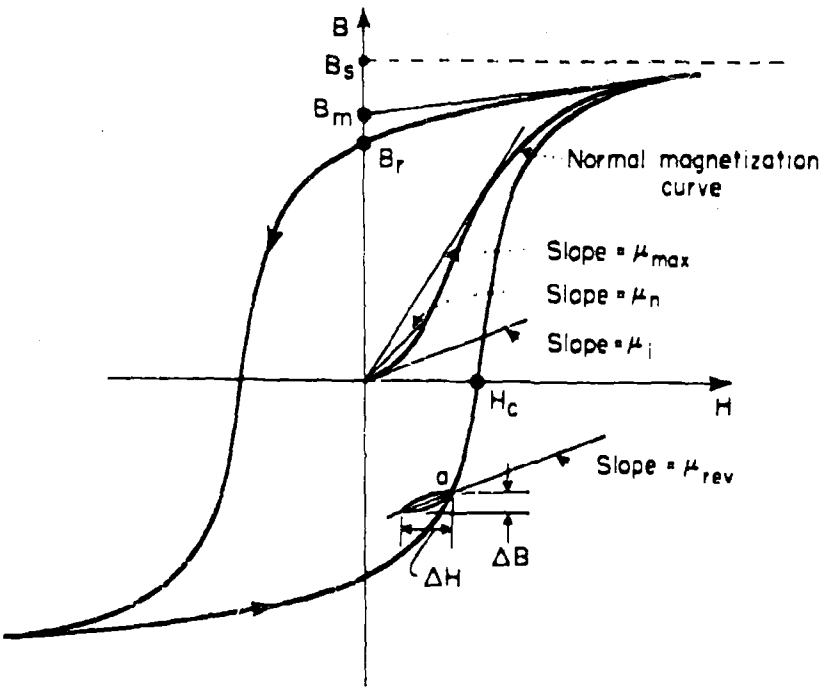

Fig. 1.1. Magnetization characteristics of a ferromagnetic material, indicating the parameters commonly used.

where w is a shape factor varying from zero for a long needle parallel to the field to 1 for such needle perpendicular to the field.

2. Measurement Techniques of the Laboratory for Insulation Research

a) Quasi-static magnetic measurements

Up to ± 2000 amp./m (25 oersteds), normal magnetization curves and hysteresis loops were plotted by a quasi-static fluxmeter (Fig. 2.1), developed by Epstein and Frackiewicz after a design by Cioffi.[3] This instrument served also for tracing the initial permeability as function of temperature up to the Curie point. For fields up to 400,000 amp./m (5,000 oersteds), the normal magnetization characteristics could be determined with a null-coil pendulum magneto-

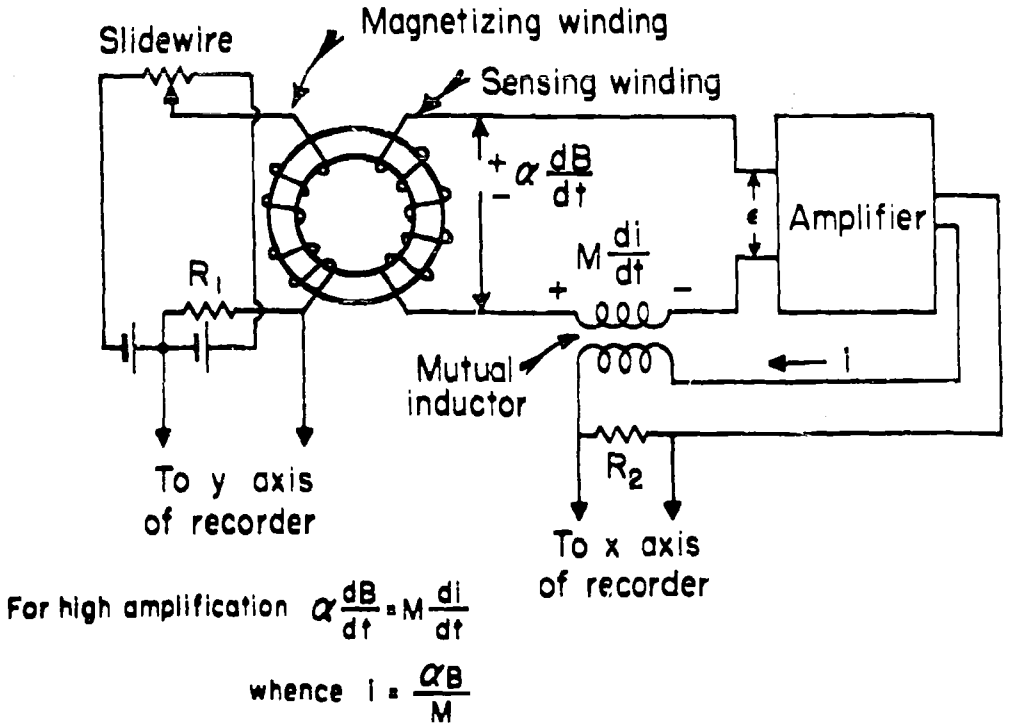

Fig. 2.1. Recording flux meter for quasi-static magnetic measurements.

3) P. P. Cioffi, Rev. Sci. Instr. 21, 624 (1950); D. J. Epstein and B. Frackiewicz, Prog. Rep. No. XIV, Lab. Ins. Res., Mass. Inst. Tech., Dec., 1953.

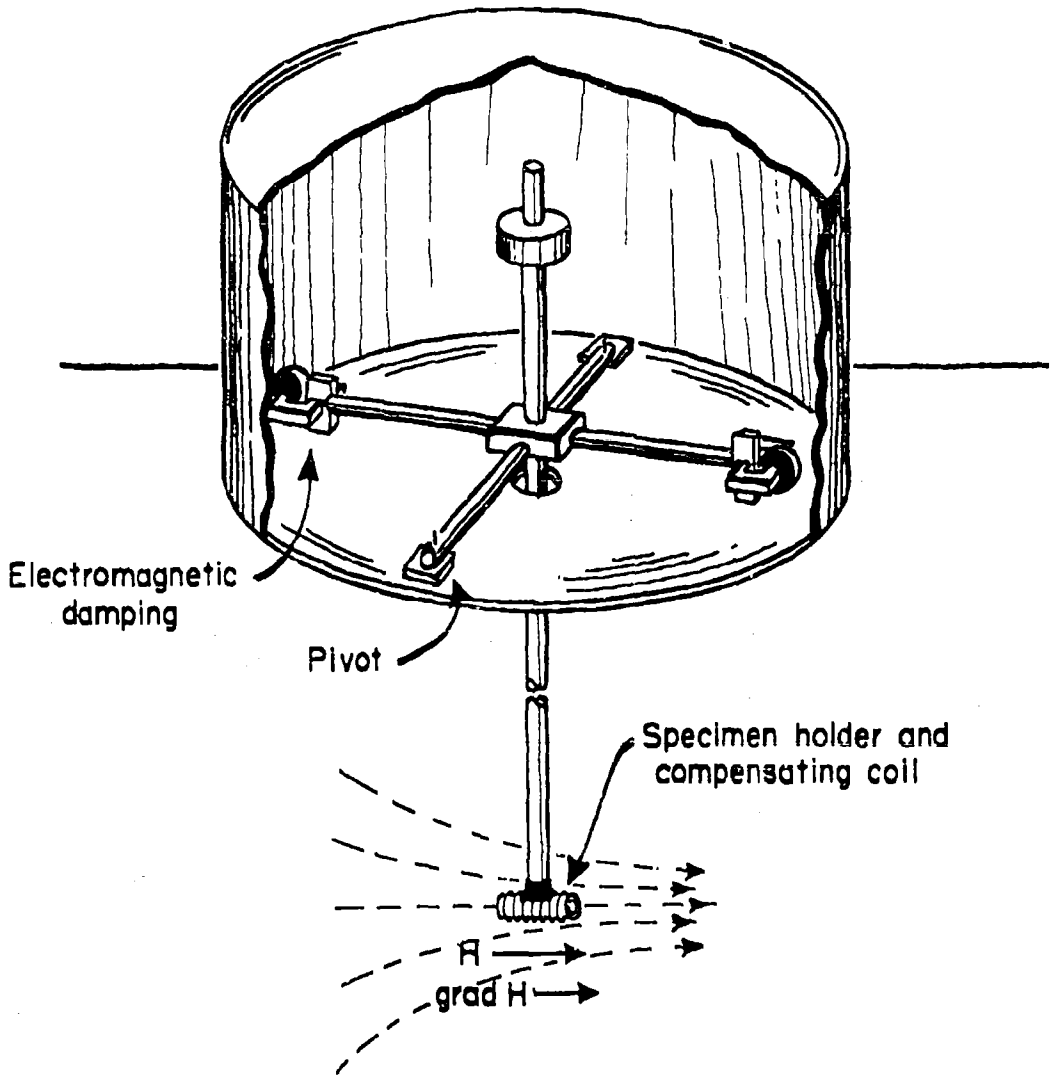

Fig. 2.2. The pendulum magnetometer.

meter, designed by Domenicali[4] (Fig. 2.2). Finally, a vibrating-coil magnetometer has been developed by Smith[5] (Fig. 2.3) for rapid measurements of magnatization and anisotropy characteristics, at high and low temperatures and high pressures; it determines the dipole field of the sample at a distance outside the oven and pressure bomb.

4) C. A. Domenicali, Rev. Sci. Instr. 21, 327 (1950).

5) D. O. Smith, Ph.D. Thesis, Mass. Inst. Tech., 1955.

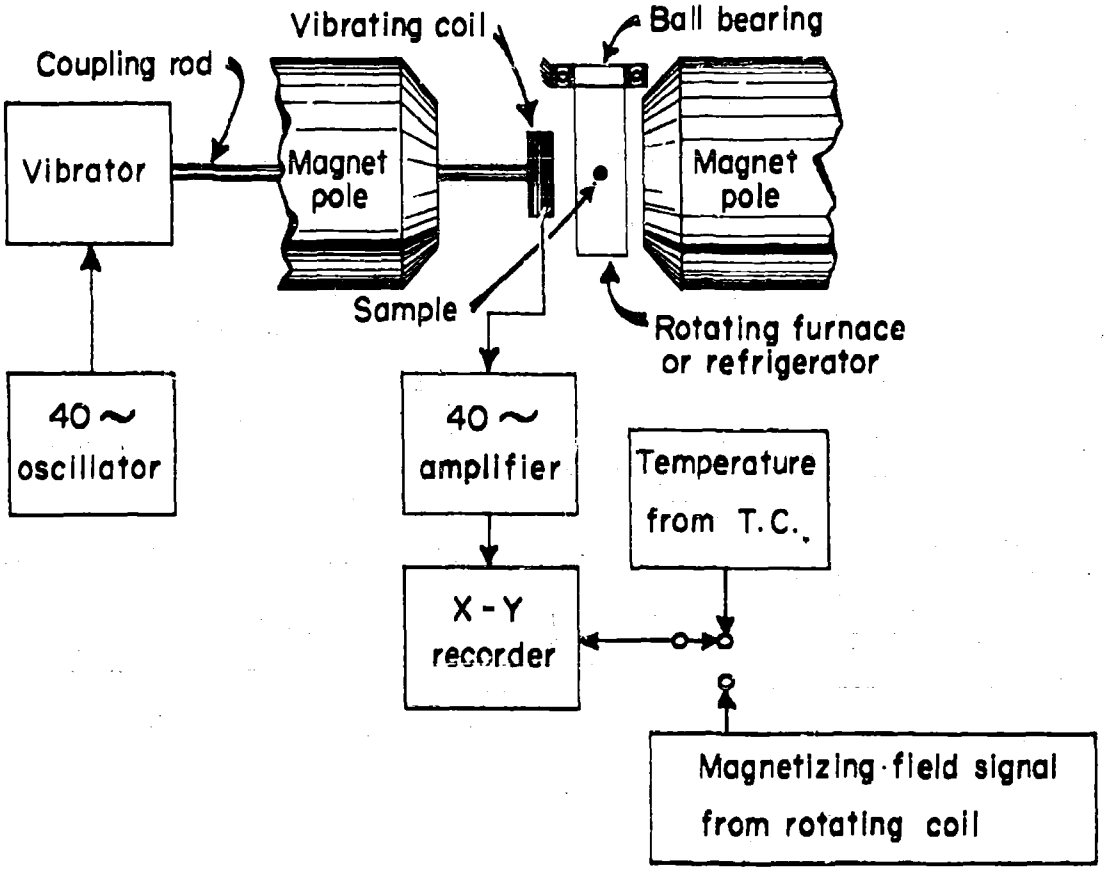

Fig. 2.3. Schematic diagram of the vibrating-coil magnetometer. A uniform maguetic field is perturbed by the presence of a magnetic sample. This perturbation induces an a-c voltage in the vibrating coil proportional to the magnetic moment of the sample.

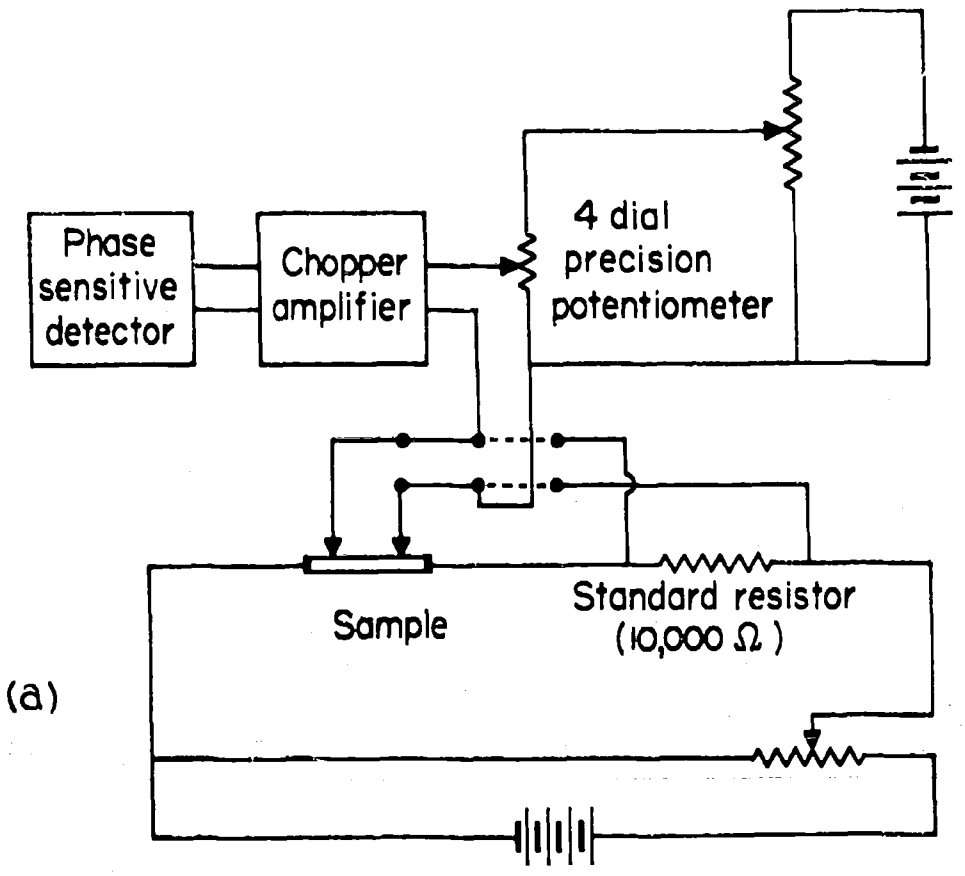

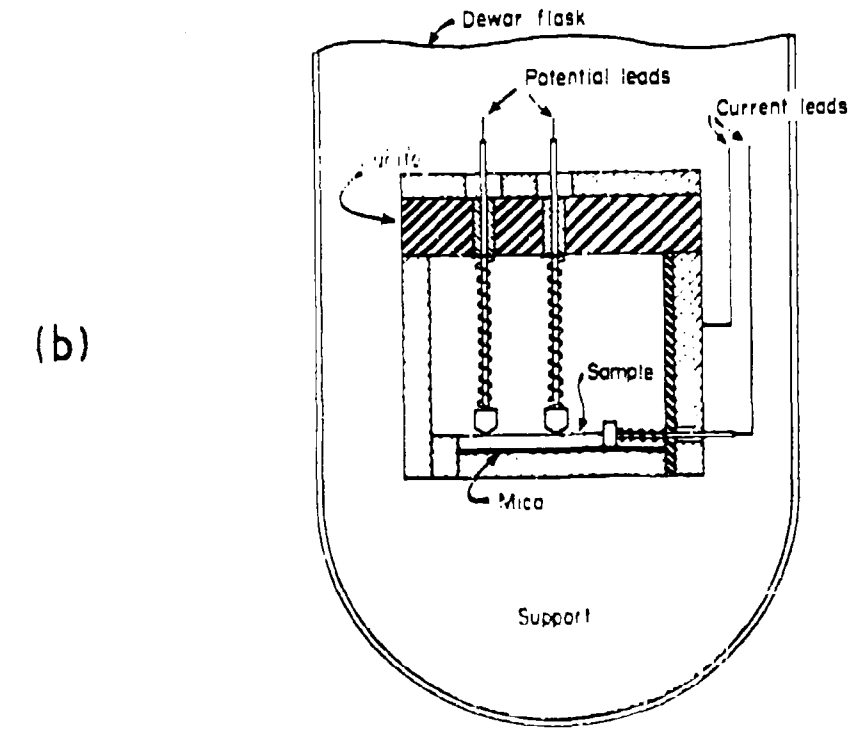

Fig. 2.4. (a) Circuit for four-terminal measurement of d-c conductivity; (b) specimen holder.

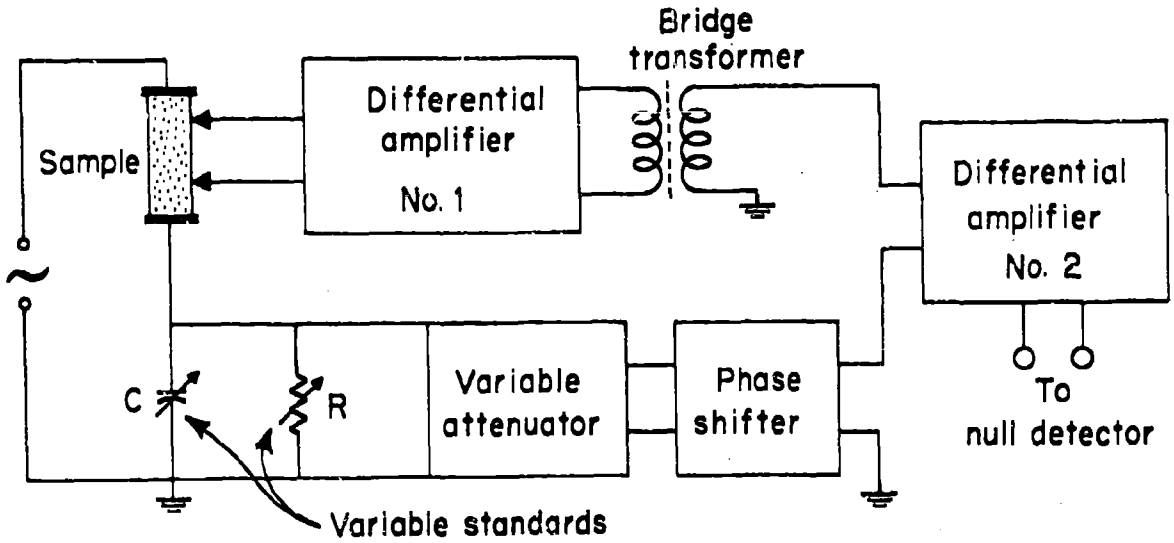

(a)

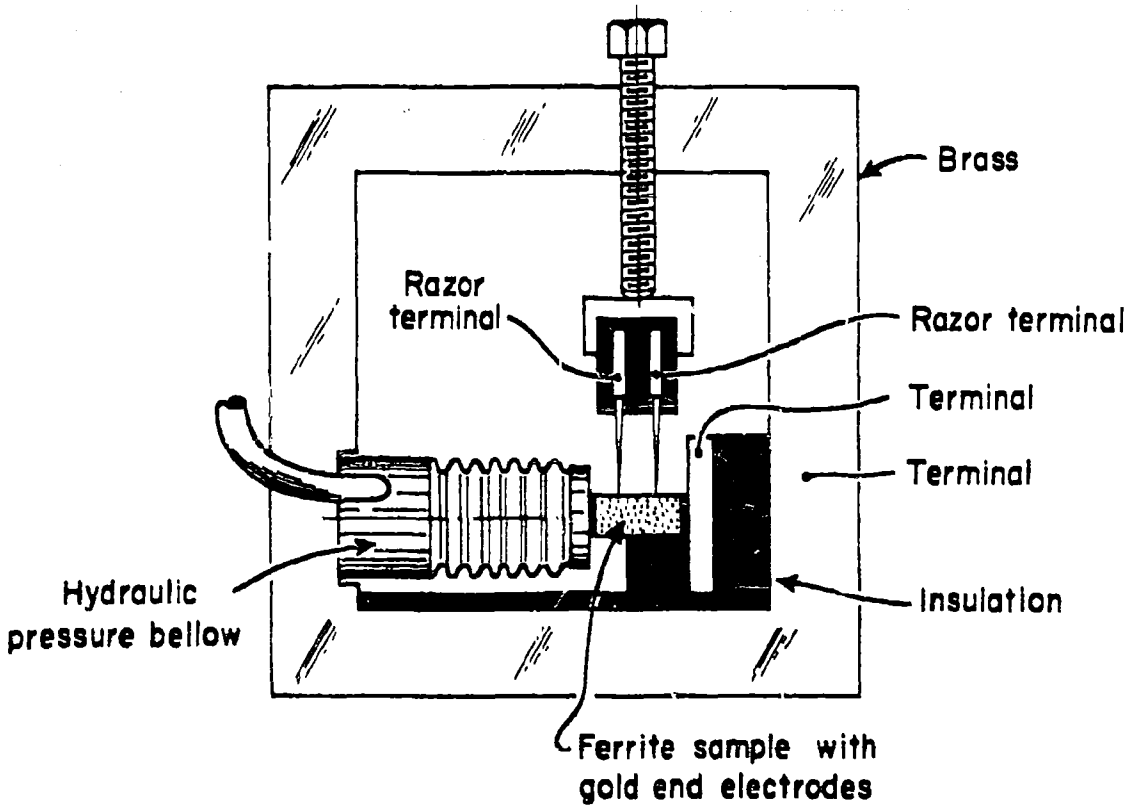

(b)

Fig. 2.5. (a) Differential-voltmeter circuit and (b) specimen holder for four-terminal a-c measurements of dielectric properties.

b) Measurements of ϵ^* by four-terminal methods

In order to avoid boundary-layer effects, semiconductors should be measured, in general, by a four-terminal arrangement. For d.c. the voltage drop across the potential electrodes was compared with that across a 10,000-ohm standard resistor (Fig. 2.4). A-c measurements up to 10^4 cps were made either with a differential voltmeter circuit (Fig. 2.5) or (in order to avoid the nonlinearity of the electronic components) in a potentiometer circuit with the coupling transformer to the detector tuned to resonance to provide a very high input impedance (Fig. 2.6).

c) Measurements of ϵ^* and μ^* at low frequencies (10^2 to 10^5 cps)

In most cases the permittivity was obtained by balancing the sample capacitor in one of the bridge circuits shown in Fig. 2.7. For permeability determinations toroid samples with windings were used and measured with a capacitance in series in the same type of bridge circuit (Fig. 2.8).

d) ϵ^* and μ^* in the medium frequency range (10^5 to 10^8 cps)

The measurements of the permittivity on lumped-capacitor samples were extended by the use of a susceptance variation circuit; dielectric constant and loss were obtained by the resonance position and half-width of the resonance curve (Fig. 2.9). For toroids in permeability determinations this technique is inferior because the distributed capacitance of the windings enters. Hence, the complex permeability was obtained on coaxial samples. For the range from 10^5 to 10^7 cps, such a sample was placed on a movable shorting plunger in a four-arm coaxial bridge (Fig. 2.10). Between 10^7 and 10^8 cps the coaxial sample could be measured at the shorted end of a fixed line section in the sample arm of a commercial radio-frequency bridge (G.R. 916-A or 1601) (Fig. 2.11).

e) Measurements in the high-frequency range (10^8 to 10^{10} cps)

Between 10^8 and 3×10^9 cps ϵ^* and μ^* were obtained in a coaxial line with

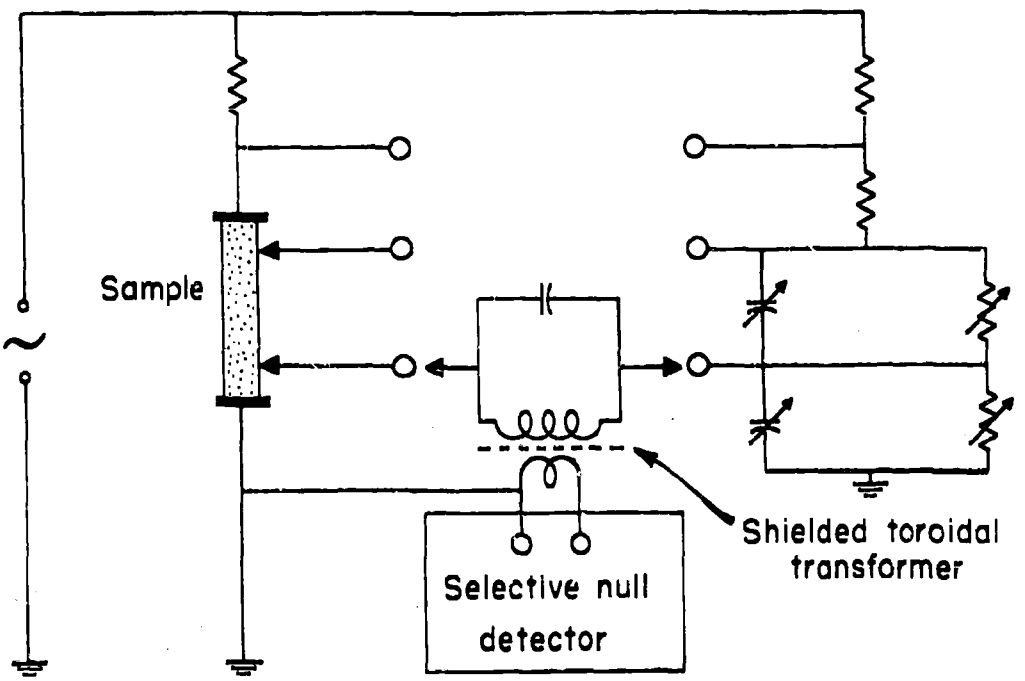

Fig. 2.6. Potentiometer circuit for four-terminal measurements.

standing-wave detector, by locating a thin sample in two successive measurements in a region of high magnetic and high electric field strength (short-circuit and open-circuit method) (Fig. 2.12). A d-c magnetic field parallel to the high-frequency field could be superposed by connecting a current source across the center conductor. At higher frequencies, the same method was used with hollow wave guides.

f) Measurements in the optical range

The absorption of the ferrites in the optical range is very high. The spectra could be recorded from 2000 to about 10,000A by a Cary instrument and from 1 to about 40 μ by an IR-3 Beckmann spectrophotometer, equipped for the far infrared in this laboratory with KRS-5 optics. For a survey study, ceramic or crystal samples were pulverized to particles of the order of 0.1 to 1 μ, mixed

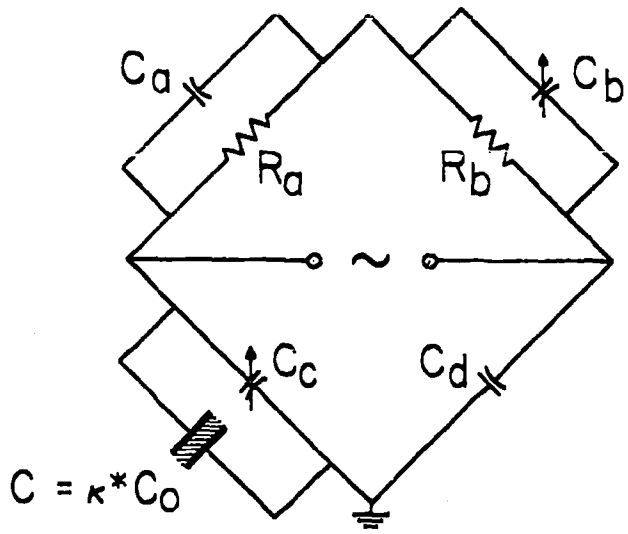

$$\kappa' = \frac{\Delta C_c + C_o}{C_a}$$

$$\kappa'' = C_d \cdot \frac{\omega R_b}{C_o} \cdot \Delta C_b$$

LOW LOSS

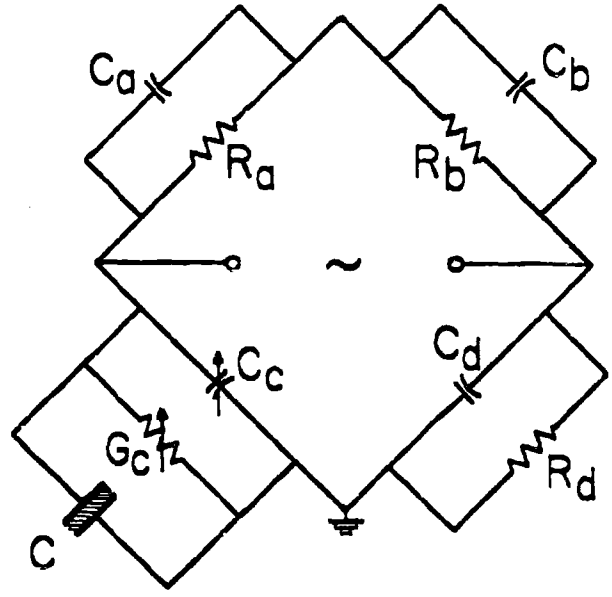

$$\kappa' = \frac{\Delta C_c}{C_o}$$

$$\kappa'' = \frac{\Delta G_c}{\omega C_o}$$

HIGH LOSS

Fig. 2.7. Bridge circuits used for dielectric measurements in the frequency range 10^2 to 10^5 cps.

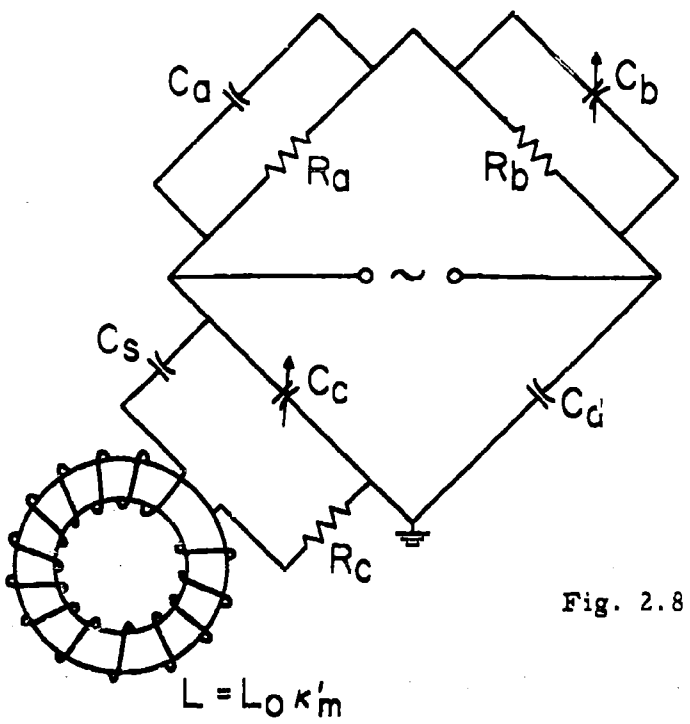

$$\kappa'_m = \frac{1}{L_o} \frac{\Delta C_c}{\omega^2 C_s (C_s + \Delta C_c)}$$

Fig. 2.8. Bridge circuit for magnetic measurements in the frequency range 10^2 to 10^5 cps.

with KBr powder and pressed to nearly transparent specimens[6] in the form of disks (ca. 1 cm dia., 2 mm thick). In the sample holder of Fig. 2.13 the temperature could be varied from -196° to +100°C. In addition to these mixed specimens, single crystal disks were measured in reflection and evaporated layers in transmission.

3. Background Information on the Frequency Dependence of the Ferromagnetic Response

The frequency response of ferromagnetics has been an important research problem of physics for more than fifty years. That it has not yet been solved to general satisfaction, is due to a variety of circumstances. Before World War II the investigations concentrated on metals; because of skin effect they are practically opaque in the decisive frequency region. The concept of a complex permeability, while visualized by Arkadiew[7] at an early date, had not been clearly

6) M. M. Stimson and M. J. O'Donnell, J. Am. Chem. Soc. 74, 1805 (1952); U. Schiedt and H. Reinwein, Z. Naturforsch. 7B, 270 (1952).

7) W. Arkadiew, Physik. Z. 14, 928 (1913).

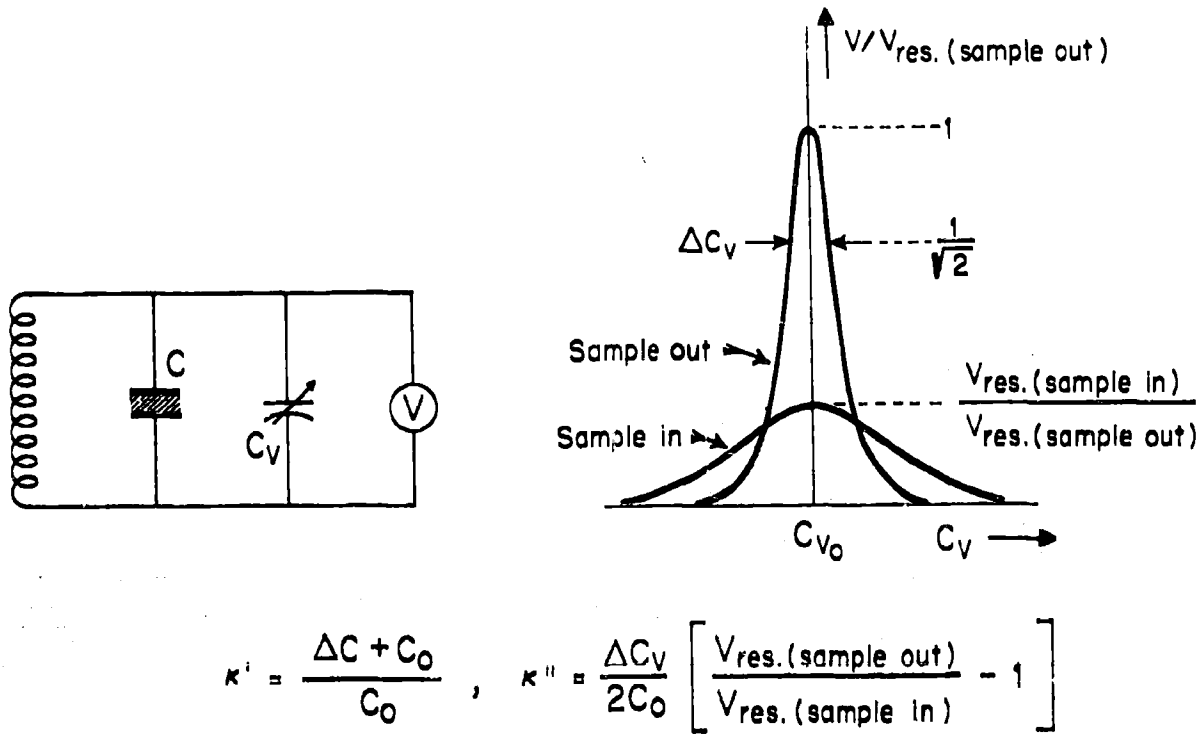

Fig. 2.9. Resonant circuit measurement of dielectric properties in the frequency range 10^5 to 10^8 cps.

formulated in a language common to physicists and electrical engineers and incorporated into the electromagnetic field theory. Techniques for measuring frequency response characteristics were not sufficiently developed, especially in the microwave region. And last, not least, the theory of ferromagnetism, after a promising start, bogged down in the uncertainties of quantum-mechanical approximations.

In spite of these handicaps, a number of decisive facts were established. Measurements on thin wires and films gave a general idea of the dispersion of the initial permeability for metals (Fig. 3.1).[8] Optical measurements by Hagen

8) J. T. Allanson, J. Inst. Elec. Engrs. 92, Part III, 247 (1945); C. Kittel, Phys. Rev. 70, 281 (1946).

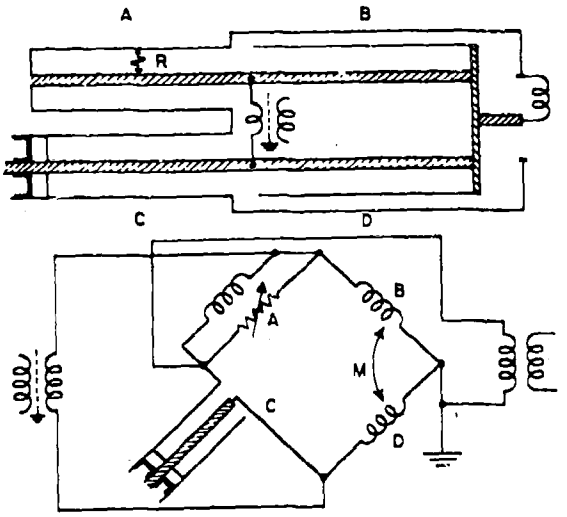

$$K'_m = \frac{\Delta\ell + d}{d} - \frac{\frac{\Delta\ell_R}{d}\left(\frac{Z_c}{R}\cdot\frac{2\pi\Delta\ell_R}{\lambda}\right)^2}{1+\left(\frac{Z_c}{R}\cdot\frac{2\pi\Delta\ell_R}{\lambda}\right)^2}$$

$$K''_m = \frac{\lambda}{2\pi d}\cdot\frac{\frac{Z_c}{R}\left(\frac{2\pi\Delta\ell_R}{\lambda}\right)^2}{\left(1+\frac{Z_c}{R}\cdot\frac{2\pi\Delta\ell_R}{\lambda}\right)^2}$$ Line loss neglected

Fig. 2.10. Coaxial line bridge for use in the frequency range 10^5 to 10^7 cps.

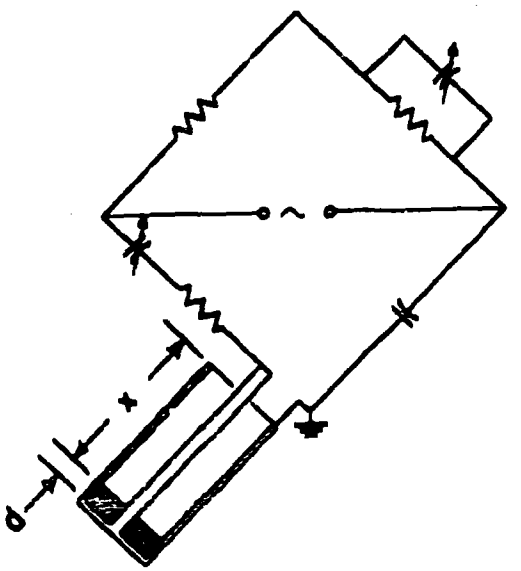

Fig. 2.11. General Radio bridges for use in the frequency range 10^7 to 10^8 cps.

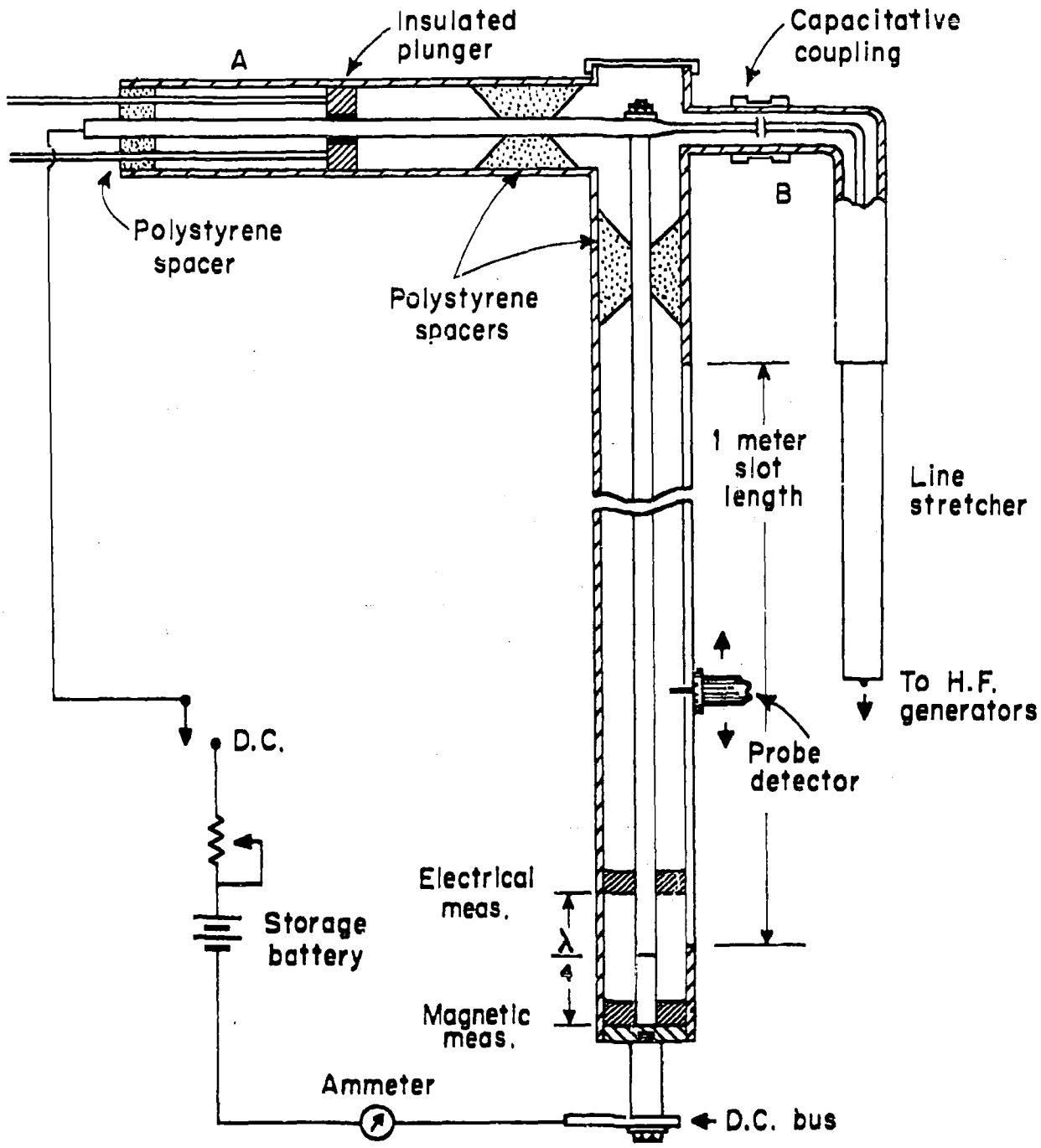

Fig. 2.12. Slotted line for dielectric and magnetic measurements using a superimposed constant magnetic field.

and Rubens[9] on the reflectivity and emissivity of iron and nickel between 1 and

9) E. Hagen and H. Rubens, Ann. Phys. [IV] 11, 873 (1903).

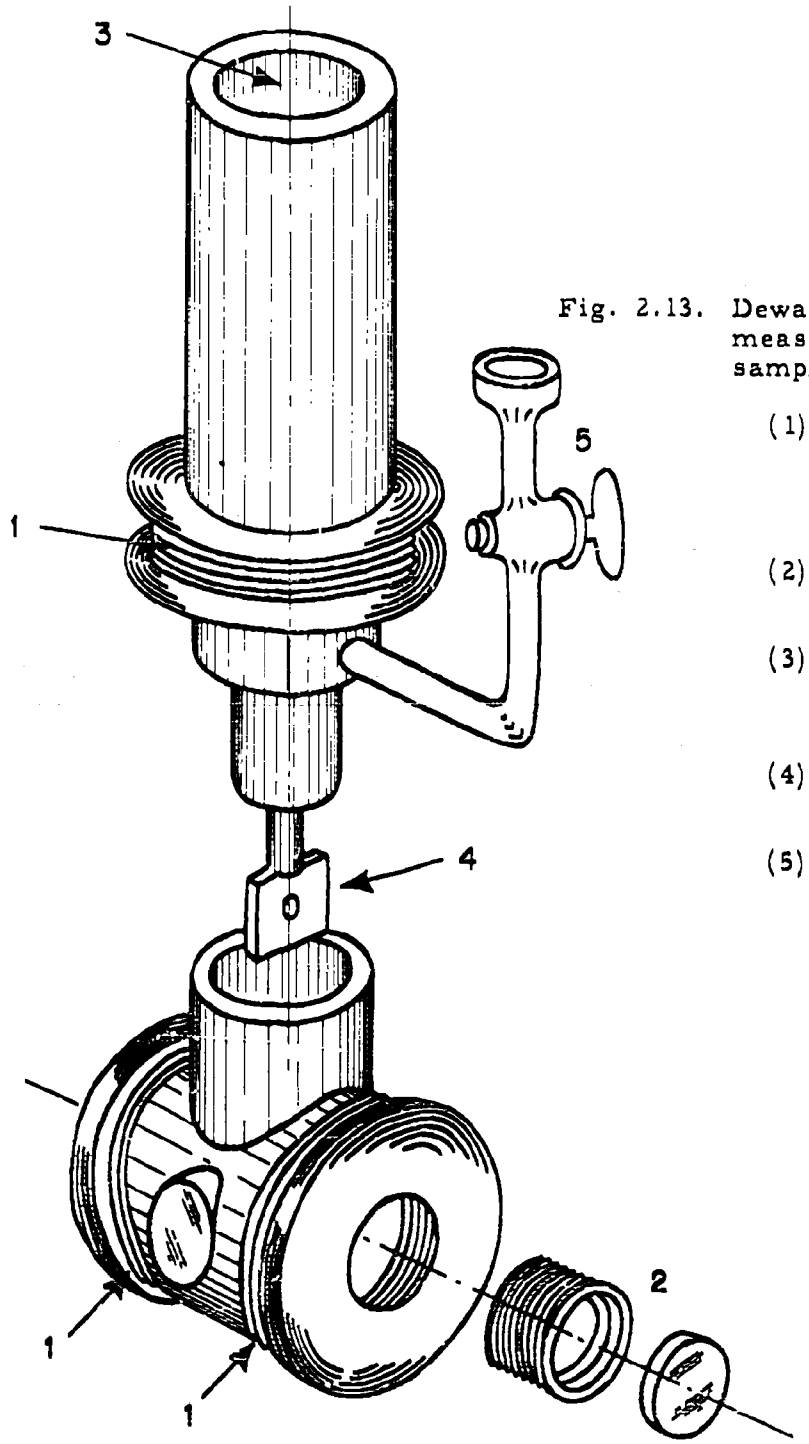

Fig. 2.13. Dewar cell for infrared measurements of solid samples:

(1) flexible bellows for focusing and centering adjustments

(2) lens or window assembly

(3) reservoir for cooling- or heating-bath

(4) micro sample holder

(5) vacuum line

25 μ showed, at an early date, that the ferromagnetic response of metals disappears in this infrared region. At low frequencies the existence of Barkhausen

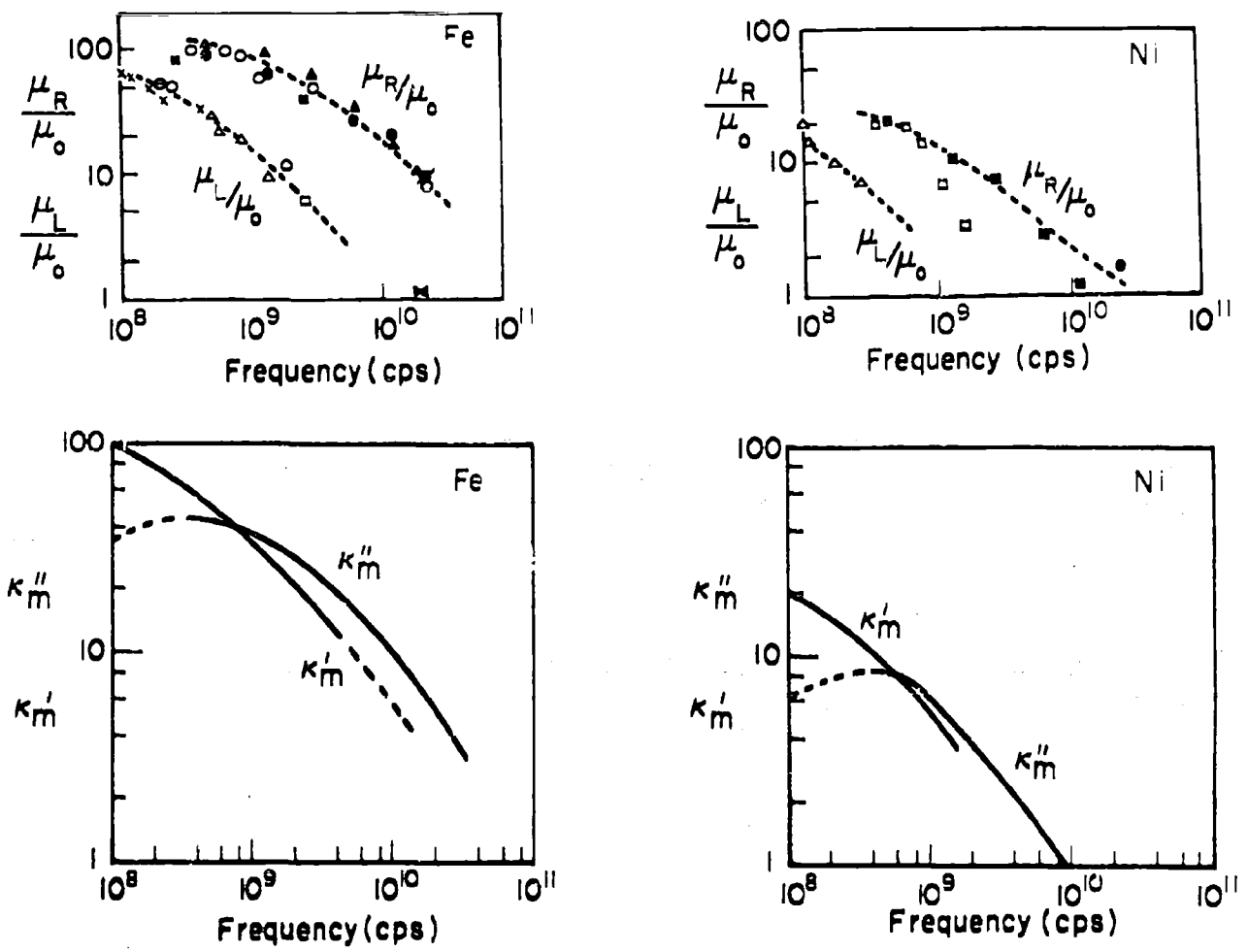

Fig. 3.1. Permeability values for iron and nickel in the frequency range 10^8 to 10^{11} cps plotted from the accumulated data of Allanson and Kittel.[8]

noise[10], and its correlation to domain-wall motion and hysteresis loops[11] made it obvious that a dispersion region caused by domain effects must exist and that this dispersion is field-strength sensitive. A description of domain walls and their motion by spin orientation was introduced by Bloch[12], while the possibility of a resonance phenomenon in ferromagnets was discussed by Landau and Lifshitz.[13]

10) H. Barkhausen, Physik. Z. 20, 401 (1919).

11) K. J. Sixtus and L. Tonks, Phys. Rev. 37, 930 (1931).

12) F. Bloch, Z. Phys. 74, 295 (1932).

13) L. Landau and E. Lifshitz, Physik. Z. Sowjetunion 8, 135 (1935).

Much has happened since these prewar days to clarify the phenomena, as well as to underline their complexities. Measurement techniques using wave guides, first introduced in the early days of the war[14], have made the microwave range accessible by a variety of precision methods.[15] The discovery of nuclear[16], paramagnetic[17] and ferromagnetic[18] resonance has led to a clearer understanding of the gyroscopic behavior of magnetic moments and of the importance of magnetic anisotropy.[19] The demand for magnetics of superior high-frequency properties caused the emergence of the ferromagnetic nonmetals from obscurity; this development, pioneered by Snoek, Verwey and co-workers of the Philips Laboratories[20], has lifted the eddy-current screen. The combination of magnetic and nonmagnetic constituents in ferrites leads to new coupling phenomena between magnetic moments, as Néel first recognized in antiferromagnetism[21], and to a new freedom of making magnetic properties to order. Much additional important work could be cited; it has been ably summarized in recent surveys.[22, 23]

14) S. Roberts and A. von Hippel, J. Appl. Phys. 17, 610 (1946).

15) Cf. W. B. Westphal and D. J. Epstein, "Dielectric Materials and Applications," Technology Press, and Wiley and Sons, New York, N.Y., 1954.

16) I. I. Rabi, Phys. Rev. 51, 652 (1937); E. M. Purcell, H. C. Torrey and R. V. Pound, Phys. Rev. 69, 37 (1946); F. Bloch, W. W. Hansen and M. Packard, Phys. Rev. 70, 474 (1946).

17) E. Zavoisky, J. Phys. (U.S.S.R.) 10, 170, 197 (1946).

18) J. H. E. Griffiths, Nature 158, 670 (1946).

19) C. Kittel, Phys. Rev. 73, 155 (1948).

20) J. L. Snoek, "New Developments in Ferromagnetic Materials," Elsevier, New York, N.Y., 1947.

21) L. Néel, Ann. Phys. [11] 5, 232 (1936); [12] 3, 137 (1948).

22) G. T. Rado, "Ferromagnetic Phenomena at Microwave Frequencies," Advances in Electronics II, 1950; A. Fairweather, F. F. Roberts and A. J. E. Welch, "Ferrites," Rep. Prog. Phys. 15, 142 (1952).

23) H. P. Wijn, Lab. Philips Gloeilampenfabrieken, Separaat 2092, 1953.

The question of the frequency response of ferrites is under investigation in various laboratories. Several resonance phenomena (cavity[24], gyromagnetic[13, 25] and domain-wall[26] resonance) and several relaxation phenomena[23] have been invoked to explain the observed characteristics. That no unanimity has been reached in these interpretations, is not surprising in view of the complexity and diffuseness of the response curves (Fig. 3.2) and the variety of the experimental and theoretical parameters.

4. Gyroscopic Effects in Magnetization Phenomena

The elementary magnetic moments $\vec{m}$ of a material are causally related to quantized angular momenta p' as

$$\vec{m} = \gamma \vec{p}' \tag{4.1}$$

(γ is the gyromagnetic ratio). They are gyroscopes, subjected in a magnetic field $\vec{H}$, according to Newton's law, to a torque

$$T = \frac{d\vec{p}'}{dt} = \vec{m} \times \mu_o \vec{H} \ , \tag{4.2}$$

which causes a temporal change of the magnetic moment

$$\frac{d\vec{m}}{dt} = \gamma \left[\vec{m} \times \mu_o \vec{H} \right] . \tag{4.3}$$

The magnetization, represented by the additive action of N dipole moments per unit volume,

$$\vec{M} = N \vec{m} \ , \tag{4.4}$$

obeys therefore the equation of motion

$$\frac{d\vec{M}}{dt} = \gamma \left[\vec{M} \times \mu_o \vec{H} \right] . \tag{4.5}$$

---

24) F. G. Brockman, P. H. Dowling and W. G. Steneck, Phys. Rev. 77, 85 (1950).

25) J. L. Snoek, Physica 14, 207 (1948); D. Polder and J. Smit, Revs. Mod. Phys. 25, 89 (1953).

26) W. Döring, Z. Naturforsch. 3A, 373 (1948); R. Becker, J. phys. radium 12, 332 (1951); G. T. Rado, R. W. Wright and W. H. Emerson, Phys. Rev. 80, 273 (1950).

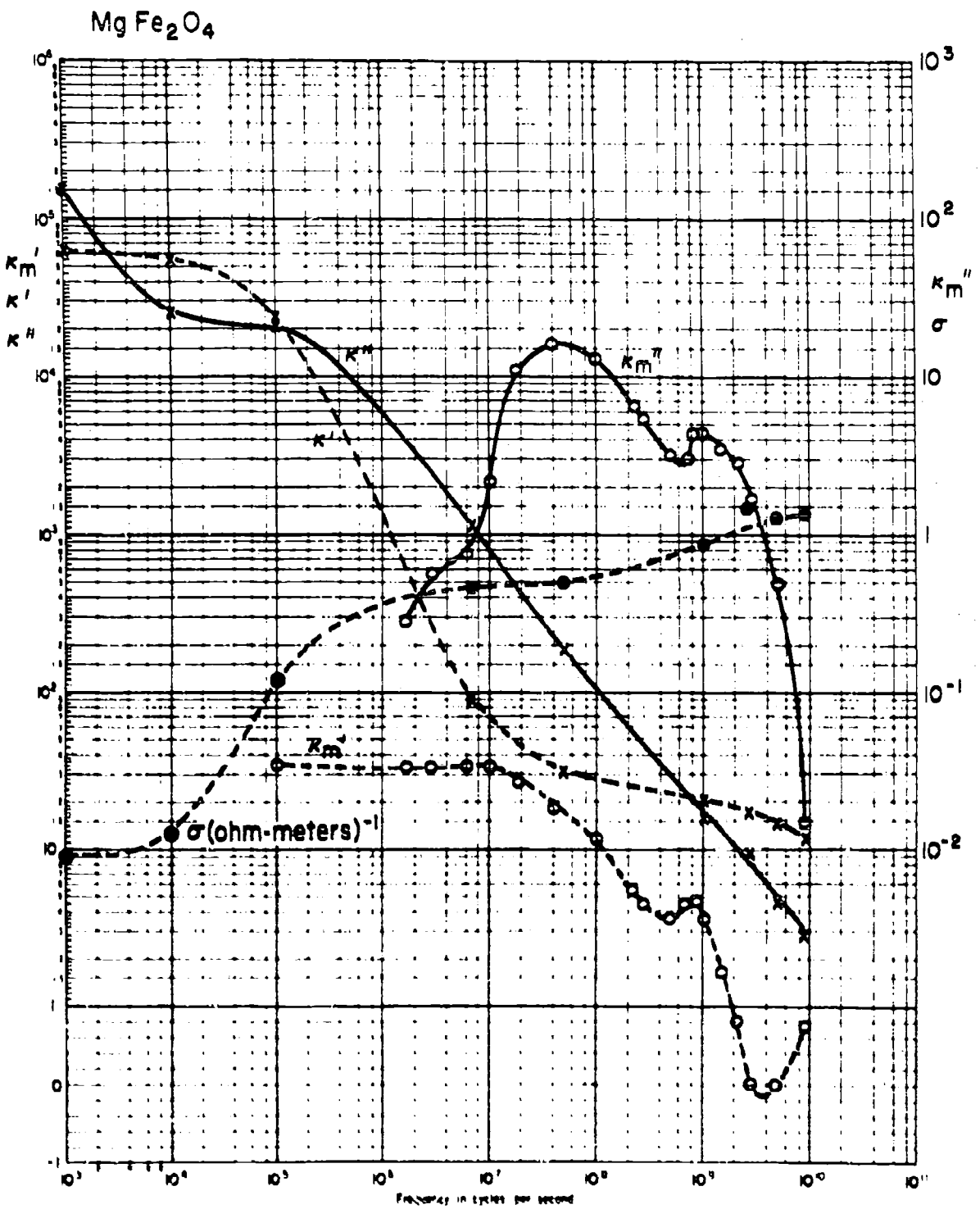

Fig. 3.2. A typical case of the dielectric and magnetic dispersions in ferrites; results for $MgFe_2O_4$.

a) Precession in static field

If $\underset{\rightarrow}{H}$ represents a static field applied in the +z direction,

$$\underset{\rightarrow}{H} = H_z = \text{constant} \quad , \tag{4.6}$$

Eq. (4.5) resolves into the differential equations

$$\begin{aligned} \frac{d^2M_x}{dt^2} &= -\gamma^2 \mu_o^2 H_z^2 M_x \\ \frac{d^2M_y}{dt^2} &= -\gamma^2 \mu_o^2 H_z^2 M_y \quad . \end{aligned} \tag{4.7}$$

The components M_x and M_y of the magnetization act like linear oscillators of the resonance frequency (Larmor frequency)

$$\omega_o = -\gamma \mu_o H_z \quad . \tag{4.8}$$

According to the coupling equation

$$\frac{dM_x}{dt} = j\omega_o M_x = \omega_o M_y \quad , \tag{4.9}$$

these two oscillating components are out of phase by 90° in space and time, hence add up to a circular rotation in the x-y plane. The magnetization vector $\underset{\rightarrow}{M}$ precesses around the magnetic field axis (Fig. 4.1).

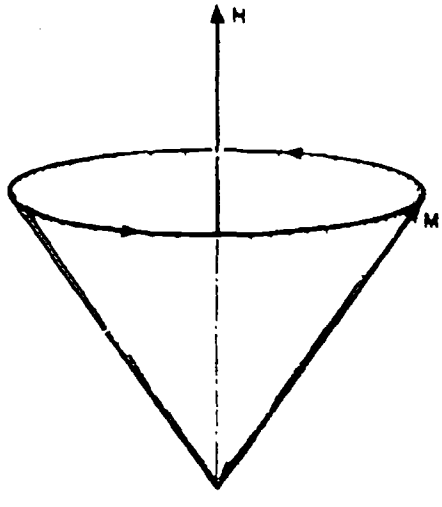

Fig. 4.1. Undamped precession of magnetization vector about the magnetic-field axis ($\gamma < 0$).

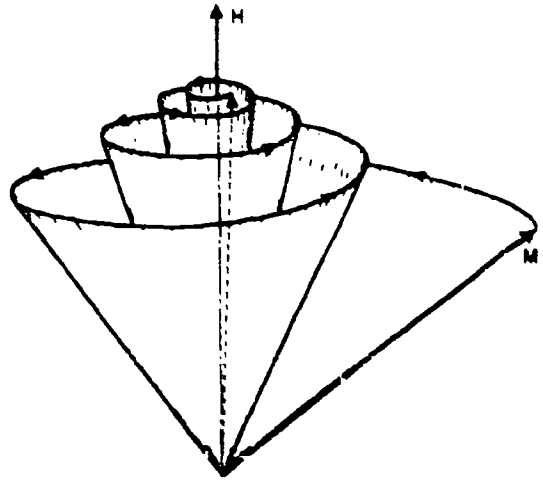

Fig. 4.2. Damped precession of magnetization vector about the magnetic-field axis ($\gamma < 0$).

In real matter, the rotational energy of the Larmor precession will be dissipated by such effects as magnetic dipole radiation, spin interaction, eddy-current damping and magneto-elastic coupling. In consequence, the magnetic momentum vector will spiral back into the z direction (Fig. 4.2). This tendency can be expressed in the equations of motion by adding to the rotational torque an erecting torque (Fig. 4.3),

$$\frac{d\vec{M}}{dt} = \gamma \left[\vec{M}\times\mu_o\vec{H}\right] - \frac{\lambda}{|M|^2}\left[\vec{M}\times(\vec{M}\times\vec{H})\right] \equiv \gamma \left[\vec{M}\times\mu_o\vec{H}\right] + \lambda\left[\vec{H} - \frac{(\vec{M}\cdot\vec{H})\vec{M}}{|M|^2}\right] \tag{4.10}$$

as first introduced by Landau and Lifshitz.[13] In the absence of a precise theory of the damping mechanism, the factor λ must be regarded as a parameter that may depend on $\vec{H}$ and $\vec{M}$. In place of Eqs. (4.7) we obtain for the magnetization components

$$\frac{d^2M_x}{dt^2} + \lambda A \frac{dM_x}{dt} + \omega_o^2 M_x + \omega_o \lambda A M_y = 0$$
$$\frac{d^2M_y}{dt^2} + \lambda A \frac{dM_y}{dt} + \omega_o^2 M_y - \omega_o \lambda A M_x = 0 \quad , \tag{4.11}$$

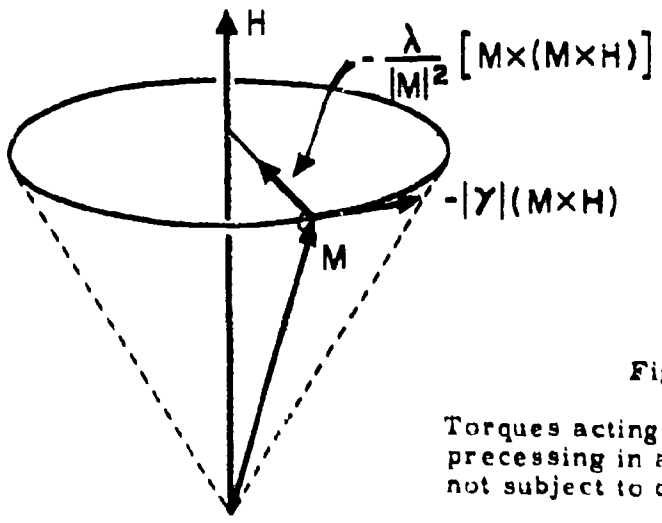

Fig. 4.3.

Torques acting on magnetic dipole precessing in a magnetic field H not subject to damping.

where

$$A \equiv \frac{(M \cdot H)}{|M|^2} \quad .$$

The M_x and M_y oscillators are now attenuated and coupled. In addition a magnetization component in the z direction appears as

$$\frac{dM_z}{dt} + \lambda \left\{ AM_z - H_z \right\} = 0 \quad . \tag{4.12}$$

The solution is

$$\begin{aligned} M_x &= M_o \cos(\omega_o t)\, e^{-at} \\ M_y &= M_o \sin(\omega_o t)\, e^{-at} \\ M_z &= M \left\{ 1 - \left(\frac{M_o}{M} \right)^2 e^{-2at} \right\} \end{aligned} \tag{4.13}$$

$$a \equiv \lambda A \quad .$$

By introducing the erecting torque, the oscillators in the x-y plane remain out of phase by 90° in space and time but are attenuated. The resonance frequency is still identical to the Larmor frequency of Eq. (4.8). However, a time-dependent M_z component has appeared which grows asymptotically to the total value $\underset{\rightarrow}{M}$.

b) Superposition of a small alternating magnetic field

After the precession of the magnetization vector $\underset{\rightarrow}{M}$ in the static field H_z has died away, the superposition of a small alternating magnetic field

$$\Delta \underset{\rightarrow}{H} = (\Delta \underset{\rightarrow}{H})_o \, e^{j\omega t} \tag{4.14}$$

again causes a precession. Without attenuation and by including only first-order terms, the torque equation (Eq. 4.5) reads

$$\frac{d(\Delta M)}{dt} = \gamma \begin{vmatrix} \underset{\rightarrow}{i} & \underset{\rightarrow}{j} & \underset{\rightarrow}{k} \\ \Delta M_x & \Delta M_y & M_z \\ \mu_o \Delta H_x & \mu_o \Delta H_y & \mu_o H_z \end{vmatrix} ; \tag{4.15}$$

that is,

$$\frac{d(\Delta M_x)}{dt} = \gamma\mu_o \left[(\Delta M_y)H_z - M_z(\Delta H_y) \right]$$

$$\frac{d(\Delta M_y)}{dt} = \gamma\mu_o \left[M_z(\Delta H_x) - (\Delta M_x)H_z \right] \qquad (4.16)$$

$$\frac{d(\Delta M_z)}{dt} = 0 \quad .$$

Differentiation and substitution leads to the differential equation

$$\frac{d^2(\Delta M_x)}{dt^2} = \gamma\mu_o \left\{ \frac{d(\Delta M_y)}{dt} H_z - M_z \frac{d(\Delta H_y)}{dt} \right\} \qquad (4.17)$$

$$= \gamma^2\mu_o^2 H_z \left\{ M_z(\Delta H_x) - (\Delta M_x)H_z \right\} - j\omega\gamma\mu_o M_z(\Delta H_y) \ ,$$

By introducing the Larmor frequency of Eq. (4.8), we arrive at the final expression for the magnetization component in the x direction

$$\Delta M_x = \frac{\omega_o^2 \frac{M_z}{H_z}}{\omega_o^2 - \omega^2} (\Delta H_x) - j \frac{\omega\omega_o \frac{M_z}{H_z}}{\omega_o^2 - \omega^2} (\Delta H_y) \equiv a(\Delta H_x) - j \frac{\omega}{\omega_o} a(\Delta H_y) \ ;$$

and, correspondingly, for the y component (4.18)

$$\Delta M_y = \frac{\omega_o^2 \frac{M_z}{H_z}}{\omega_o^2 - \omega^2} (\Delta H_y) + j \frac{\omega\omega_o \frac{M_z}{H_z}}{\omega_o^2 - \omega^2} (\Delta H_x) \equiv a(\Delta H_y) + j \frac{\omega}{\omega_o} a(\Delta H_x) \ ,$$

where $a \equiv \dfrac{\omega_o^2 \frac{M_z}{H_z}}{\omega^2 - \omega^2}$.

Both field components in the x-y plane cause a precession of the $\underrightarrow{M}$ vector around the field axis, H_z. For very low frequencies in relation to the Larmor frequency, the $\underrightarrow{M}$ vector practically oscillates in the direction of and in phase with the driving field; for very high frequencies ($\omega >> \omega_o$), the magnetization vector is essentially out of phase by 90° in space and 180° in time; at the Larmor frequency itself, the $\underrightarrow{M}$ vector describes a circular precession motion in the x-y plane (Fig. 4.4).

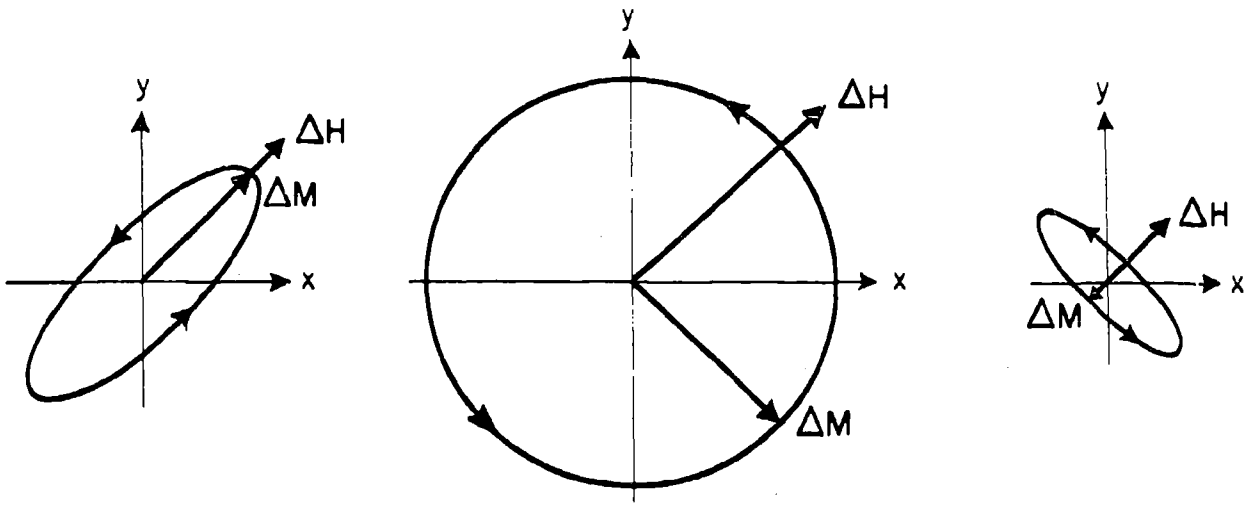

$\omega << \omega_0$ $\omega = \omega_0$ $\omega >> \omega_0$

Fig. 4.4. Projection in the x-y plane of the motion of the magnetization vector ($\gamma < 0$) under the influence of a constant field H_z and an oscillatory field ΔH.

Expressing the relation between the magnetization and field components by a susceptibility matrix for the magnetic susceptibility χ_m (cf Eqs. 1.14 and 1.17), we obtain with $\chi_{11} = \chi_{22} = a$, and $\chi_{12} = -\chi_{21} = -j\frac{\omega}{\omega_o} a$,

$$\chi_m = \begin{vmatrix} \chi_{11} & \chi_{12} & 0 \\ \chi_{21} & \chi_{22} & 0 \\ 0 & 0 & 0 \end{vmatrix} \tag{4.19}$$

If attenuation is introduced by the Landau-Lifshitz torque term, we find in place of Eq. (4.18) for the same first-order approximation

$$\Delta M_x = \frac{\omega_o\omega' + \lambda^2 A + j\omega\lambda}{\omega_o^2 + (j\omega + \lambda A)^2} \Delta H_x - \frac{j\omega\omega'}{\omega_o^2 + (j\omega + \lambda A)^2} \Delta H_y$$

$$\Delta M_y = \frac{j\omega\omega'}{\omega_o^2 + (j\omega + \lambda A)^2} \Delta H_x + \frac{(\omega_o\omega' + \lambda^2 A + j\omega\lambda)}{\omega_o^2 + (j\omega + \lambda A)^2} \Delta H_y \tag{4.20}$$

$$\omega' \equiv -\mu_o \gamma M_z$$

$$\Delta M_z = 0$$

Thus,

$$\begin{aligned} \Delta M_x &= a'(\Delta H_x) - jb'(\Delta H_y) \\ \Delta M_y &= a'(\Delta H_y) + jb'(\Delta H_x) \end{aligned} \quad , \tag{4.21}$$

where

$$a' \equiv \frac{\omega_o\omega' + \lambda^2 A + j\omega\lambda}{\omega_o^2 + (j\omega + \lambda A)^2} = \frac{\omega_o^2 \frac{M_z}{H_z} + \lambda(j\omega + \alpha)}{\omega_o^2 + (j\omega + \alpha)^2} \quad ,$$

$$b' \equiv \frac{\omega\omega'}{\omega_o^2 + (j\omega + \alpha)^2}$$

The magnetization components are coupled to the exciting-field components as previously, but the forced oscillations are attenuated and their resonance frequency has been raised from the Larmor frequency ω_o to $\sqrt{\omega_o^2 + \alpha^2}$.

c) Propagation of an electromagnetic plane wave through a premagnetized dielectric*

The small magnetic disturbance $\Delta\vec{H}$ of the preceding section is coupled according to Maxwell's equations with an electric field $\Delta\vec{E}$ as

$$\begin{aligned} \vec{\nabla} \times (\Delta\vec{E}) &= -\frac{\partial(\Delta\vec{B})}{\partial t} \\ \vec{\nabla} \times (\Delta\vec{H}) &= \frac{\partial\vec{D}}{\partial t} \end{aligned} \tag{4.22}$$

Hence an electromagnetic wave travels through the material, assumed here to be a plane wave

$$\begin{aligned} \Delta\vec{E} &= \Delta\vec{E}_o\, e^{j\omega t - \gamma(\vec{k}^o \cdot \vec{r})} \\ \Delta\vec{H} &= \Delta\vec{H}_o\, e^{j\omega t - \gamma(\vec{k}^o \cdot \vec{r})} \end{aligned} \tag{4.23}$$

* The discussion given here of the gyroscopic effects is a generalization of the well-known derivation of Polder[27], expressed in our language.

27) D. Polder, Phil. Mag. [7] 40, 99 (1949).

The unit vector $\underset{\rightarrow}{k}^{o}$ indicates the direction of propagation; $\underset{\rightarrow}{r}$ represents a vector pointing from some origin into space, and $\underset{\rightarrow}{k}^{o} \cdot \underset{\rightarrow}{r}$ is a general distance co-ordinate measured along the propagation direction (Fig. 4.5). The vectors $\underset{\rightarrow}{k}^{o}$, $\underset{\rightarrow}{E}$ and $\underset{\rightarrow}{H}$ form a right-hand screw system.

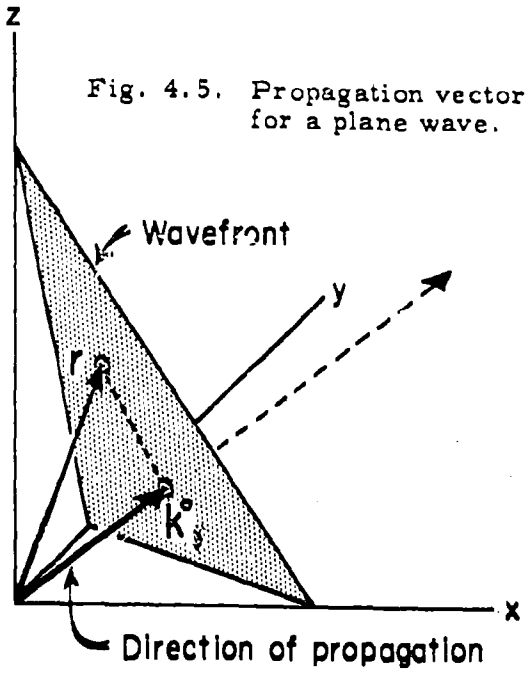

Fig. 4.5. Propagation vector $\underset{\rightarrow}{k}^{o}$ for a plane wave.

Introducing the plane-wave solution, we may rewrite Maxwell's equations

$$-\gamma(\underset{\rightarrow}{k}^{o} \times \Delta\underset{\rightarrow}{E}) = -j\omega\Delta\underset{\rightarrow}{B}$$
$$-\gamma(\underset{\rightarrow}{k}^{o} \times \Delta\underset{\rightarrow}{H}) = j\omega\Delta\underset{\rightarrow}{D} \qquad (4.24)$$

Neglecting attenuation ($\alpha = 0$, $\underset{\rightarrow}{B} = \mu'\underset{\rightarrow}{H}$, $\underset{\rightarrow}{D} = \epsilon'\underset{\rightarrow}{E}$), we replace the propagation factor γ (cf. Eq. 1.7) by its phase factor

$$\gamma \simeq j\beta = j\frac{2\pi}{\lambda} \qquad (4.25)$$

and obtain, in place of Eq. (4.24),

$$\frac{2\pi}{\omega\lambda}(\underset{\rightarrow}{k}^{o} \times \Delta\underset{\rightarrow}{E}) = \mu'\Delta\underset{\rightarrow}{H}$$
$$\frac{2\pi}{\omega\lambda}(\Delta\underset{\rightarrow}{H} \times k^{o}) = \epsilon'\Delta\underset{\rightarrow}{E} \qquad (4.26)$$

Substitution of $\Delta\underset{\rightarrow}{E}$ from the second into the first equation,

$$\left(\frac{2\pi}{\omega\lambda}\right)^{2}\left[\underset{\rightarrow}{k}^{o} \times (\Delta\underset{\rightarrow}{H} \times k^{o})\right] \equiv \frac{1}{v^{2}}\Delta\underset{\rightarrow}{H} = \epsilon'\mu'\Delta\underset{\rightarrow}{H}\,, \qquad (4.27)$$

leads, since $\epsilon'\mu' = \kappa'\kappa'_{m}/c^{2}$, to a generalized Maxwell relation (cf. Eqs. 1.7 and 1.10)

$$n^{2} \equiv \left(\frac{c}{v}\right)^{2} = \kappa'\kappa'_{m}\,. \qquad (4.28)$$

In our premagnetized dielectric, the index of refraction n will depend on

the angle θ between the direction of propagation $\underset{\rightarrow}{k}^{o}$ and the z axis. The change in magnetic induction

$$\Delta\underset{\rightarrow}{B} = \mu_o \Delta\underset{\rightarrow}{H} + \mu_o \Delta\underset{\rightarrow}{M} = \mu \Delta\underset{\rightarrow}{H} \quad , \tag{4.29}$$

according to Eq. (4.19), is given for the loss-free material by the permeability matrix

$$\mu' = \begin{vmatrix} \mu_{11} & \mu_{12} & 0 \\ \mu_{21} & \mu_{22} & 0 \\ 0 & 0 & \mu_o \end{vmatrix}$$

with

$$\begin{aligned} \frac{\mu_{11}}{\mu_o} &= \frac{\mu_{22}}{\mu_o} = (1 + a) \equiv c_1 \\ \frac{\mu_{12}}{\mu_o} &= -\frac{\mu_{21}}{\mu_o} = -j\frac{\omega}{\omega_c} a \equiv -jc_2 \quad . \end{aligned} \tag{4.30}$$

Hence

$$\begin{aligned} \frac{\Delta B_x}{\mu_o} &= c_1 \Delta H_x - jc_2 \Delta H_y \\ \frac{\Delta B_y}{\mu_o} &= jc_2 \Delta H_x + c_1 \Delta H_y \\ \frac{\Delta B_z}{\mu_o} &= \Delta H_z \end{aligned} \tag{4.31}$$

By introducing these induction components into Maxwell's equations, a general equation for the index of refraction results

$$n_{\pm}^2 \equiv \kappa' \kappa'_{m_{\pm}} = \frac{\kappa'}{2} \frac{(c_1^2 - c_1 - c_2^2)(\sin^2\theta) + 2c_1 \pm \left\{(c_1^2 - c_1 - c_2^2)^2 (\sin^4\theta) + 4c_2^2 \cos^2\theta\right\}^{1/2}}{(c_1 - 1)(\sin^2\theta) + 1} \quad . \tag{4.32}$$

For any angle θ we have two values for the index of refraction, that is, for the magnetic permeability. The expressions become especially simple for the propagation direction parallel to the magnetic-field axis ($\theta = 0$), where two circularly

polarized waves may exist with indices

$$n_+^2 = \kappa'(c_1 + c_2)$$
$$n_-^2 = \kappa'(c_1 - c_2) \quad ; \tag{4.33}$$

and for the direction perpendicular to the field axis ($\theta = \pi/2$), where two linearly polarized waves may propagate with

$$n_+^2 = \kappa' \frac{c_1^2 - c_2^2}{c_1}$$
$$n_-^2 = \kappa' \tag{4.34}$$

To understand graphically the meaning of this double refraction, we insert for c_1 and c_2 in Eq. (4.32) the values previously derived (cf. Eqs. 4.18 and 4.30)

$$c_1 = 1 + a = 1 + \frac{\omega_o^2 \frac{M_z}{H_z}}{\omega_o^2 - \omega^2} \quad ,$$
$$c_2 = \frac{\omega}{\omega_o} a = \frac{\omega\omega_o \frac{M_z}{H_z}}{\omega_o^2 - \omega^2} \quad . \tag{4.35}$$

Thus

$$n_{\pm}^2 = \kappa' \kappa'_{m_{\pm}} =$$

$$\kappa' \frac{\omega_o^2 \frac{B_z}{\mu_o H_z}\left(1 + \frac{M_z}{2H_z}\sin^2\theta\right) - \omega^2 \pm \left\{\left(\omega_o^2 \frac{B_z}{\mu_o H_z}\frac{M_z}{2H_z}\sin^2\theta\right)^2 + \left(\omega\omega_o \frac{M_z}{H_z}\cos\theta\right)^2\right\}^{1/2}}{\omega_o^2\left\{1 + \frac{M_z}{H_z}\sin^2\theta\right\} - \omega^2} \quad . \tag{4.36}$$

In the general case, the role of the Larmor frequency ω_o has been taken over by a modified resonance frequency

$$\omega_o'' = \omega_o \left\{1 + \frac{M_z}{H_z}\sin^2\theta\right\}^{1/2} \quad , \tag{4.37}$$

which depends on the angle between propagation direction and magnetic-field axis.

In the special cases of parallel or perpendicular incidence we obtain

$$(\text{for } \theta = 0) \qquad n^2_{\pm\parallel} = \kappa' \frac{\omega_o^2 - \omega^2 + \omega_o^2 \frac{M_z}{H_z}\left\{1 \pm \frac{\omega}{\omega_o}\right\}}{\omega_o^2 - \omega^2} \tag{4.38}$$

and

$$(\text{for } \theta = \tfrac{\pi}{2}) \qquad n^2_{\pm\perp} = \kappa' \frac{\omega''^2_o - \omega^2 + \omega''^2_o \frac{M_z}{2H_z}\left\{1 \pm 1\right\}}{\omega''^2_o - \omega^2} \quad .$$

At the resonance frequency, the value n_+^2 becomes infinite and that of n_-^2 equals κ'.

Let us visualize the situation. Propagation direction and magnetic-field axis (z direction) together designate a plane of incidence, the x-z plane of Fig. 4.6. The magnetic field $\Delta\vec{H}$ has a component ΔH_n normal to this plane pointing always in the y direction, while the component parallel to the plane ΔH_p is composed of components in the x and the z direction:

$$\begin{aligned} \Delta\vec{H} &= \Delta\vec{H}_n + \Delta\vec{H}_p \quad , \\ \Delta H_x &= \Delta H_p \cos\theta \quad , \\ \Delta H_y &= \Delta H_n \quad , \\ \Delta H_z &= \Delta H_p \sin\theta \quad . \end{aligned} \tag{4.39}$$

If the incident wave is linearly polarized at 45° to the plane of incidence ($\Delta H_p = \Delta H_n$), the case of parallel incidence ($\theta = 0$; Eq. 4.33) corresponds to $\Delta H_x = \Delta H_y$. This linearly polarized incident wave may be split into two circularly polarized waves of 1/2 amplitude, the one rotating in the direction of the precession motion ($+\omega$), the other counterclockwise ($-\omega$). The two indices of refraction, n_+^2 and n_-^2, refer to these two waves. The clockwise circularly-polarized wave exercises the torque discussed in 4b, as can be verified from Eq. (4.18) by rewriting

$$\Delta\vec{M}_+ = \frac{\omega_o^2 \frac{M_z}{H_z} + j\omega\omega_o \frac{M_z}{H_z}}{\omega_o^2 - \omega^2} \Delta\vec{H} \quad . \tag{4.40}$$

The relative magnetic permeability, in accord with Eq. (4.38), is

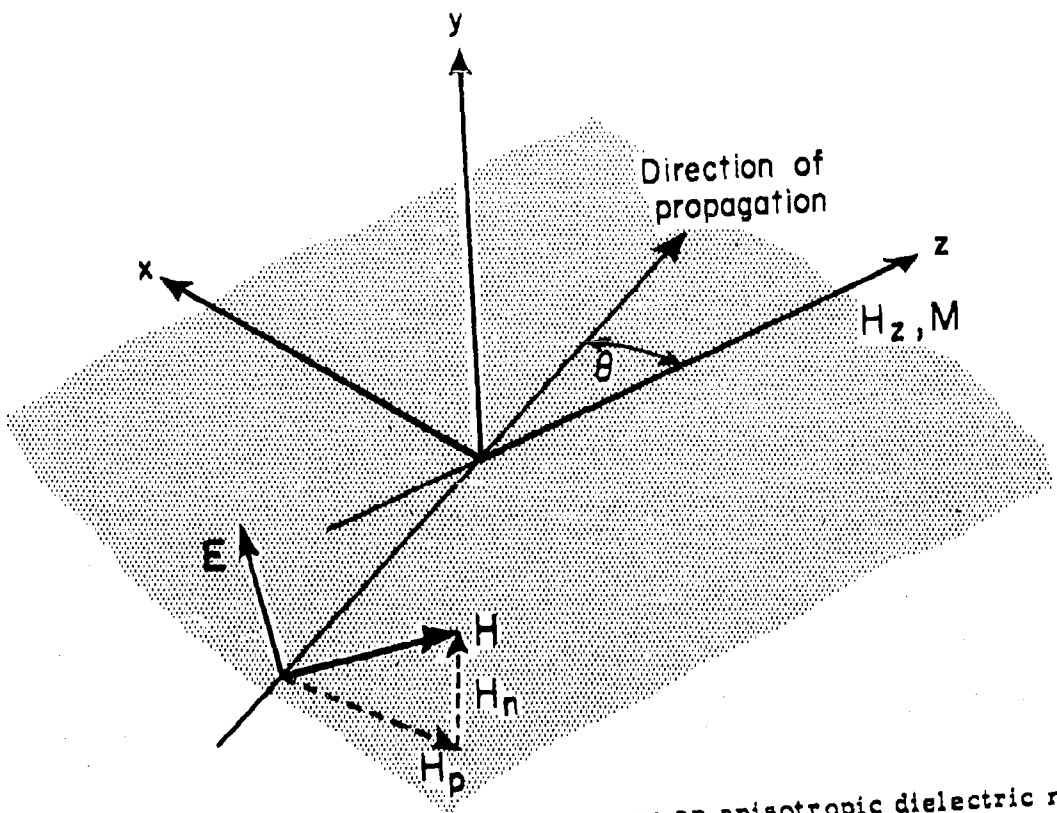

Fig. 4.6. Incidence of an electromagnetic wave on an anisotropic dielectric medium

$$\kappa'_{m_{+\|}} = 1 + \frac{|\Delta M|}{|\Delta H|} = \frac{\omega_o^2 - \omega^2 + \omega_o^2 \frac{M_z}{H_z}\left\{1 + \frac{\omega}{\omega_o}\right\}}{\omega_o^2 - \omega^2} = \frac{n^2_{+\|}}{\kappa'} \quad . \tag{4.41}$$

The case $n^2_{+\|}$ represents the microwave Faraday effect used in gyrators.

Increase of the angle θ leads to a weakening of the ΔH_x component, until at $\theta = \pi/2$ it disappears. As a replacement, the ΔH_z component comes into play, but as the material is magnetized to saturation in that direction, this component does not contribute to the magnetization of the material in this first-order approximation. In consequence, the magnetization produced by the ΔH_x and ΔH_y components has a component in the direction of propagation (ΔM_ℓ). Since the divergence of $\underset{\rightarrow}{B}$ must be zero, this longitudinal magnetization component produces a longitudinal field component

$$\Delta \underset{\rightarrow}{H}_\ell = - \Delta \underset{\rightarrow}{M}_\ell \quad , \tag{4.42}$$

that is, the wave is no longer strictly a transverse wave. This expresses itself

in an increase of the Larmor frequency. At $\theta = \pi/2$ we have to substitute for ω_o^2 the term $\omega_o\omega_1$, where

$$\omega_o = -\mu_o\gamma H_z$$
$$\omega_1 = -\gamma B_z \quad . \tag{4.43}$$

That for parallel incidence a term proportional to ω appears, while for perpendicular incidence it is absent (cf. Eqs. 4.38), results from the fact that in the former case both field components, ΔH_x and ΔH_y, magnetize normal to the propagation direction and in the latter case only the ΔH_y component. Thus for parallel incidence the magnetization contains a contribution caused by the field component normal to its direction, and this contribution varies according to Eq. (4.18) proportionally to ω.

If we introduce attenuation through the Landau-Lifshitz torque, the real permeabilities of Eq. (4.30) have to be replaced by the complex permeabilities (cf. Eq. 4.21)

$$\frac{\mu_{11}}{\mu_o} = \frac{\mu_{22}}{\mu_o} = (1 + a') = c_1'$$
$$\frac{\mu_{12}}{\mu_o} = -\frac{\mu_{21}}{\mu_o} = -jb' \equiv -jc_2' \quad , \tag{4.44}$$

and the index of refraction of Eq. (4.32) has to be discussed by substituting c_1' and c_2' for c_1 and c_2. The resonance frequency of the Faraday effect for parallel incidence now shifts to $\sqrt{\omega_o^2 + a^2}$ and the absorption shows a line width $2a$ (Fig. 4.7).

5. Domain Walls

As the Curie point of a ferromagnetic is approached from higher temperature, the elementary spins spontaneously align in long dipole chains and saturation magnetization $\underline{M}$ develops in a preferred crystallographic direction. Several equivalent lattice directions are available and are normally chosen by the

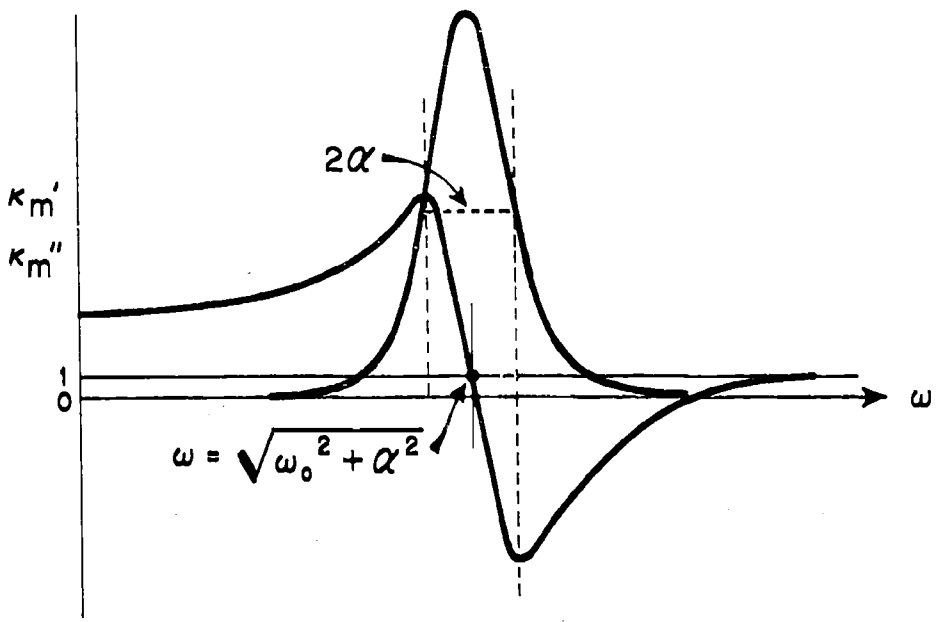

Fig. 4.7. Dispersion of permeability for a clockwise, circularly-polarized wave propagated along the magnetic-field axis.

magnetic axes, in order to produce a domain pattern approaching a constellation of minimum free energy. The domain walls separating adjacent spin arrays of different orientation are transition regions of finite thickness through which the spins change their direction gradually (Fig. 5.1)

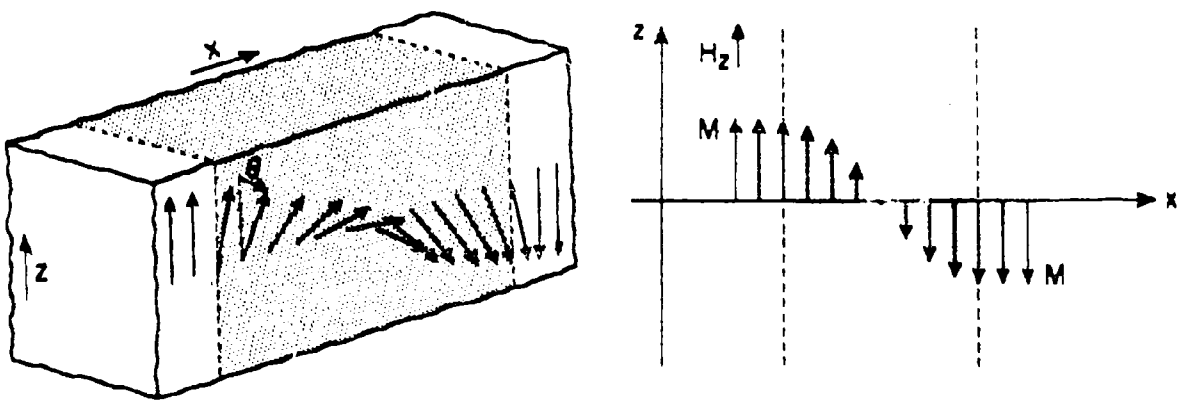

Fig. 5.1. 180°-domain-wall structure.

a) Wall statics[28)]

For a simple calculation one assumes a wall of infinite extent in the y and z directions, of a thickness d in the x direction, and the spins at both sides beyond x = 0 and x = d lined up in the +z and -z direction, respectively. The infinite side-wise extension of such a 180° wall keeps the spins orientated in the y-z planes, as long as no external field acts, because thus they may form endless dipole chains and avoid creating a demagnetizing field. If θ designates the angle between a spin moment $\underrightarrow{m}$ and the +z direction, the spin components are

$$m_x = 0,\ m_y = m \sin\theta,\ m_z = m \cos\theta \ . \qquad (5.1)$$

The alignment angle θ of the spins in the wall changes as f(x).

As the ferrites considered here are cubic, the anisotropy energy of the spins must have cubic symmetry. If a_1, a_2, a_3 designate the direction cosines of the magnetization in reference to the three axes, the magnetic anisotropy energy in a layer of unit cross section and of the thickness dx is in first approximation

$$\Delta W_a = K_1(a_1^2a_2^2 + a_2^2a_3^2 + a_3^2a_1^2)dx = K_1 \mathfrak{E}(\theta)dx \ , \qquad (5.2)$$

with K_1 the first-order anisotropy constant. The anisotropy energy increases with the thickness of the wall, because more spins are thrown out of optimum alignment.

The exchange energy per unit area of the wall between neighboring spins deviating by small angles θ is for the same layer element

$$\Delta W_e = A\left[(\nabla a_1)^2 + (\nabla a_2)^2 + (\nabla a_3)^2\right]dx = A\left(\frac{d\theta}{dx}\right)^2 dx \ ; \qquad (5.3)$$

A represents the exchange factor[28)] for spins placed uniformly in a cubic array with lattice distance a. If it is assumed that the spin orientation changes uniformly from θ = 0 to θ = π across the wall thickness d, $\frac{d\theta}{dx} = \pi a/d$, and we obtain

28) C. Kittel, Revs. Mod. Phys. 21, 541 (1949).

$$\int_0^d \Delta W_e = A \frac{\pi^2 a^2}{d^2} \cdot d \sim \frac{1}{d} \quad . \tag{5.4}$$

Thus the larger the wall thickness d, the smaller the exchange energy.

Consequently, the wall adjusts itself to a certain thickness and bunching of spins by balancing the two energy terms

$$K_1 \int_0^d \mathcal{E}(\theta) \cdot dx = A \int_0^d \left(\frac{d\theta}{dx}\right)^2 dx \; ; \; * \tag{5.5}$$

that is,

$$\frac{dx}{d\theta} = \sqrt{\frac{A}{K_1}} \Big/ \sqrt{\mathcal{E}(\theta)} \quad . \tag{5.6}$$

Hence the wall energy becomes

$$W_\ell = 2K_1 \int_0^\pi \mathcal{E}(\theta) \frac{dx}{d\theta} \, d\theta = 2K_1 \int_0^\pi \sqrt{\mathcal{E}(\theta) d\theta} \quad , \tag{5.7}$$

with

$$\delta \equiv \sqrt{\frac{A}{K_1}} \tag{5.8}$$

designating the wall-thickness parameter.[24]

In any but an ideal case, these energy terms will be modified by magnetostriction and residual strains.

b) Wall dynamics [26, 29]

The application of an external field H_z produces a torque on the magnetic spins in the wall proportionally to sin θ. Since the spins are gyroscopes, a precession around the z axis tends to develop, carrying the spins out of the y-z planes. Because the spins are coupled and staggered, an actual precession cannot take place, but a wall deformation results producing a magnetization in the x

* Strictly speaking, the wall lacks precisely defined limits, and the integration should be taken between - ∞ and + ∞ .

29) J. K. Galt, J. Andrus and H. G. Hopper, Revs. Mod. Phys. 25, 93 (1953).

direction. This component M_x creates a closing field

$$H_x = - M_x \tag{5.9}$$

because div $B_x = 0$ (div B_y and div B_z are, a priori, zero for a wall of infinite sidewise extension).

The torque exerted by H_z, and hence the wall distortion and the M_x components are a maximum in the middle of the wall, where the closing field H_x may be appreciably larger than the applied field H_z.

A second precession motion about H_x ensues, and this, coupled with the damping torques directed towards H_x and H_z according to the Landau-Lifshitz expression erects the moments into the z direction and causes the wall to move in the x direction.

The structure of the wall is assumed to remain unchanged during translation, while the individual spins are left behind just as particles in any wave motion. For the individual dipoles the instantaneous angular velocity for precession around the x axis is given by (cf. Fig. 5.1 and Eq. 4.8)

$$\omega_o \equiv \frac{d\theta}{dt} = - \gamma \mu_o H_x \quad , \tag{5.10}$$

and determines the translation velocity v as

$$- \frac{d\theta}{dt} = \frac{d\theta}{dx} \cdot v \quad ; \tag{5.11}$$

hence (cf. Eq. 5.6)

$$H_x = \frac{v}{\mu_o \gamma} \frac{d\theta}{dx} = \frac{v}{\mu_o \gamma} \cdot \frac{\sqrt{\mathcal{E}(\theta)}}{\delta} \quad . \tag{5.12}$$

In moving a unit distance, the potential energy of the system is reduced by the reversal of moment $2\underset{\rightarrow}{M}$ per unit area of wall. The associated energy $2\mu_o M H_z$ must be transferred to the lattice by the damping mechanism operating on the precessing dipole moments in the wall. This mechanism gives a dissipation rate $\mu_o H \cdot \frac{dM}{dt} \simeq \mu_o \lambda H_x^2$, according to Eq. (4.10), since for low damping $H_x >> H_z$ in the center of the wall. The consequence of the introduction of the Landau-Lifshitz

term is to give a rate of damping which increases with wall distortion, and hence with wall velocity.

The equilibrium velocity is given by the balance of the rates of energy creation and dissipation

$$2MH_z\mu_o v = \int_{-\infty}^{\infty} \mu_o \lambda H_x^2 \, dx = \frac{\mu_o \lambda v^2}{\mu_o^2 \gamma^2 \delta} \int_o^{\pi} \sqrt{\mathcal{E}(\theta)} \, d\theta \quad , \tag{5.13}$$

whence

$$v = \frac{2M\gamma^2 \mu_o^2 \delta}{\lambda \int_o^{\pi} \sqrt{\mathcal{E}(\theta)} \, d\theta} H_z \quad . \tag{5.14}$$

The wall distortion giving rise to H_x involves an increase in the energy stored in the wall structure. This added distortion energy is given, per unit area, by

$$\begin{aligned} \Delta W &= -\frac{\mu_o}{2} \int_{-\infty}^{\infty} M_x H_x \, dx = \frac{\mu_o}{2} \int_{-\infty}^{\infty} H_x^2 dx \\ &= \frac{v^2}{2} \frac{\int_o^{\pi} \sqrt{\mathcal{E}(\theta)}}{\gamma^2 \mu_o \delta} \, d\theta \quad . \end{aligned} \tag{5.15}$$

The coefficient of $v^2/2$ may be interpreted as an effective wall mass

$$m = \frac{1}{\gamma^2 \mu_o \delta} \int_o^{\pi} \sqrt{\mathcal{E}(\theta)} \, d\theta \quad . \tag{5.16}$$

When a wall is stabilized in position by the presence of impurities, cavities, stress patterns, etc., a restoring force of the type $F_x = -kx$ exists for small displacements.[11, 29] Thus the equation of motion of the wall may be written as that of an harmonic oscillator of the mass m subjected to a frictional damping. Since this damping leads to the constant velocity v for the free wall, as given in Eq. (5.14), the damping constant is

$$\beta = \frac{\text{driving force}}{\text{velocity}} = \frac{2M\mu_o H_z}{v} = \lambda m \quad . \tag{5.17}$$

In consequence, the trapped wall obeys the harmonic oscillator equation

$$m\ddot{x} + \beta\dot{x} + kx = 2\mu_o M H_z \quad , \tag{5.18}$$

with

$$\beta = \frac{\lambda}{\gamma^2 \mu_o \delta} \int_o^{\pi} \sqrt{\mathcal{E}(\theta)}\, d\theta = \lambda m \quad .$$

If $H_z = |H_z|\ e^{j\omega t}$, the apparent susceptibility $\Delta M_z/H_z = \frac{2Mx}{H_z}$ corresponding to this motion, becomes

$$\chi_z \equiv \frac{\Delta M_z}{H_z} = \frac{4\mu_o M^2/m\ell}{\omega_o^2 - \omega^2 + j\omega\lambda} \quad , \tag{5.19}$$

where $\omega_o^2 = k/m$ and ℓ in the width of the specimen. The ratio of dynamic to static susceptibility is therefore

$$\frac{\chi_z}{\chi_s} = \frac{\omega_o^2}{\omega_o^2 - \omega^2 + j\omega\lambda} = \frac{k}{k - m\omega^2 + j\omega\beta} \quad . \tag{5.20}$$

This resonance response approximates in the case of dominating damping ($\beta >> m\omega$) a relaxation response

$$\frac{\chi_z}{\chi_s} \simeq \frac{k}{k + j\omega\beta} = \frac{1}{1 + j\omega\tau} \quad . \tag{5.21}$$

with the relaxation time $\tau = \frac{\beta}{k}$.

6. Effective Field and Spin Resonance

In Eq. (4.8) we assumed that the Larmor frequency is determined by the applied field H_z. This is true only in isotropic magnetic media without domain and crystal boundaries.

a) Anisotropy effect

Normally we deal with magnetically anisotropic materials and, as Kittel first showed, an "effective" field results from the restoring torque exercised on

the magnetic moment vector when it is deflected from the direction of easy magnetization. This torque can be calculated from the change of the anisotropy energy (cf. Eq. 5.2) and leads to an effective field expression for a single-domain crystal of spherical shape and cubic crystal symmetry[19]

$$H_{eff} = \frac{2K_1}{\mu_o M_s} \quad \text{for } K_1 \text{ positive (easy direction [100])}$$

and (6.1)

$$H_{eff} = -\frac{3K_1}{2\mu_o M_s} \quad \text{for } K_1 \text{ negative (easy direction [111])} .$$

For $K_1 = -6.2 \times 10^4$ joules/m^3 at room temperature (nickel ferrite), H_{eff} becomes ca. 28,000 amp./m, that is, the Larmor precession resonance should occur approximately at 1000 Mc/sec.

b) Shape factor

For ellipsoids the position of minimum energy for an isotropic ferromagnetic is the direction of the long axis, because the smallest demagnetizing field results (cf. Eq. 1.18). Hence, deviation of the magnetization from this direction gives rise to a torque tending to restore the minimum energy state. Expressed in terms of an effective field, for a single-domain ellipsoid, polarized in the z direction by a field H_z, one obtains[30]

$$H_{eff} = \left[H_z + (w_x - w_z) M_z \right]^{1/2} \left[H_z + (w_y - w_z) M_z \right]^{1/2} . \qquad (6.2)$$

The maximum value is reached for a long needle

$$H_{eff} = H_z + \frac{1}{2} M_s . \qquad (6.3)$$

c) Induced moments on domain boundaries

An even greater effective field may be obtained, as Folder and Smit showed[25], by demagnetizing fields which may arise on domain boundaries. Figure 6.1 shows an x-y cross section through a ferromagnetic body containing

30) C. Kittel, Phys. Rev. 71, 270 (1947).

a 180° domain orientated in the ±z direction with thin walls in the z-y planes. Application of an oscillatory field in the ±x direction, that is, perpendicular to the wall, produces a Larmor precession around the z direction with the sense of rotation opposite in the up-and-down domains.

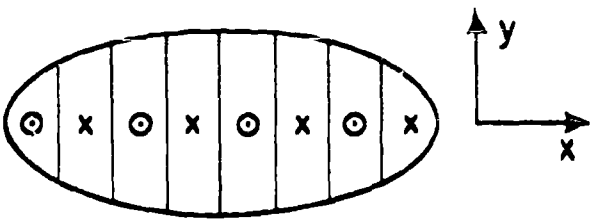

Fig. 6.1. x-y projection of a domain pattern leading to a modified resonance frequency.[25]

In consequence, the poles created in the x direction at the walls appear in phase and therefore add to dipole chains, producing the normal shape magnetization factor w_x of the overall body. The poles created in the y directions are in opposition and their demagnetizing effect cancels ($w_{x_{eff}} = w_x$, $w_{y_{eff}} = 0$, $w_z = 0$).

If the oscillatory field stands in the ±y direction, on the other hand, the free poles induced on the domain walls pile up in alternating sheets and lead to very strong closing fields in the individual domains ($w_{x_{eff}} = 1$; $w_{y_{eff}} = w_y$; $w_z = 0$). Since the shape factor in the y direction can vary between 0 and 1, the highest effective field would arise in a body very short in the y direction ($w_{y_{eff}} = 1$). The total effect in this case is equivalent to $H_{eff} = H_z + M_s$ as far as the Larmor frequency is concerned (cf. Eq. 6.2).

The field action of induced moments invoked by Polder and Smit can be generalized; any domain arrangement pointing at various angles to an applied oscillatory field should produce a distribution of Larmor frequencies.

7. Structure of Ferrites

The ferrites considered here have the spinel structure, a closest-packed cubic array of O^{2-} spheres with compensating cations in interstitial positions. Adjecent to each oxygen ion are 14 interstices: 6, located in the cube-edge directions, surrounded by six oxygen ions (ocatahedral sites), 8 placed in the space-

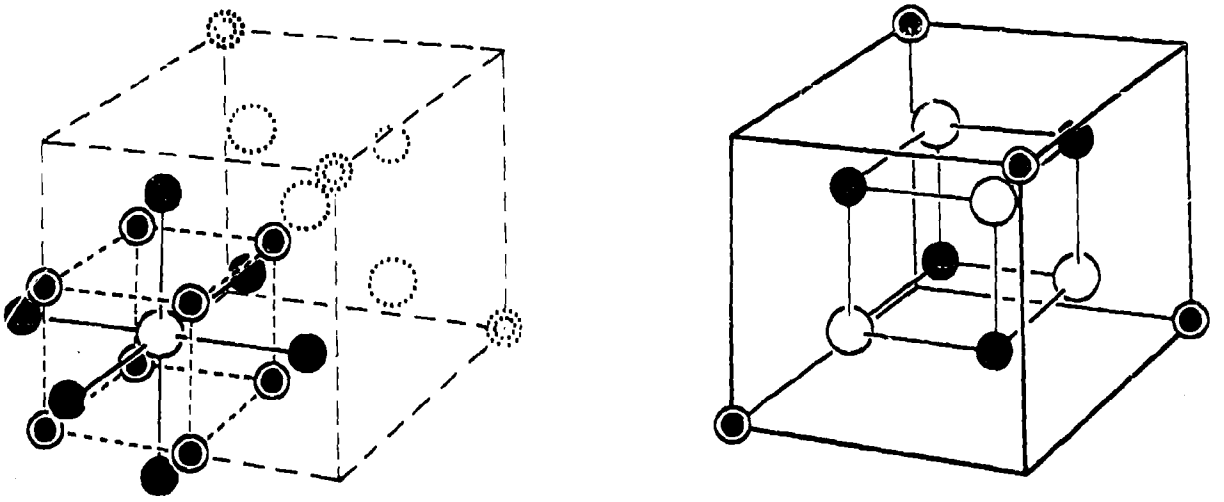

Fig. 7.1. (a) Cation positions surrounding oxygen ions arranged in a close-packed lattice; (b) the cation positions occupied in the ferrite lattice.

diagonal directions, surrounded by four oxygen ions (tetrahedral sites) (Fig. 7.1).

The prototype of these ferromagnetic spinels is magnetite (Fe_3O_4). Here each anion is balanced by 3/4 of a cation; hence, placing around each oxygen "a" cations in the octahedral and "b" cations in the tetrahedral positions, we have to fulfill the condition

$$\frac{a}{6} + \frac{b}{4} = \frac{3}{4} \quad ; \qquad (7.1)$$

that is,

$$a = 3, \quad b = 1$$

or

$$a = 0, \quad b = 3 \quad .$$

The cations repel each other and therefore should be placed at maximum possible separation. If, in addition, we require that a repetition of the oxygen-cation configuration in space should produce a symmetrical and stable lattice structure, the observed unit cell of magnetite is obtained with 32 oxygens and 24 cations in the arrangement a = 3, b = 1. The unit cell comprises 8 Fe_3O_4 groups (Fig. 7.2).[31]

31) J. H. Epstein, MS Thesis, Mass. Inst. Tech., 1954.

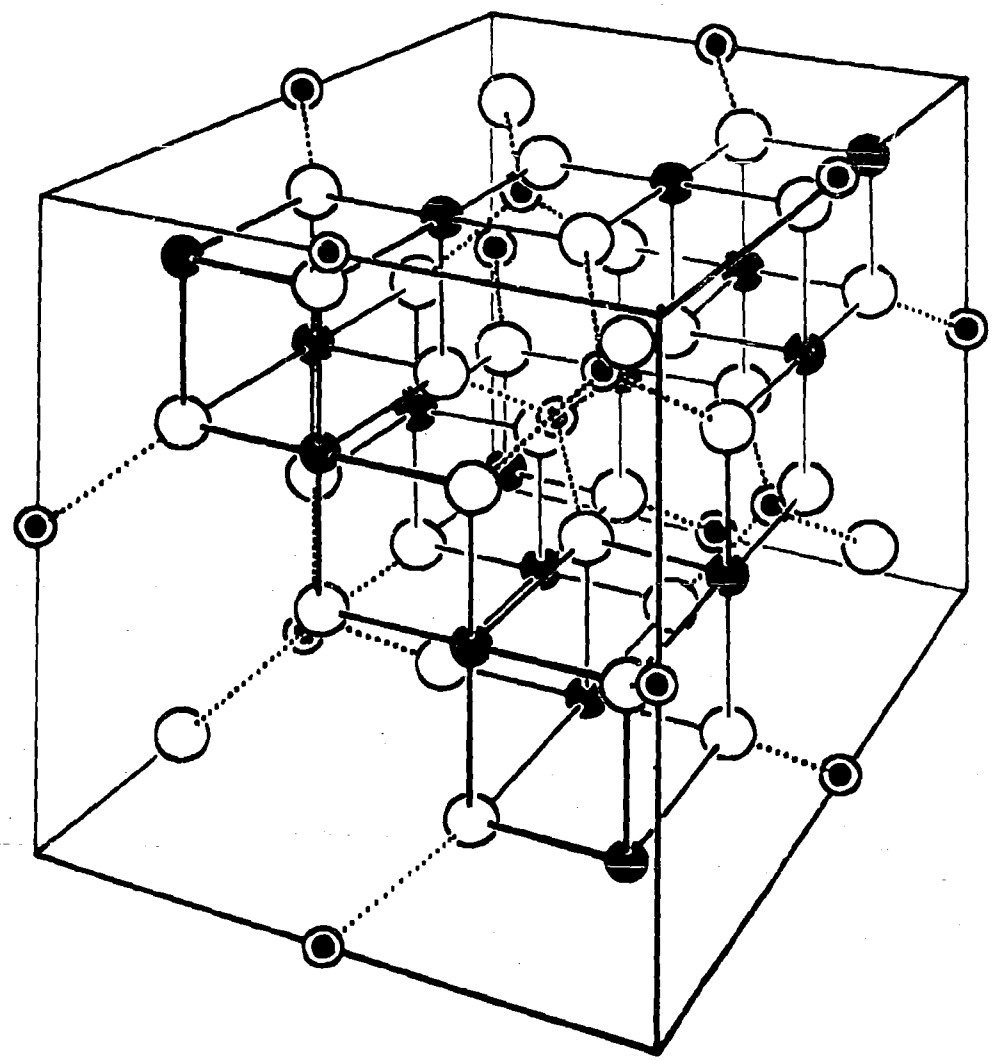

	(a)	(b)
Octahedral cation sites	$\frac{1}{8}, \frac{7}{8}, \frac{1}{8}$ $\frac{3}{8}, \frac{5}{8}, \frac{1}{8}$ $\frac{5}{8}, \frac{3}{8}, \frac{1}{8}$ $\frac{7}{8}, \frac{1}{8}, \frac{1}{8}$	Fe^{+++}
	$\frac{1}{8}, \frac{3}{8}, \frac{5}{8}$ $\frac{3}{8}, \frac{1}{8}, \frac{5}{8}$ $\frac{5}{8}, \frac{7}{8}, \frac{5}{8}$ $\frac{7}{8}, \frac{5}{8}, \frac{5}{8}$	
	$\frac{1}{8}, \frac{5}{8}, \frac{3}{8}$ $\frac{3}{8}, \frac{7}{8}, \frac{3}{8}$ $\frac{5}{8}, \frac{1}{8}, \frac{3}{8}$ $\frac{7}{8}, \frac{3}{8}, \frac{3}{8}$	Fe^{++}
	$\frac{1}{8}, \frac{1}{8}, \frac{7}{8}$ $\frac{3}{8}, \frac{3}{8}, \frac{7}{8}$ $\frac{5}{8}, \frac{5}{8}, \frac{7}{8}$ $\frac{7}{8}, \frac{7}{8}, \frac{7}{8}$	
Tetrahedral cation sites	$0, \frac{1}{2}, 0$ $\frac{1}{4}, \frac{1}{4}, \frac{1}{4}$ $0, 0, \frac{1}{2}$ $\frac{1}{4}, \frac{3}{4}, \frac{3}{4}$	Fe^{+++}
	$\frac{1}{2}, 0, 0$ $\frac{3}{4}, \frac{3}{4}, \frac{1}{4}$ $\frac{1}{2}, \frac{1}{2}, \frac{1}{2}$ $\frac{3}{4}, \frac{1}{4}, \frac{3}{4}$	

Fig. 7.2. Ferrite unit cell: (a) occupied cation sites; (b) cation sites as occupied in ordered magnetite structure.

Thus far we pretended that each iron ion has the valence $Fe^{8/3+}$. Actually, a chemist would write for magnetite $Fe_3O_4 = Fe^{2+}\ O^{2-}\ Fe_2^{3+}\ O_3^{2-}$, that is, postulate 8 ferrous and 16 ferric ions per unit cell. In structures of the spinel type, the distribution of cations over the permissible sites may lie anywhere between the two extreme cases of 8 divalent ions on tetrahedral sites and 16 trivalent ions on octahedral sites (normal spinel) or 8 trivalent ions on tetrahedral sites and the remaining 8 divalent and 8 trivalent ions on octahedral sites (inverse spinel). The physicist finds that, in magnetite, 8 Fe^{3+} ions are located in tetrahedral sites (inverse spinel), but the sixteen remaining cations in the octahedral sites can be separated only artificially at room temperature into 8 Fe^{3+} and 8 Fe^{2+} ions (Fig. 7.2a). The electron exchange between the ferrous and ferric ions at identical lattice sites is so rapid (as the high conductivity of magnetite testifies; $\sigma \cong 10^2$ ohm^{-1} m^{-1}), that an average charge of +2.5 should be assigned to these iron atoms in octahedral positions.

Each iron ion is the carrier of a magnetic moment; hence the two different cation sites form two magnetic sublattices. According to Néel[21], the coupling between the tetrahedral and octahedral sublattices tends to enforce antiferromagnetism; thus the saturation magnetization of magnetite at 0°K should correspond to that of the ferrous ions of the chemical formula. The ordering of the magnetic moments of the cations is:

Filled cation sites per unit cell:	Octahedral (16)	Tetrahedral (8)	Resultant moment
Magnetic moment ordering	8 $Fe^{++}\uparrow$ 8 $Fe^{+++}\uparrow$	8 $Fe^{+++}\downarrow$	8 $Fe^{++}\uparrow$

Near -160°C an electronic order-disorder transition is observed; the electron exchange between Fe^{2+} and Fe^{3+} has slowed down so much that the lattice can respond to the whereabouts of the electrons by distortion and freezes in an ordered $Fe^{2+}Fe^{3+}$ structure. In Néel's sense, we should now distinguish between three magnetic sub-

lattices (cf. Fig. 7.2b). By substituting other cations for Fe^{2+} and/or Fe^{3+}, a tremendous variety of ferrite-type materials can be made in which the resulting magnetic properties depend in a complicated manner on the spin interactions in and between such sublattices.

A satisfactory physical analysis of the ferrites requires accurate knowledge of the cation distribution, of the electron exchange between multivalent ions, and of the origin and coupling of the magnetic moments. In this connection it must be considered that a purely ionic description of the structure may not be justified. Furthermore, the magnetic anisotropy of the materials enters: the magnetic moments tend to align themselves in preferential crystallographic orientations. Table 1 summarizes room temperature observations of magnetic

Table 7.1. Magnetic anisotropy, magnetostriction, and Curie temperatures of various ferrites.

	K_1 (joules/m^3)	$\overline{\lambda}$	T_c Temp.
$LiFe_5O_8$	-	-	590°C
$MnFe_2O_4$	- 2,600	-	295
$Mn_{0.45}Zn_{0.55}Fe_2O_4$	- 380	-	100
Fe_3O_4	-11,000	41×10^{-6}	580
$CoFe_2O_4$	ca. $+10^5$	ca. -200×10^{-6}	515
$NiFe_2O_4$	- 6,200	-	600
$CuFe_2O_4$	-	-	410

anisotropy and the Curie temperatures for some simple ferrites. It also indicates the magnetostriction: the relative change in length of a polycrystalline specimen accompanying magnetization.

Dielectric Analysis

8. Broad-Band Spectroscopy

At first sight, the broad-band spectrum of a ferrite evokes a feeling of complexity and inarticulation (Fig. 8.1). A number of effects appear superposed, and some analytical approach is needed to reduce the integrated characteristic into its components. Remembering that interaction effects in macroscopic systems lead to resonance and relaxation spectra, we may try to dissolve the frequency-response characteristic into a meaningful sequence of resonance and relaxation spectra and to check and correct such a tentative analysis by further experiments. This procedure requires a fingertip feeling for revealing trends in the experimental curves. By focussing on the detailed shape of resonance and relaxation characteristics, one acquires some experience for this purpose.

9. Resonance Spectra

(a) Permittivity

While there is no certainty that the behavior of a physical system showing a resonance-type absorption can be described in terms of a simple circuit of inductive, capacitive, and resistive elements, it is helpful to start with such equivalent circuits. For example, the admittance of a capacitor filled with a lossy dielectric may be represented by (Fig. 9.1)

$$Y_{cap.} = j\omega\kappa^* C_o = \frac{1}{R + j\omega L + \frac{1}{j\omega C}} + j\omega C_o \quad , \tag{9.1}$$

with C_o the air capacitance of the condenser. Thus

$$\chi^* = \kappa^* - 1 = \frac{1}{LC_o} \frac{1}{\omega_o^2 - \omega^2 + j\omega 2a} \quad , \tag{9.2}$$

with the static value $\chi_s = \frac{1}{LC_o\omega_o^2} = \frac{C}{C_o}$; $\omega_o = \frac{1}{\sqrt{LC}}$; $a = \frac{R}{2L}$. The ratio of dynamic to static permittivity for this equivalent circuit is therefore

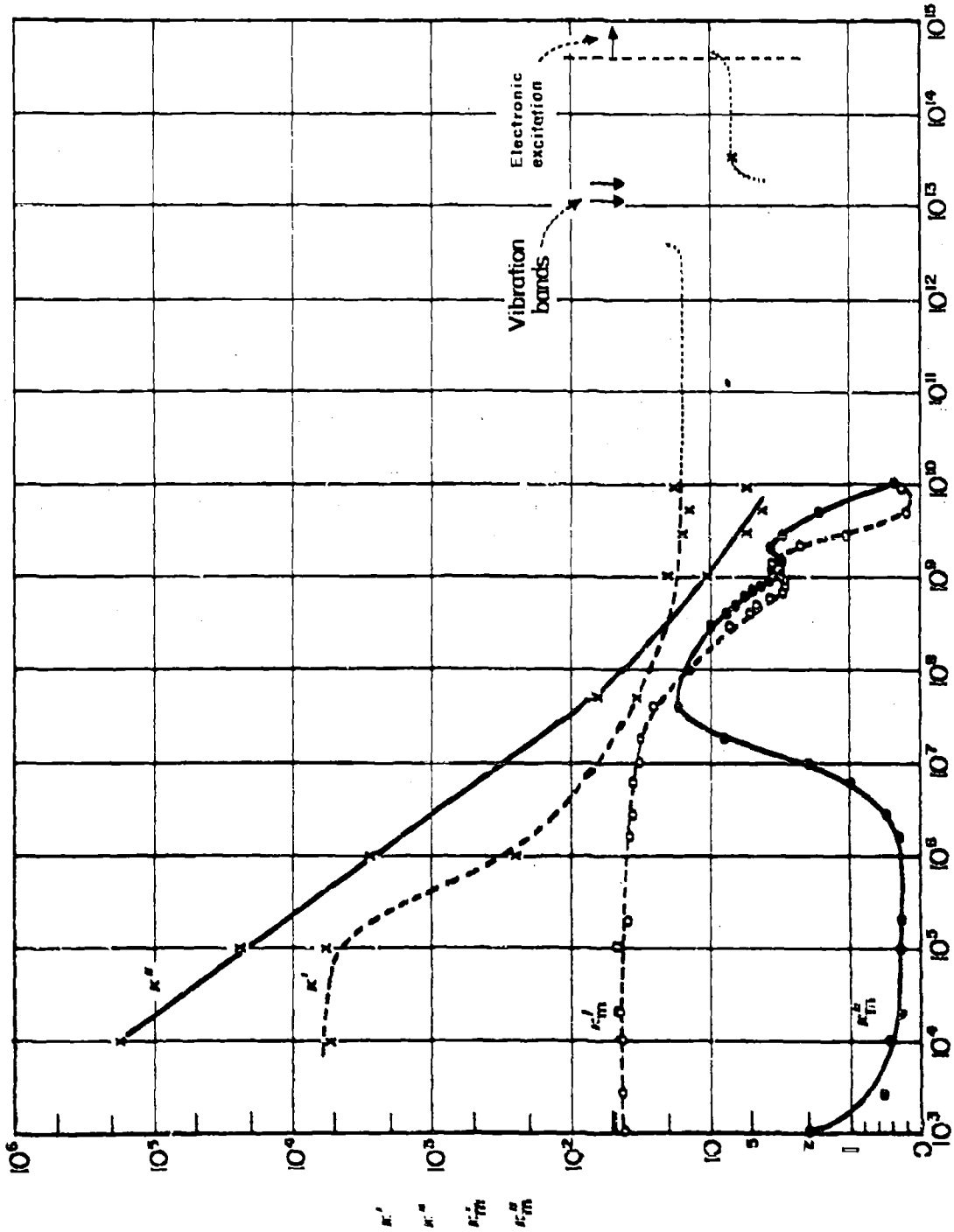

Fig. 8.1. Frequency dependence of the permittivity and permeability of nickel ferrite.

$$\frac{\chi^*}{\chi_s} = \frac{\omega_o^2}{\omega_o^2 - \omega^2 + j\omega 2a}$$

$$\frac{\chi'}{\chi_s} = \frac{\omega_o^2(\omega_o^2 - \omega^2)}{(\omega_o^2 - \omega^2)^2 + (2a\omega)^2} = \frac{1 - w^2}{(1 - w^2)^2 + (\frac{w}{Q})^2} \qquad (9.3)$$

$$\frac{\chi''}{\chi_s} = \frac{2\omega_o^2\, \omega a}{(\omega_o^2 - \omega^2)^2 + (2a\omega)^2} = \frac{\frac{w}{Q}}{(1 - w^2)^2 + (\frac{w}{Q})^2}$$

In the right-hand expressions of Eq. (9.3), the relative frequency w and the "Q" of the resonance circuit have been introduced as normalizing parameters: $w = \omega/\omega_o$, $Q = \omega_o/2a$. The shapes of the normalized dispersion and absorption curves for this resonance polarization are shown in Fig. 9.1 with Q parameters of 10, 2, and 1. The out-of-phase components balance for $\omega = \omega_o$, while the in-phase component (loss factor) reaches a maximum when $\omega^2 \simeq \omega_o^2 - a^2$.

(b) Permeability

Similarly a coil of the air inductance L_o, when filled with a material showing resonant-type magnetic losses, may be represented by the circuit of Fig. 9.2 with

$$Z_{coil} = j\omega\kappa_m^* L_o = \frac{j\omega L(1 + j\omega RC)}{1 - \omega^2 LC + j\omega RC} + j\omega L_o \,. \qquad (9.4)$$

Hence

$$\chi_m^* = \kappa_m^* - 1 = \frac{L}{L_o} \frac{\omega_o^2 + j\omega 2a}{\omega_o^2 - \omega^2 + j\omega 2a} \,, \qquad (9.5)$$

with the static susceptibility value $\chi_{ms} = L/L_o$; $\omega_o = \frac{1}{\sqrt{LC}}$; $a = \frac{R}{2L}$; that is,

$$\frac{\chi_m^*}{\chi_{ms}} = \frac{\omega_o^2 + j\omega 2a}{\omega_1^2 - \omega^2 + j\omega 2a}$$

$$\frac{\chi_m'}{\chi_{ms}} = \frac{(1 - w^2) + (\frac{w}{Q})^2}{(1 - w^2)^2 + (\frac{w}{Q})^2} \qquad (9.6)$$

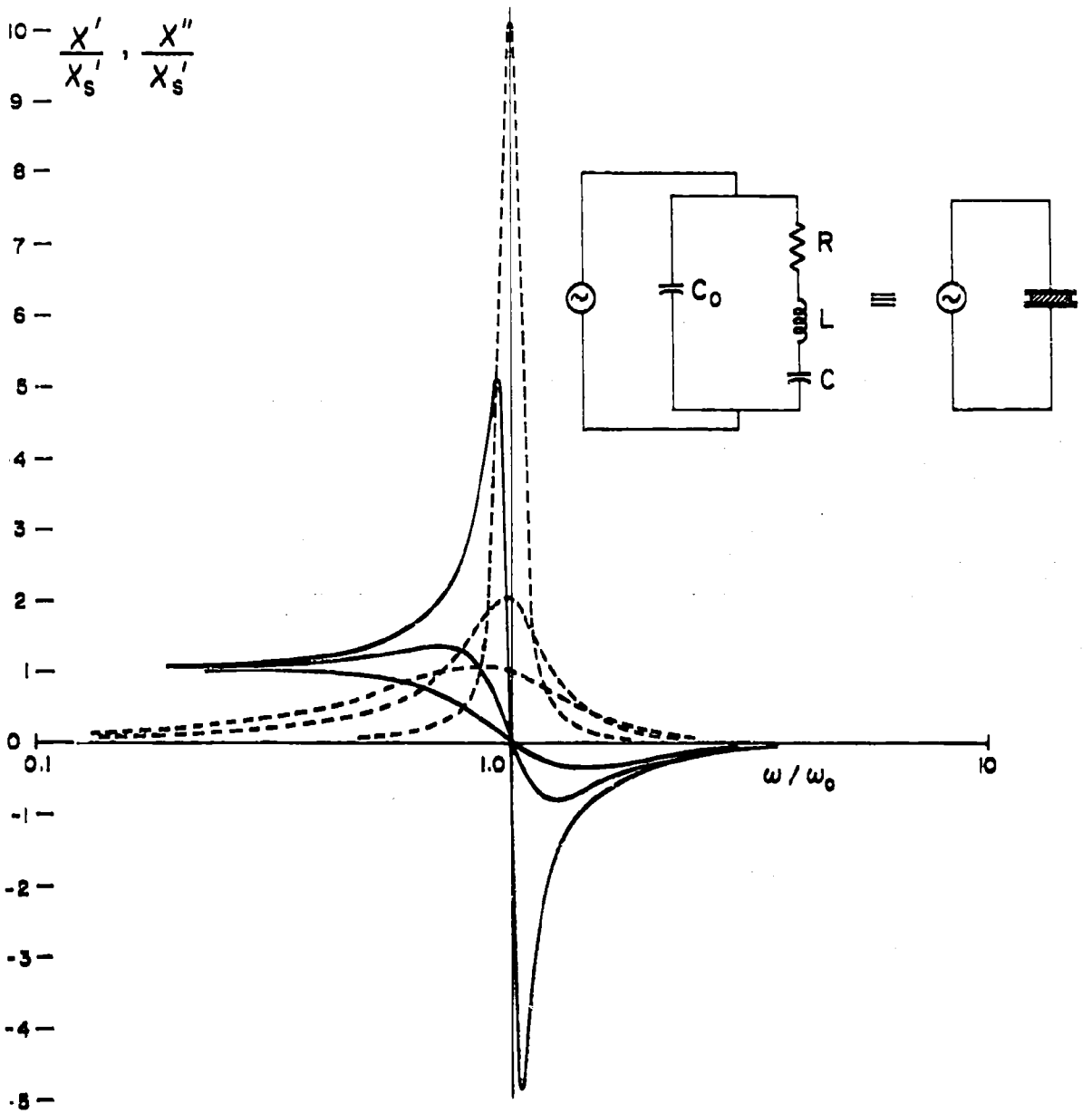

Fig. 9.1. Equivalent circuit and dispersion of dielectric constant and loss for a capacitor filled with a dielectric showing a resonance-type dispersion.

$$\frac{\chi_m''}{\chi_{ms}} = \frac{w^2 \left(\frac{w}{Q}\right)}{(1 - w)^2 + \left(\frac{w}{Q}\right)^2} .$$

The resonance frequency ω_o', at which the out-of-phase currents balance ($\chi_m'/\chi_{ms} = 0$), becomes

$$\omega_o' = \frac{\omega_o^2}{\sqrt{\omega_o^2 - (2a)^2}} , \qquad (9.7)$$

that is, $\omega_o'^2 \simeq \omega_o^2 + 2a^2$ for $2a \ll \omega_o$.

The loss component reaches a maximum when $\omega^2 \simeq \omega_o^2 + a^2$ Figure 9.2 shows the value of χ_m'/χ_{ms} and χ_m''/χ_{ms} as functions of w for Q equals 10, 2, and 1.

The attenuation introduced in the magnetic precession theory by the Landau-Lifshitz term pulls the resonance frequency up, but by a different amount. According to Eq. (4.21)

$$\chi_{ms} = \frac{\Delta M_x}{\Delta H_x} = \frac{\gamma^2 H_z M_z + \frac{\lambda^2 H_z}{M} + j\omega\lambda}{\gamma^2 H_z^2 + \frac{\lambda^2 H_z^2}{M^2} - \omega^2 + 2j\omega \frac{\lambda H_z}{M_z}} = \frac{M_z}{H_z} \cdot \frac{\omega_o^2 + a^2 + j\omega a}{\omega_o^2 + a^2 - \omega^2 + j\omega 2a} , \qquad (9.8)$$

where $\omega_o = \mu_o H_z$, $a = \frac{\lambda H_z}{M_z}$. Hence

$$\frac{\chi_m^*}{\chi_{ms}} = \frac{\omega_o^2 + a^2 + j\omega a}{\omega_o^2 + a^2 - \omega^2 + j\omega 2a}$$

$$\frac{\chi_m'}{\chi_{ms}} = \frac{(\omega_o^2 + a^2)^2 - \omega^2(\omega_o^2 - a^2)}{(\omega_o^2 + a^2 - \omega^2)^2 + 4a^2\omega^2} = \frac{\left[1 + \left(\frac{1}{2Q}\right)^2\right]^2 - w^2\left[1 - \left(\frac{1}{2Q}\right)^2\right]}{1 + \left(\frac{1}{2Q}\right)^2 - w^2\,^2 + \left(\frac{w}{Q}\right)^2} \qquad (9.9)$$

$$\frac{\chi_m''}{\chi_{ms}} = \frac{a\omega(\omega_o^2 + a^2 + \omega^2)}{(\omega_o^2 + a^2 - \omega^2)^2 + 4a^2\omega^2} = \frac{\frac{w}{2Q}\left[1 + \left(\frac{1}{2Q}\right)^2 + w^2\right]}{\left[1 + \left(\frac{1}{2Q}\right)^2 - w^2\right]^2 + \left(\frac{w}{Q}\right)^2}$$

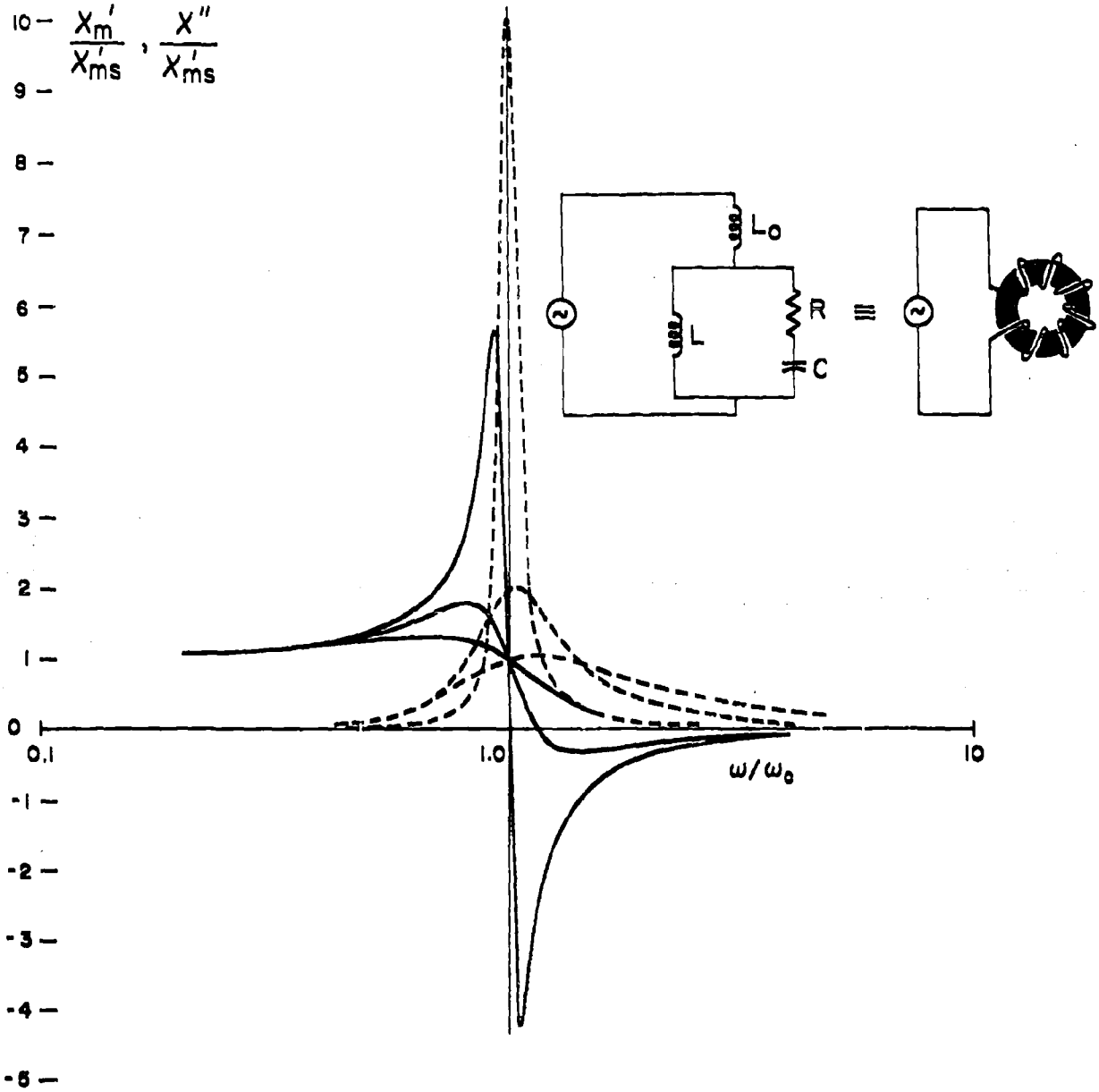

Fig. 9.2. Equivalent circuit and dispersion of magnetic susceptibility and loss for a coil filled with ferromagnetic material showing a resonance-type dispersion.

The out-of-phase components balance when $\omega^2 \simeq \omega_o^2 + 3a^2$, while the loss reaches a maximum when $\omega^2 \simeq \omega_o^2 + a^2$. Figure 9.3 shows the values of χ_m'/χ_{ms} and χ_m''/χ_{ms} as functions of w when Q equals 10, 2, and 1, and gives an equivalent circuit of the correct frequency response when $R_1 = \frac{R}{4} + \frac{1}{CR}$, $C_1 = \frac{L}{4R^2}$. As before, $\omega_o^2 = 1/LC$, $a = R/2L$. This circuit, with its third branch, reflects the introduction of the coupling between the M_x and M_y components in the Landau-Lifshitz approach (cf. Eq. 4.10).

10. Relaxation Spectra

(a) Permittivity

The simplest kind of relaxation spectrum representing the complex permittivity is obtained by equating the admittance of the RC circuit Fig. 10.1 with that of lossy capacitor:

$$Y_{circuit} = j\omega\left(C_1 + \frac{C_2}{j\omega C_2 R_2 + 1}\right)$$

$$Y_{cap.} = j\omega\kappa^* C_o \qquad (10.1)$$

Hence

$$\kappa^* = \frac{C_1}{C_o} + \frac{C_2/C_o}{j\omega R_2 C_2 + 1} \quad ; \qquad (10.2)$$

or, by introducing the static ($\omega = 0$) and optical ($\omega = \infty$) dielectric constants κ_s' and κ_∞' and the relaxation time τ as

$$\kappa_s' = \frac{C_1}{C_o} + \frac{C_2}{C_o}$$

$$\kappa_\infty' = \frac{C_1}{C_o} \qquad (10.3)$$

$$\tau \equiv \frac{1}{a} = R_2 C_2 \ ,$$

the ratio of the dynamic to static permittivity may be written

$$\frac{\kappa^* - \kappa_\infty'}{\kappa_s' - \kappa_\infty'} = \frac{1}{1 + j\omega\tau}$$

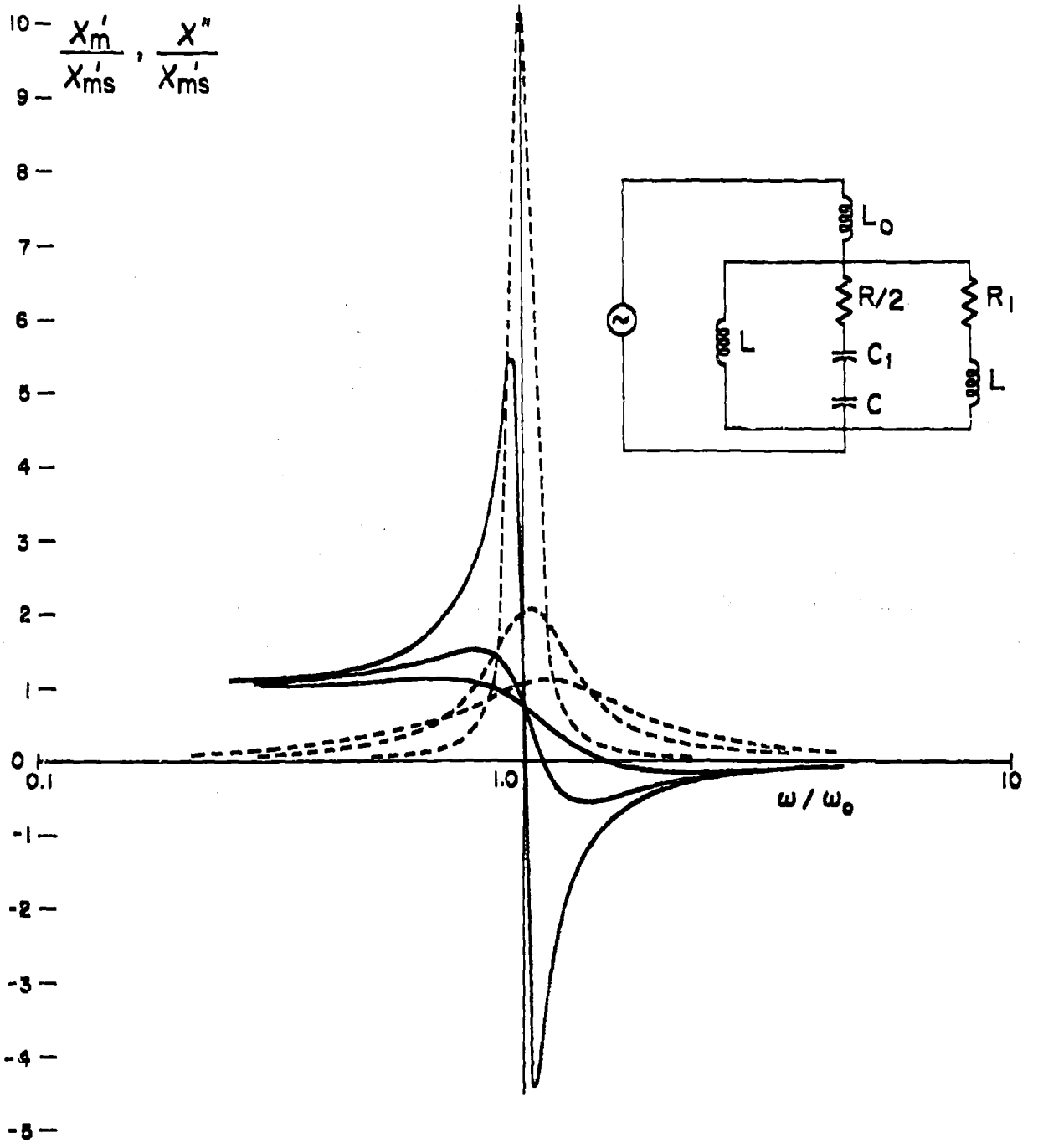

Fig. 9.3. Equivalent circuit and dispersion of magnetic susceptibility and loss for a coil filled with a ferromagnetic material showing a resonance-type dispersion described by Eq. 9.9.

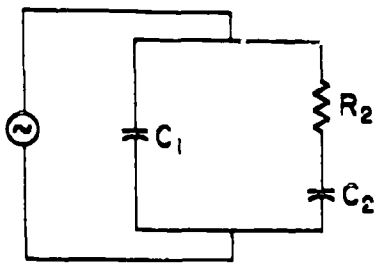

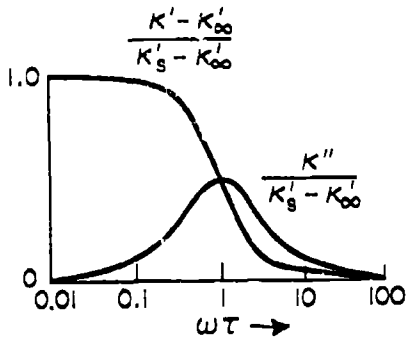

Fig. 10.1.

Equivalent circuit and dielectric constant for a material which shows a relaxation-type dispersion.

$$\frac{\kappa' - \kappa'_\infty}{\kappa'_s - \kappa'_\infty} = \frac{1}{1 + (\omega\tau)^2} \tag{10.4}$$

$$\frac{\kappa''}{\kappa'_s - \kappa'_\infty} = \frac{\omega\tau}{1 + (\omega\tau)^2}$$

To normalize the characteristic (Fig. 10.1), we introduce the new variable

$$z = \ln \omega\tau \tag{10.5}$$

and obtain

$$\frac{\kappa' - \kappa'_\infty}{\kappa'_s - \kappa'_\infty} = \frac{e^{-z}}{e^{z} + e^{-z}}$$

$$\frac{\kappa''}{\kappa'_s - \kappa'_\infty} = \frac{1}{e^{z} + e^{-z}} \tag{10.6}$$

(b) Permeability

If a resonant circuit becomes overdamped its frequency response tends to a relaxation type. This can be seen by allowing the Q of the circuit of Fig. 9.2 to become very low either by making R large, thus increasing the factor a, or by making C large thus lowering the frequency ω_o, while keeping a constant. In either case Eq. 9.6 approximates the form

$$\frac{\chi_m^*}{\chi_{ms}} \simeq \frac{j\omega 2a}{-\omega^2 + j\omega 2a} = \frac{1}{1 + j\omega\tau} \quad , \tag{10.7}$$

where $\tau = 1/2a$. Use of the Landau-Lifshitz term gives the corresponding expres-

sion (cf. Eq. 9.9) in which $\tau = 1/a$:

$$\frac{\chi_m^*}{\chi_{ms}} \simeq \frac{a^2 + j\omega a}{a^2 - \omega^2 + j\omega 2a} = \frac{a^2(a^2 - \omega^2) + 2a^2\omega^2 - j\omega a(-a^2 + \omega^2 + 2a^2)}{(a^2 - \omega^2)^2 + 4a^2\omega^2} = \frac{1}{1 + j\omega\tau} \qquad (10.8)$$

(c) Conductivity

In addition to the relaxation spectra caused by electric and magnetic dipoles, relaxation effects may originate from the migration of charge carriers. The normal concept of conduction is that of a free flow of charges with an ohmic conductivity σ given by the mobility b of the free carriers and their number per unit volume N as

$$\sigma = N e b \quad . \qquad (10.9)$$

The drift velocity v of the carriers increases according to Stokes's law proportionally to the field strength E, and the number of free carriers increases exponentially with temperature in case they can be held in traps by an activation energy U; that is,

$$v = bE \text{ and } N = N_o e^{-U/2kT} \quad . \qquad (10.10)$$

Actually, this type of unimpeded conduction is the exception. It requires that the carriers can be freely discharged at one electrode and freely replaced at the counterelectrode; in addition, the carriers must not be trapped firmly in the volume or on interfaces. In general, one or the other of these stringent prerequisites is not fulfilled, and field distortion by space-charge formation results. The outside observer notices an increase in dielectric constant accompanying a decrease in transconductance due to the build-up of space charge or interfacial polarization.

The classical example of this type of polarization is the Maxwell-Wagner two-layer condenser[32], in which the dielectric consists of two parallel sheets of material (1) and (2), characterized by dielectric constant, conductivity and thick-

32) K. W. Wagner, Arch. Elektrotech. 2, 371 (1914).

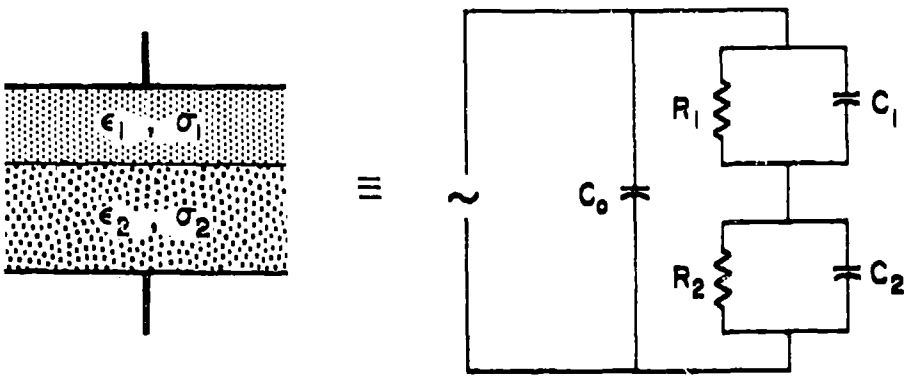

Fig. 10.2.

Two-layer capacitor and equivalent circuit.

ness (Fig. 10.2). By comparing the admittance of the equivalent circuit with that of a lossy capacitor

$$Y_{circuit} = \frac{1}{R_1 + R_2} \frac{(1 + j\omega\tau_1)(1 + j\omega\tau_2)}{1 + j\omega\tau} + j\omega C_o \,,$$

$$Y_{cap.} = j\omega\kappa^* C_o \,, \tag{10.11}$$

where $\tau_1 = C_1R_1$, $\tau_2 = C_2R_2$, and $\tau = \frac{R_1\tau_2 + R_2\tau_1}{R_1 + R_2}$, the complex permittivity results

$$\kappa^* = \frac{(\tau_1 + \tau_2) + j\omega(\tau_1 \cdot \tau_2 - \frac{1}{\omega^2})}{(R_1 + R_2)C_o\left\{1 + j\omega\tau\right\}} \,. \tag{10.12}$$

Introducing the static and optical dielectric constant

$$\kappa'_s = \frac{\tau_1 + \tau_2 - \tau}{(R_1 + R_2)C_o}$$

$$\kappa'_\infty = \frac{\tau_1\tau_2}{(R_1 + R_2)C_o} \,, \tag{10.13}$$

we obtain the normalized form

$$\frac{\kappa' - \kappa'_\infty}{\kappa'_s - \kappa'_\infty} = \frac{1}{1 + \omega^2\tau^2} \equiv \frac{e^{-z}}{e^z + e^{-z}}$$

$$\frac{\kappa''}{\kappa'_s - \kappa'_\infty} = \frac{\omega\tau}{1+\omega^2\tau^2} + \frac{1}{\omega}\,\frac{1}{\tau_1 + \tau_2 - \tau - \dfrac{\tau_1\tau_2}{\tau}} \qquad (10.14)$$

$$\equiv \frac{1}{e^z + e^{-z}} + \frac{1}{\omega}\,\frac{1}{(\kappa'_s - \kappa'_\infty)(R_1 + R_2)C_o} \quad .$$

The dispersion caused by the two-layer condenser is identical with that of the dipole polarization of Eq. (10.6); the absorption contains, in addition, the ohmic conductance effe[illegible]produced by the series resistors R_1 and R_2.

To normalize also the conduction part of the absorption characteristic, we introduce a relation between the time constants τ_1 and τ_2 by prescribing

$$\begin{aligned} \tau_1 &= R_1C_1 \\ \tau_2 &= R_2C_2 \cong aR_1bC_1 = ab\tau_1 \quad , \end{aligned} \qquad (10.15)$$

that is, the dielectric constant and conductivity of medium 2 is chosen as being multiplied by factors a and b in reference to those of medium 1. It follows that

$$\tau_1 + \tau_2 - \tau - \frac{\tau_1\tau_2}{\tau} = \frac{\tau}{a}\left(\frac{1-ab}{1+b}\right)^2$$

or

$$\frac{\kappa''}{\kappa'_s - \kappa'_\infty} = \frac{1}{e^z + e^{-z}} + \frac{1}{e^z}\,a\left(\frac{1+b}{1-ab}\right)^2 \quad . \qquad (10.16)$$

Figure 10.3 shows the two-layer absorption characteristic with a as parameter, and with b chosen arbitrarily as 2000 and κ'_∞ as 10, orders of magnitude frequently observed.

11. Features Distinguishing Resonance from Relaxation

The presence of a resonance dispersion in a composite characteristic of the type Fig. 8.1 may be detected by the presence of a maximum or minimum in the κ' curve, or by a loss curve with a steeper slope than a relaxation loss. Table 11.1 gives the conditions under which maxima and minima of κ' exist for the three types of resonance considered.

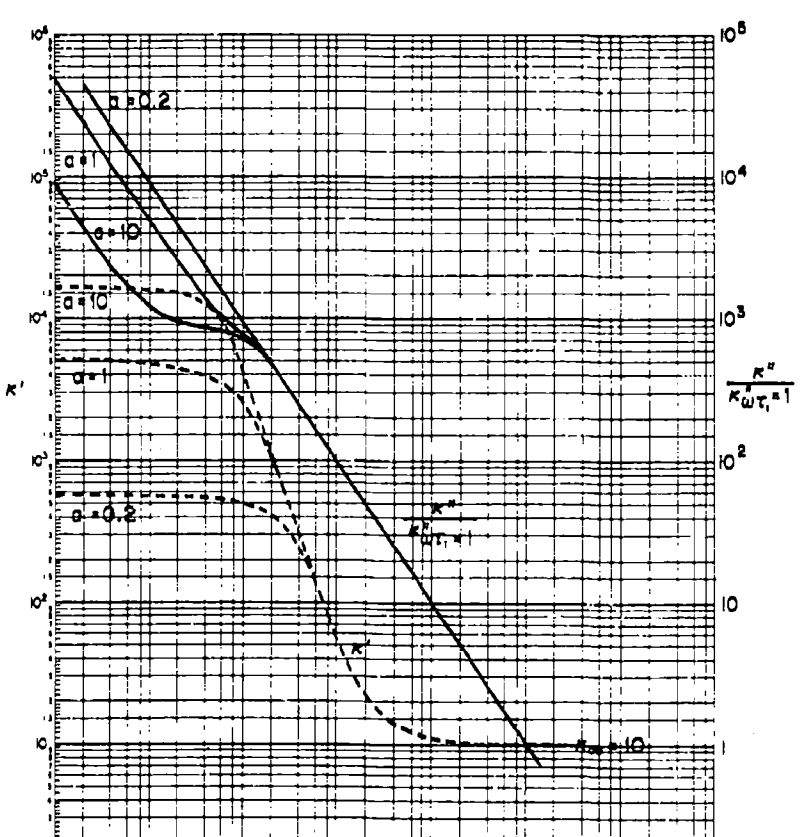

Fig. 10.3. The dispersion of dielectric constant and loss for a Maxwell-Wagner double layer.

Table 11.1. Condition for existence of resonance maxima and minima.

Resonance type	κ' maximum	κ' minimum
Circuit Fig. 9.1	$\omega_o > 2a$	ω_o finite
Circuit Fig. 9.2	$\omega_o > 0$	$\omega_o > 2a$
Landau-Lifshitz damping (Fig. 9.3)	$\omega_o > a$	$\omega_o > a$

The κ'' curve for a simple relaxation when plotted on a log-log scale (Fig. 11.1), shows a maximum positive slope of +1 and a maximum negative slope of -1;

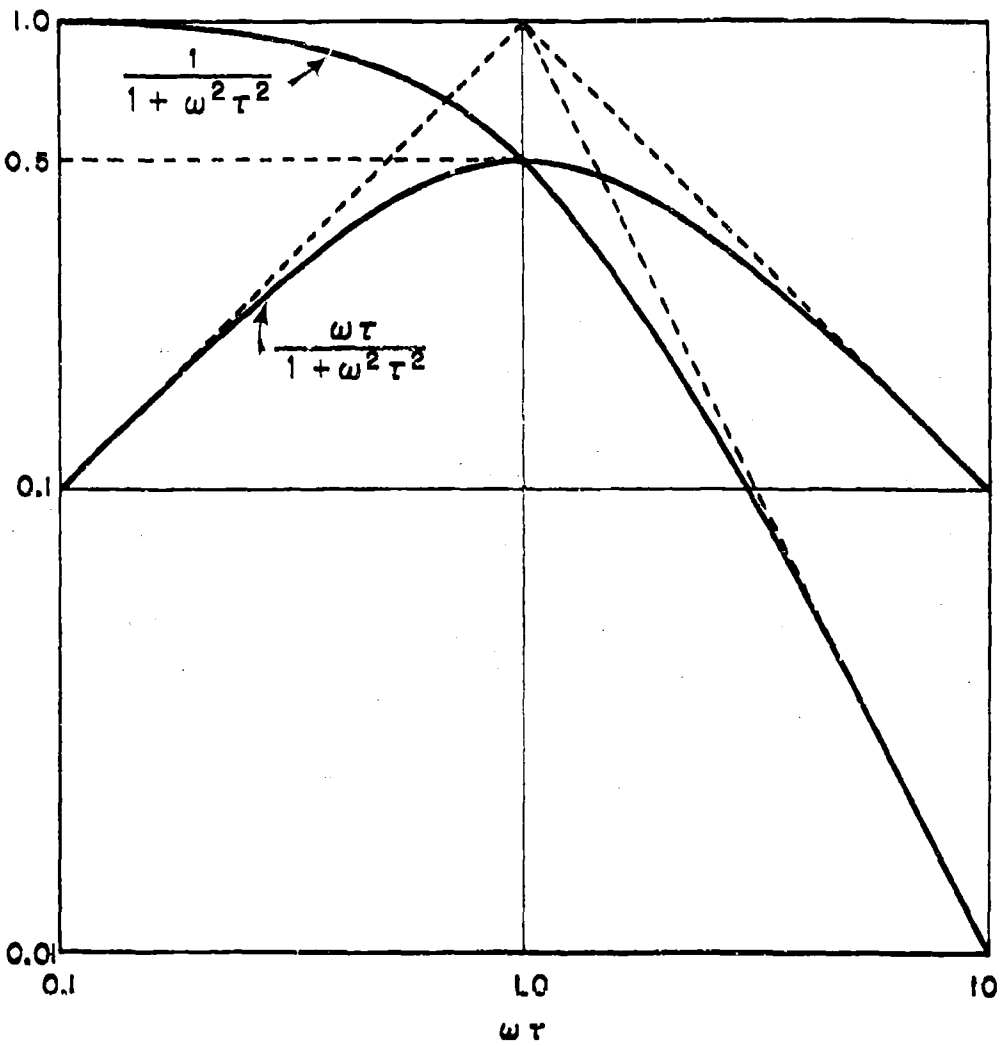

Fig. 11.1. Relaxation-type dispersion of dielectric constant and loss (*cf.* Eq. 10.4).

the loss due to interfacial polarization also gives a maximum negative slope of -1 (Fig. 10.3). Thus the occurrence of a loss peak with slopes greater than 1 on a log-log scale indicates resonance.

12. Polarization in the Optical Range

The ferrites here considered absorb strongly in the optical region, and transmission measurements on single crystals have to await the completion of grinding and etching techniques which will reduce sizeable crystal sections to a

thickness below 1 micron.

Tentative conclusions as to the optical dielectric constant can be drawn from transmission measurements on the more transparent aluminates and from transmission and reflection measurements in the near infrared on some ferrites. Table 12.1 gives the square of the index of refraction (n^2); according to Maxwell's relation it equals the dielectric constant κ' for loss-free media.

Table 12.1. n^2 for some double metal oxides.

(λ = 5393A)	n^2	(λ = 15360A)	n^2
$MgAl_2O_4$	2.97	$MgFe_2O_4$	5.5
$CaAl_2O_4$	2.95	$CaFe_2O_4$	6.6
$ZnAl_2O_4$	3.17		
$FeAl_2O_4$	3.25		

In addition, reflectivity measurements on a single crystal of nickel ferrite gave a value of 7.0 ± 0.5 for κ' on the high frequency side of the infrared bands.

Hence, the electronic polarization, with its resonance absorption in the ultraviolet and further absorptions in the visible and near infrared, appears to make a contribution of ca. 7 to the dielectric constant at low frequencies.

The detailed optical absorption spectrum and its interpretation are complicated because a variety of excitation effects enter. Figure 12.1 shows the transmission characteristic of magnetite, obtained on an evaporated iron layer, oxidized to Fe_3O_4. We expect: absorption caused by the conduction electrons migrating between the iron ions of the octahedral sites; absorption caused by transitions from 3d to 4s states; and, finally, transitions from the O^{2-} ions to the various cations. These effects may express themselves in Fig. 12.1 in overlapping absorption regions. Transmission measurements at low temperature on single crystals should show improved resolution and are in preparation.

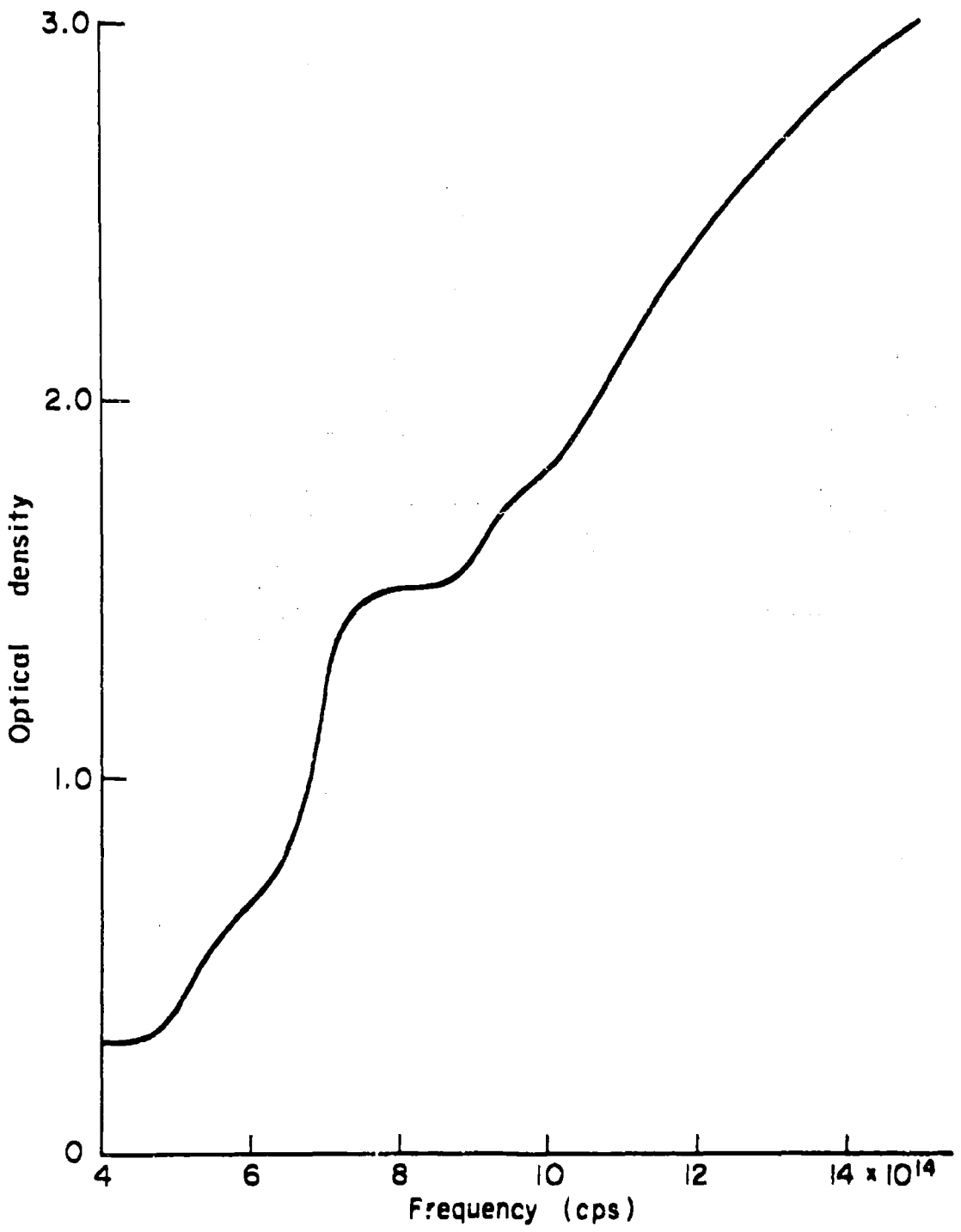

Fig. 12.1. Absorption in the optical range for a film of magnetite.

13. Infrared Vibrations

The unit cell of magnetite contains 8 Fe_3O_4 groups, that is, 56 particles (cf. Fig. 7.2). Each of these possesses three degrees of freedom, hence the unit cell has 168 normal vibrations. This inconveniently large number can be cut down by a factor of four by dividing the unit cell into four primitive rhombohedral subcells (Fig. 13.1). If we write the chemical formula of the ferrites MFe_2O_4, where M stands for a divalent metal ion, the rhombohedral cell ($M_2Fe_4O_8$) contains 14 ions which can be lumped into two MO_4 and one Fe_4 tetrahedral subgroups.

Of the 42 possible modes only those are optically active which create a change in dipole moment ($\frac{\partial \vec{\mu}}{\partial r} \neq 0$). As Waldron in this laboratory has shown in detail[33], only the eight vibratory modes of Fig. 13.1 fulfill this condition; three of these (ν_5, ν_6, ν_7) become inactivated because the overall dipole moment change in the subcell is zero; a fourth one (ν_8) is a zero-frequency translation. Hence, four optically active modes remain and are in phase throughout the lattice, when the subcells are joined together.

The highest frequency mode (ν_1) corresponds to the vibrations of the oxygen ions along the tetrahedral bond directions, the [111] crystal directions; the next lower mode (ν_2) represents a motion of the oxygen ions in a direction almost perpendicular to the first one; the remaining two modes (ν_3, ν_4) correspond to oscillations of the metal ions in the force fields of their octahedral and tetrahedral oxygen environments.

In absorption measurements, one usually obtains the real part α of the propagation constant γ. For a nonmagnetic material, γ may be expressed in terms of the dielectric constant $\kappa^* = \kappa' - j\kappa''$ as:

$$\gamma = \alpha + j\beta = \gamma_o\left(\frac{|\kappa^*| - \kappa'}{2}\right)^{1/2} + j\gamma_o\left(\frac{|\kappa^*| + \kappa'}{2}\right)^{1/2} . \qquad (13.1)$$

However, when the material is powdered and imbedded in a loss-free dielectric,

33) R. D. Waldron, Technical Report 94, March, 1955.

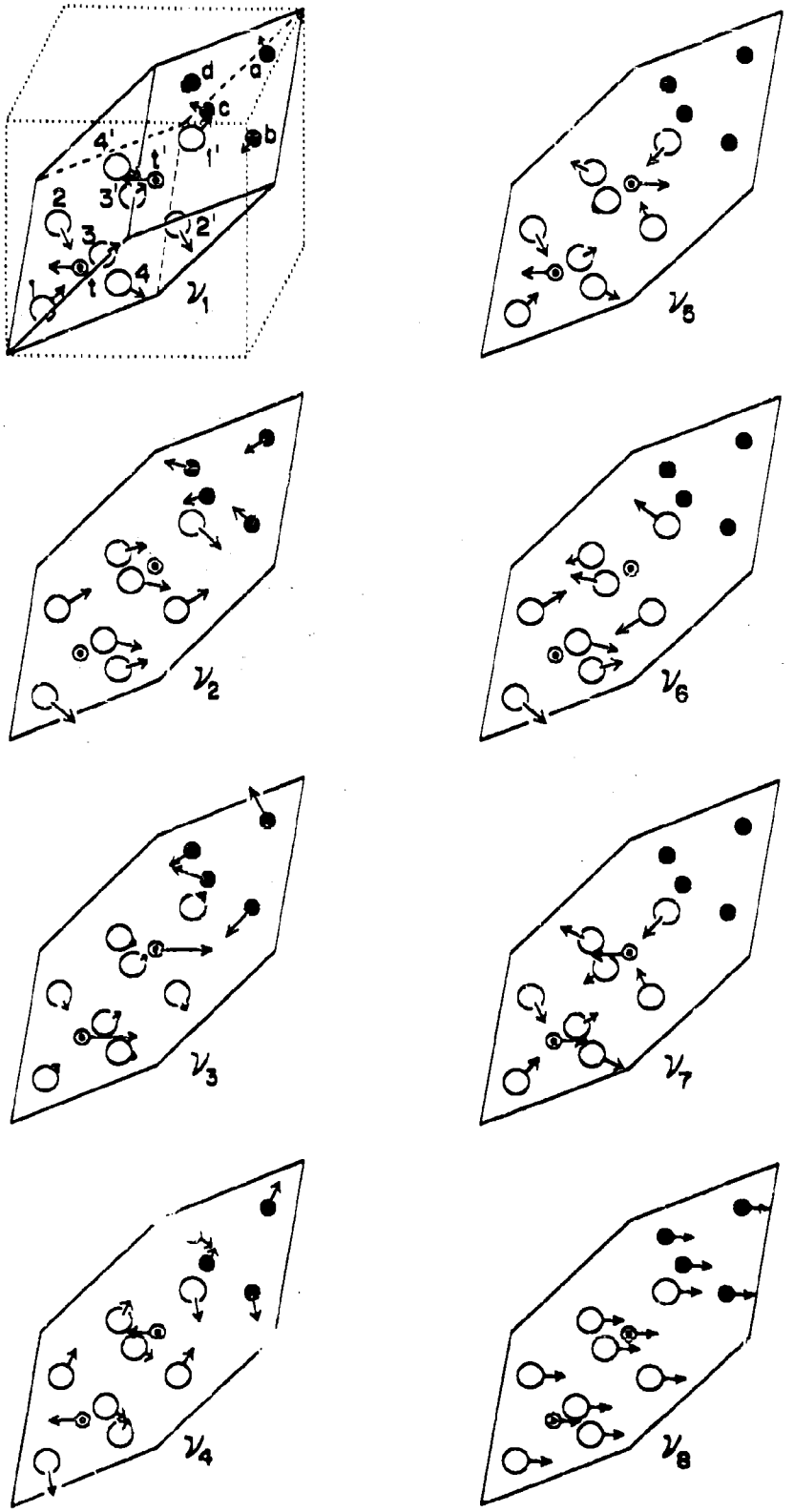

Fig. 13.1. Vibratory modes of the ferrite primitive cell giving rise to a dipole in the ion subgroups (cf. Fig. 7.2).

one measures the absorption coefficient of the resultant mixture, and this is not simply the coefficient for the material, reduced in magnitude by the dilution. There is the possibility of 2-layer condenser-type absorption (see Sec. 10), although in the present case the great dilution of the more conducting component (1 part in 800) makes this effect of no importance. Furthermore, pronounced scattering will occur when the particle sizes become of the order of the wavelength. In the present work this situation is being approached only in the visible range. For particles very much smaller than the wavelength, the absorption may be expected to follow the variations in the dielectric loss factor κ'' for the ferrite and to show peaks at the vibrational resonance frequencies.

The observed absorption spectra for six simple ferrites are shown in Fig. 13.2. Two main bands occur with peaks in the vicinity of 550 and 400 cm^{-1}, which we attribute to the two highest modes; the two lower bands lie apparently beyond the range of our instrument. $ZnFe_2O_4$ is a "normal" spinel, that is, the Zn^{2+} ion occupies the tetrahedral lattice sites, while Fe_3O_4, $NiFe_2O_4$ and $CoFe_2O_4$ are "inversed" spinels. $MgFe_2O_4$ and $MnFe_2O_4$ are intermediate cases, depending on firing conditions and cooling of the samples.[34] Obviously, the relative intensity and shape of the bands is sensitive to the type of cation in the tetrahedral sites, and infrared spectroscopy may provide a powerful, nondestructive tool for the analysis of ferrite structures.

In order to obtain values for the individual constants κ' and κ'' of nickel ferrite, a series of reflection measurements was made on a single-crystal specimen. Unfortunately, the experimental error involved in measurements with polarized radiation at infrared frequencies is sufficient to cause the derived permittivity values to vary between wide limits. On the high frequency side of the infrared absorption bands a reliable value of κ' was obtained, viz., 7.0 ± 0.5. This comes

34) G. Economos, Technical Report 78.

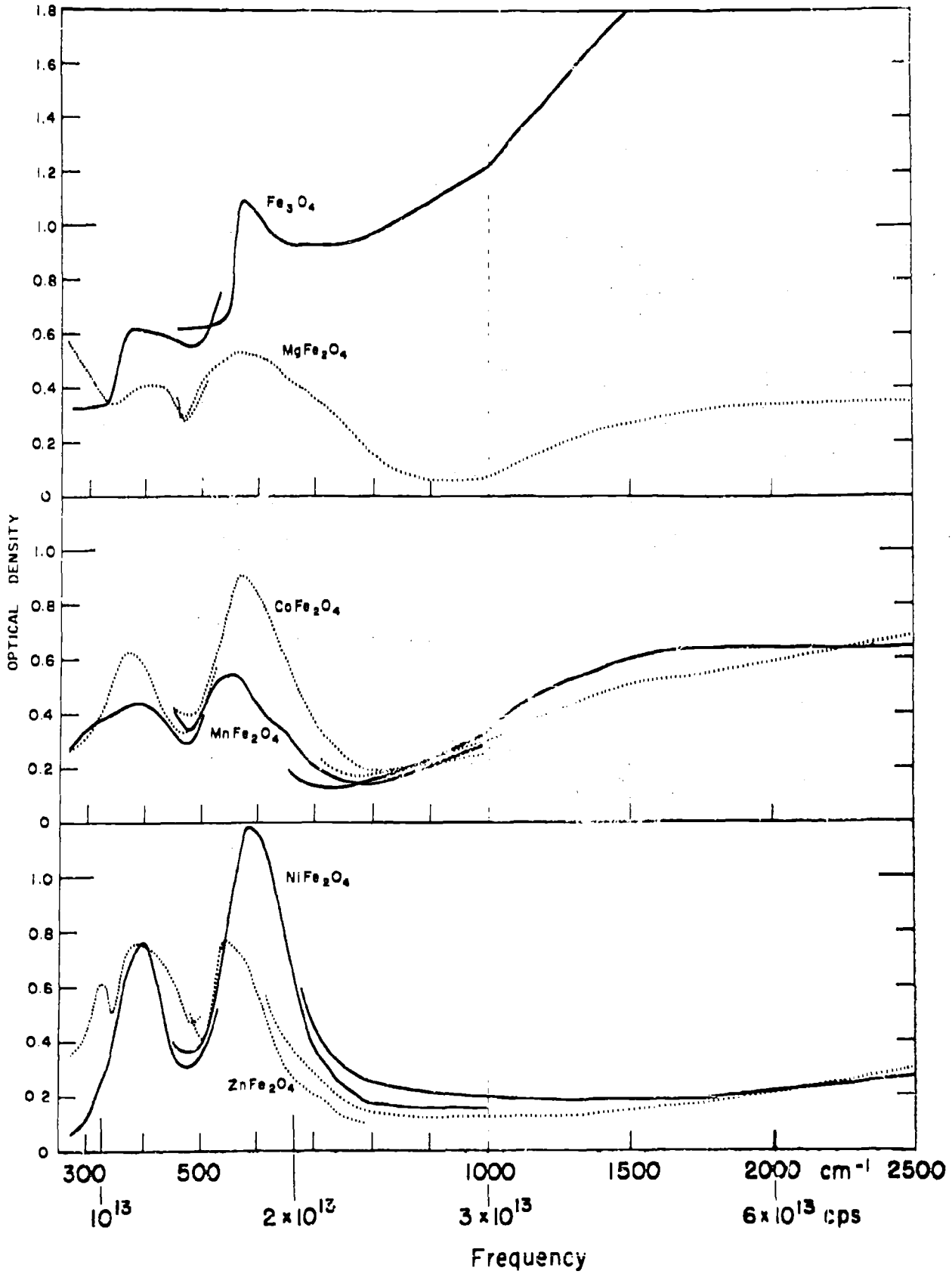

Fig. 13.2. Infrared absorption measurements for several ferrites.

from the electronic polarization (cf. Sec. 12), and since the value of κ' at microwave frequencies is of the order of 17, the atomic polarization must contribute about 10 to the low-frequency dielectric constant.

14. Polarization in the Electrical Range

In the microwave range, the ferrites show a dielectric constant of about 17; at low frequencies, κ' may rise to values of 10^4 and even higher. This general behavior is typical of many conducting materials in which the current transfer is impeded by grain boundaries and barrier layers. For a first analysis the simple equivalent circuit of the Maxwell-Wagner two-layer condenser (cf. Fig. 10.2) can serve. We assume that the ferrite proper represents medium 2 (R_2, C_2) distributed as spherical particles in an interface medium 1 (R_1, C_1). The prerequisite "spherical" is needed in order to preserve the simple relaxation spectrum with one time constant only.[35]

The amount of medium 1 is obviously small in comparison to that of medium 2 and its resistivity high, hence $C_1 \gg C_2$, $R_1 \gg R_2$, $\tau_1 \gg \tau_2$. In consequence, at sufficiently high frequencies the interface medium is shorted out and one observes the dielectric constant and conductivity of the ferrite proper. This conductivity, as our measurements on the nickel zinc ferrite series demonstrate (Figs. 14.1 to 14.9), is however not frequency independent but rises appreciably from 10^9 towards 10^{11} cps. A similar behavior has been observed, for example, for glasses.[36] Simultaneously, we find that the microwave conductivity of a typical nickel-zinc ferrite increases slowly with decreasing temperature (Fig. 14.10), while the d-c conductivity shows the exponential decrease with $1/T$ as a

35) R. W. Sillars, J. Inst. Elec. Engrs. 80, 378 (1937).

36) Lab. Ins. Res., Mass. Inst. Tech., Tables of Dielectric Materials, Vol. IV, Tech. Rep. 57, January, 1953; L. Hartshorn, J. W. Perry and R. Rushton, Proc. Inst. Elec. Engrs. 100, Part IIA, 23 (1953).

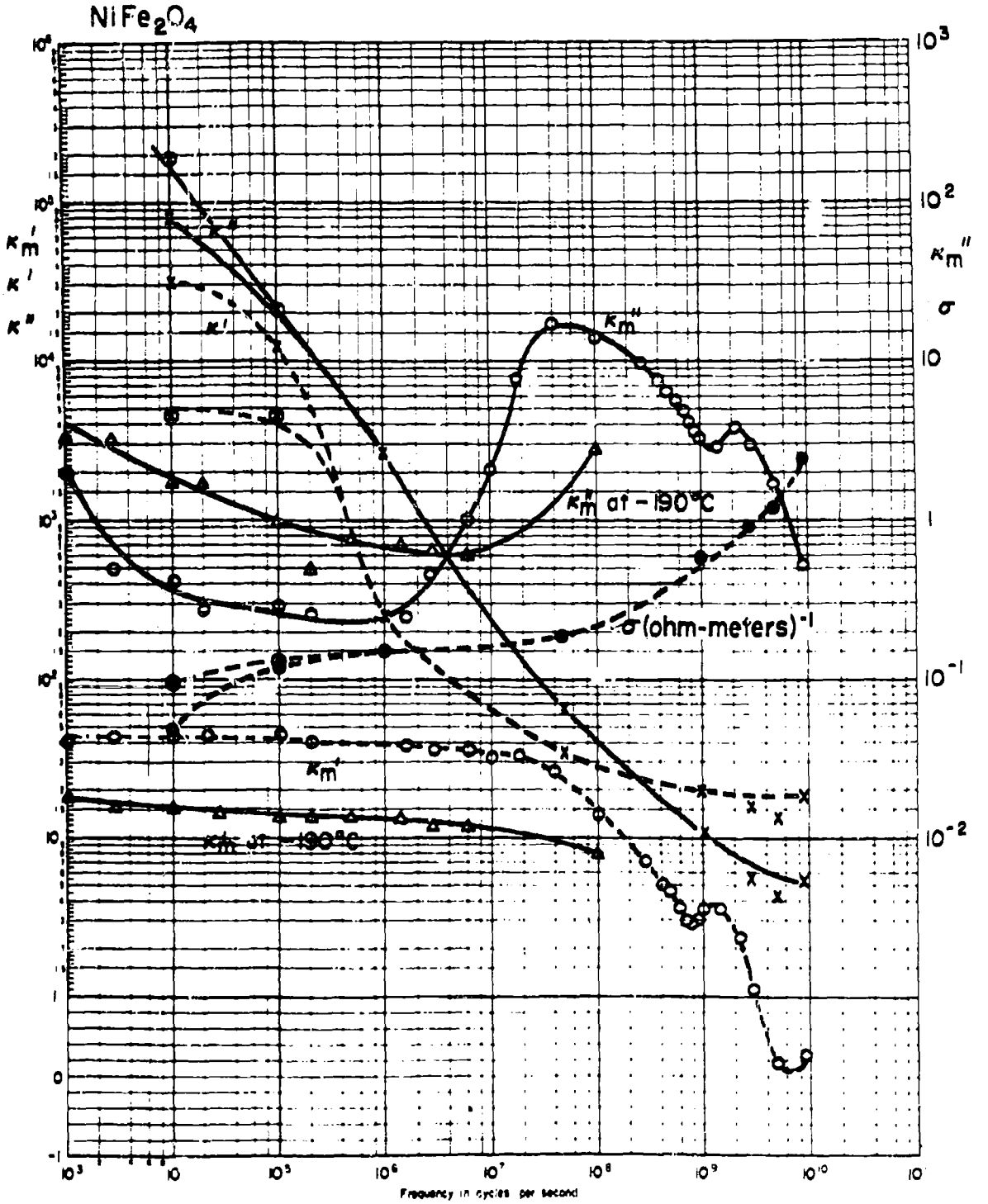

Fig. 14.1. Dielectric constant and loss, magnetic permeability and loss for $NiFe_2O_4$.

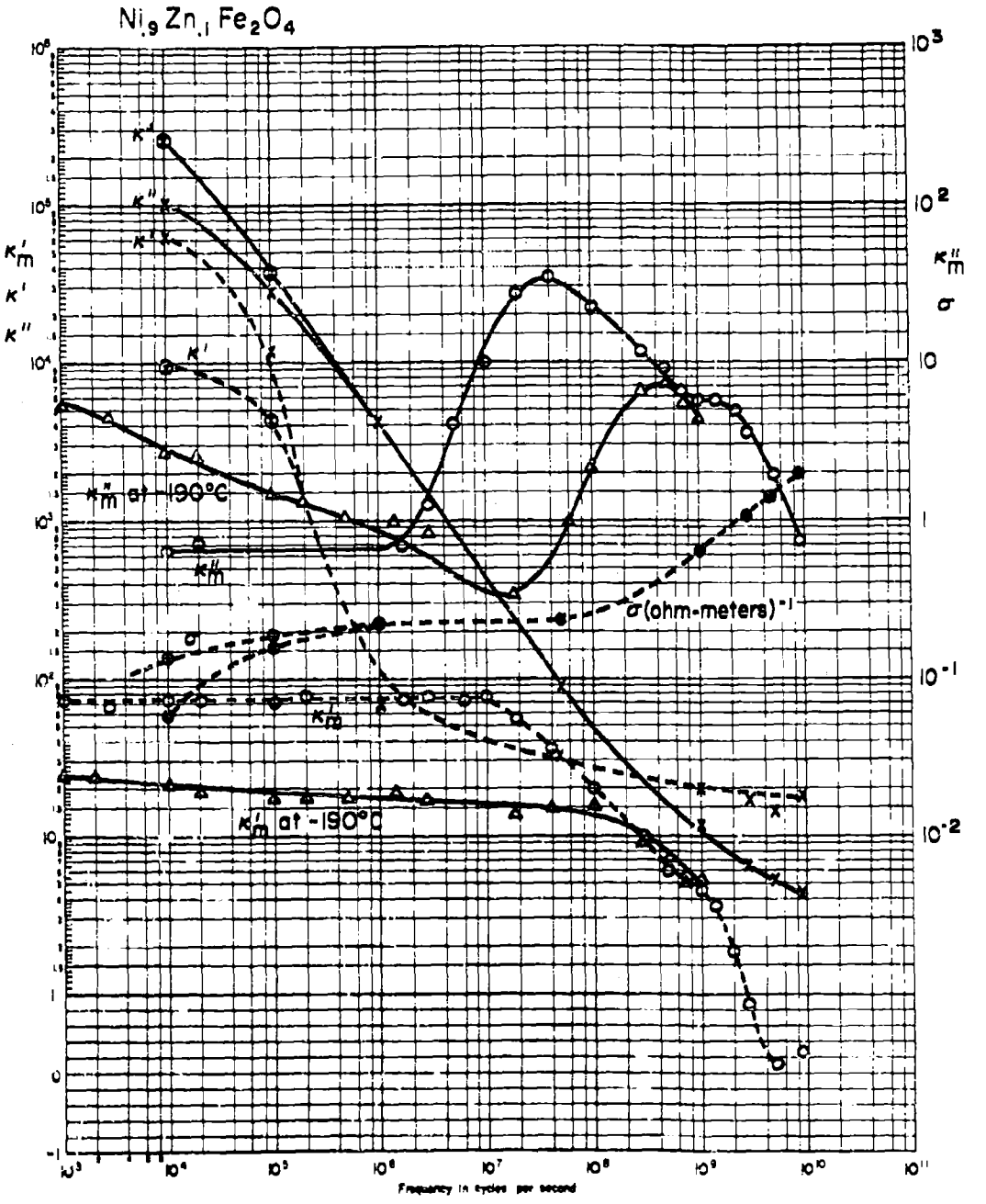

Fig. 14.2. Dielectric constant and loss, magnetic permeability and loss for $Ni_{0.9}Zn_{0.1}$.

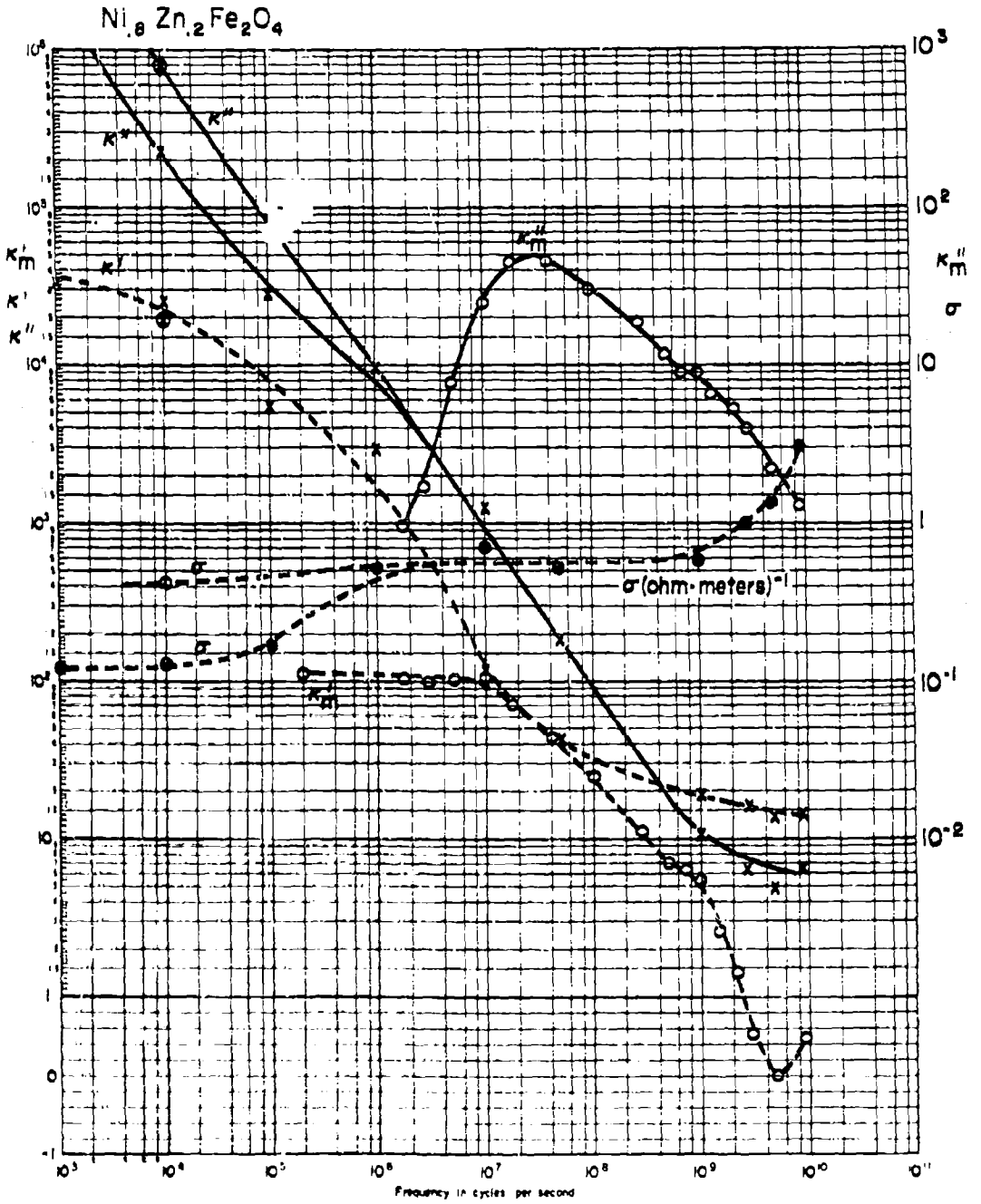

Fig. 14.3. Dielectric constant and loss, magnetic permeability and loss for $Ni_{0.8}Zn_{0.2}$.

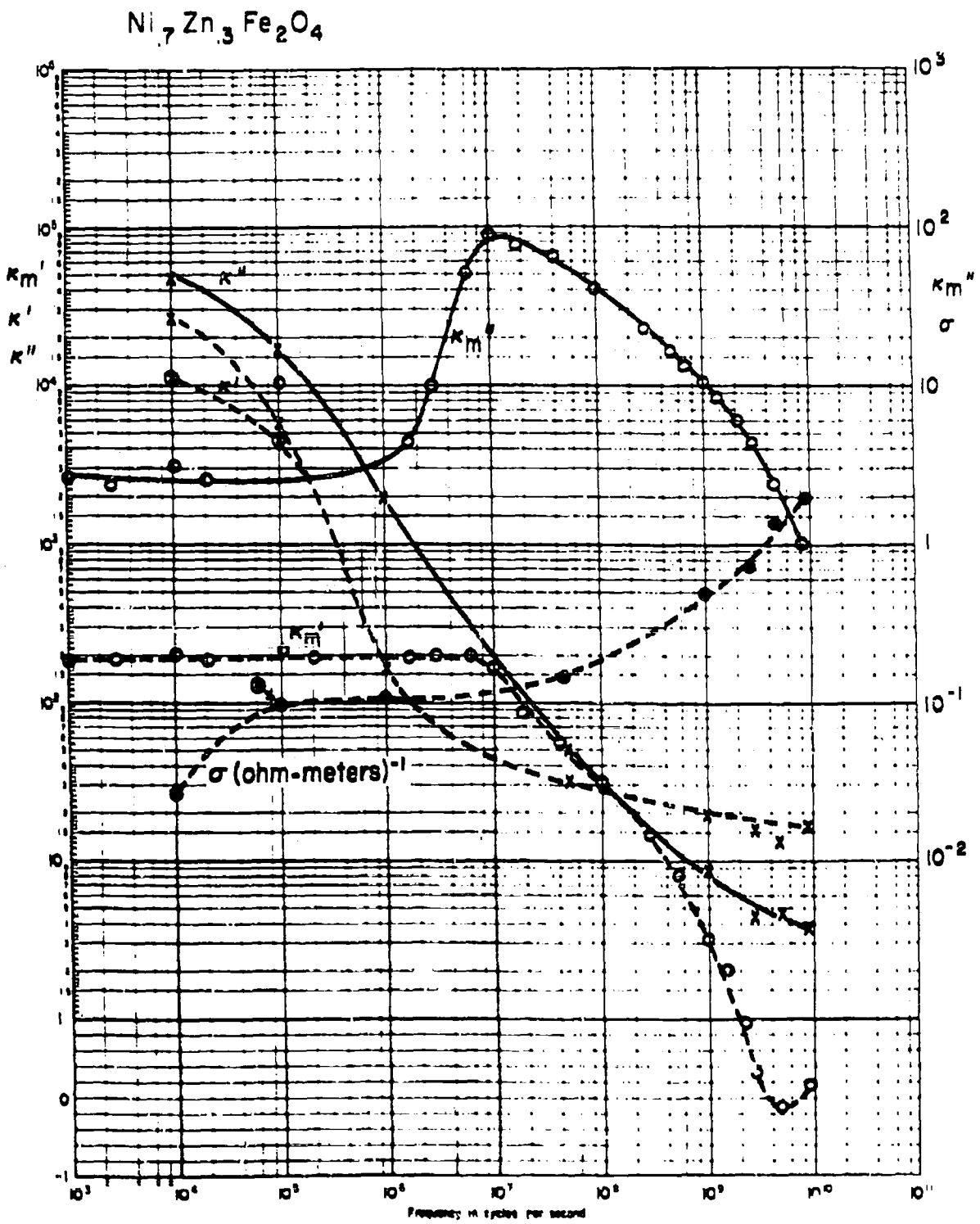

Fig. 14.4. Dielectric constant and loss, magnetic permeability and loss for $Ni_{0.7}Zn_{0.3}$

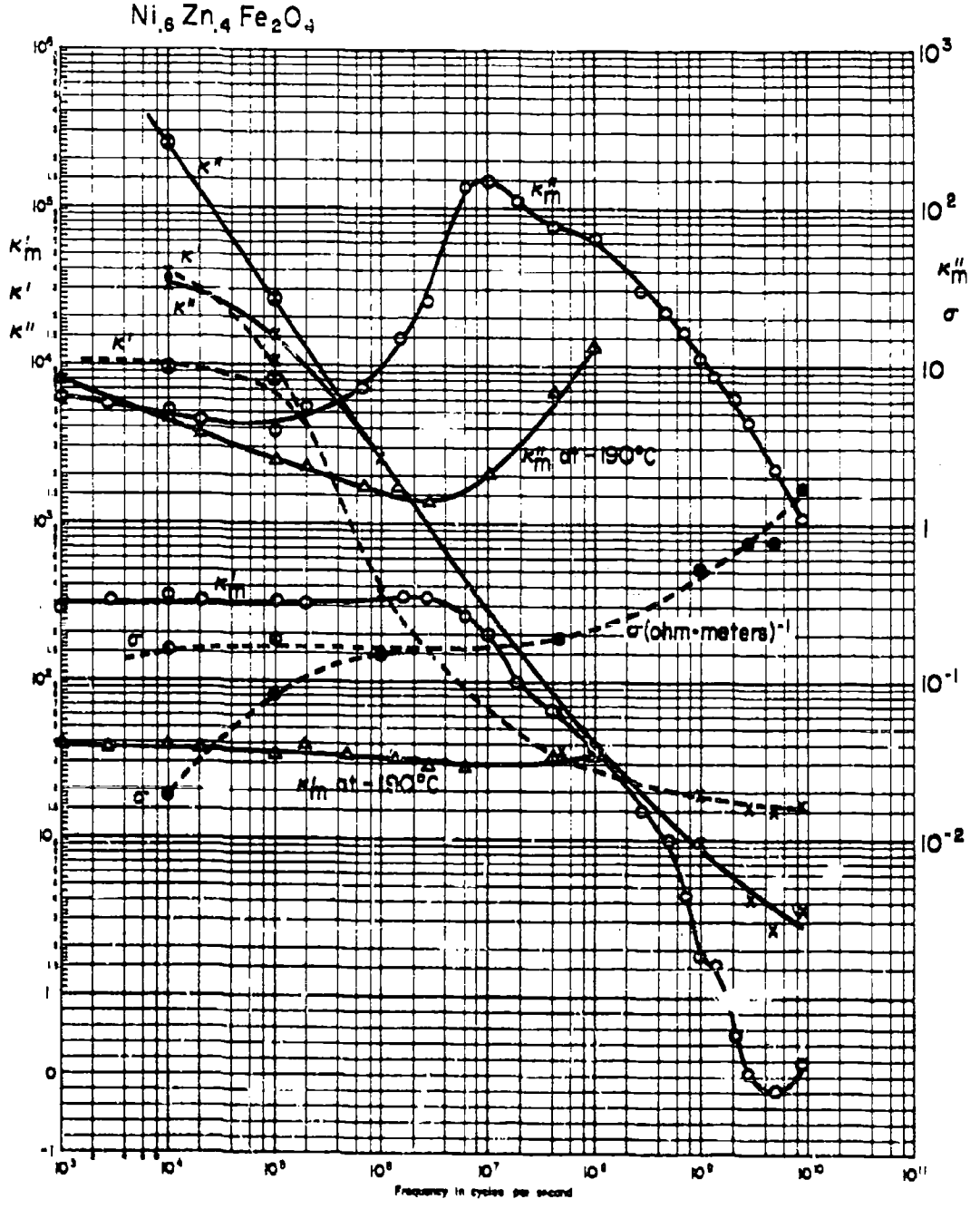

Fig. 14.5. Dielectric constant and loss, magnetic permeability and loss for $Ni_{0.6}Zn_{0.4}$

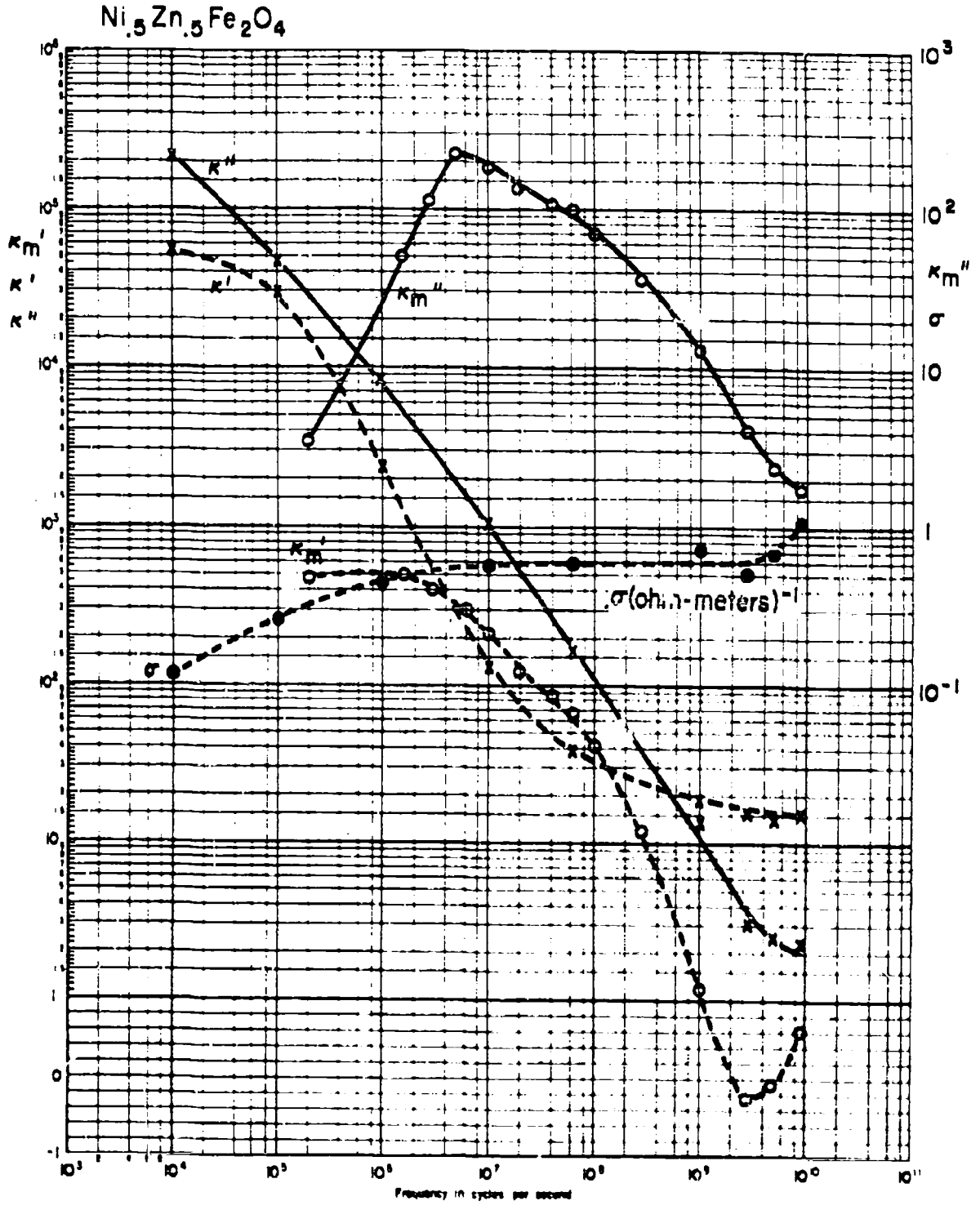

Fig. 14.6. Dielectric constant and loss, magnetic permeability and loss for $Ni_{0.5}Zn_{0.5}$

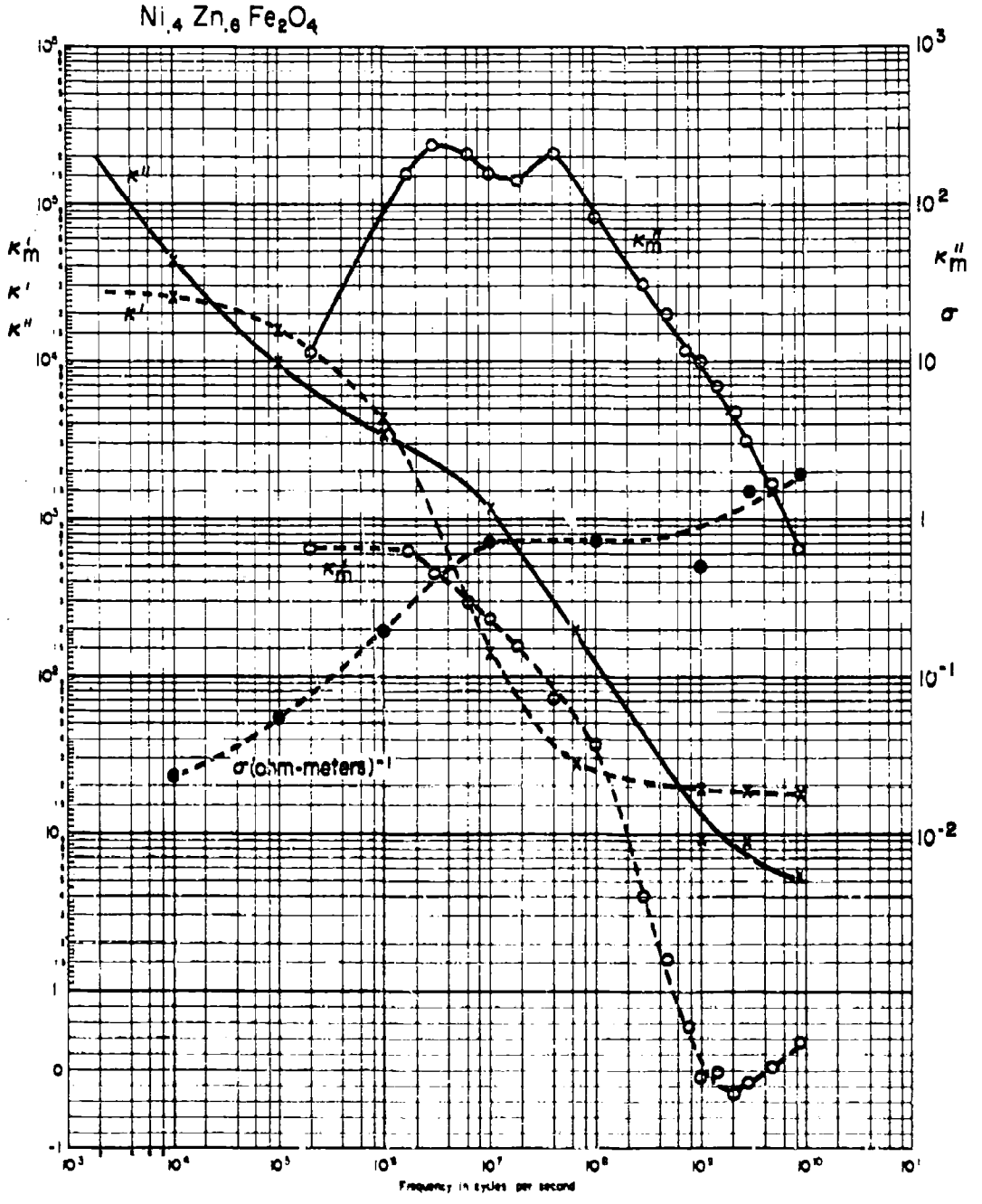

Fig. 14.7. Dielectric constant and loss, magnetic permeability and loss for $Ni_{0.4}Zn_{0.6}$.

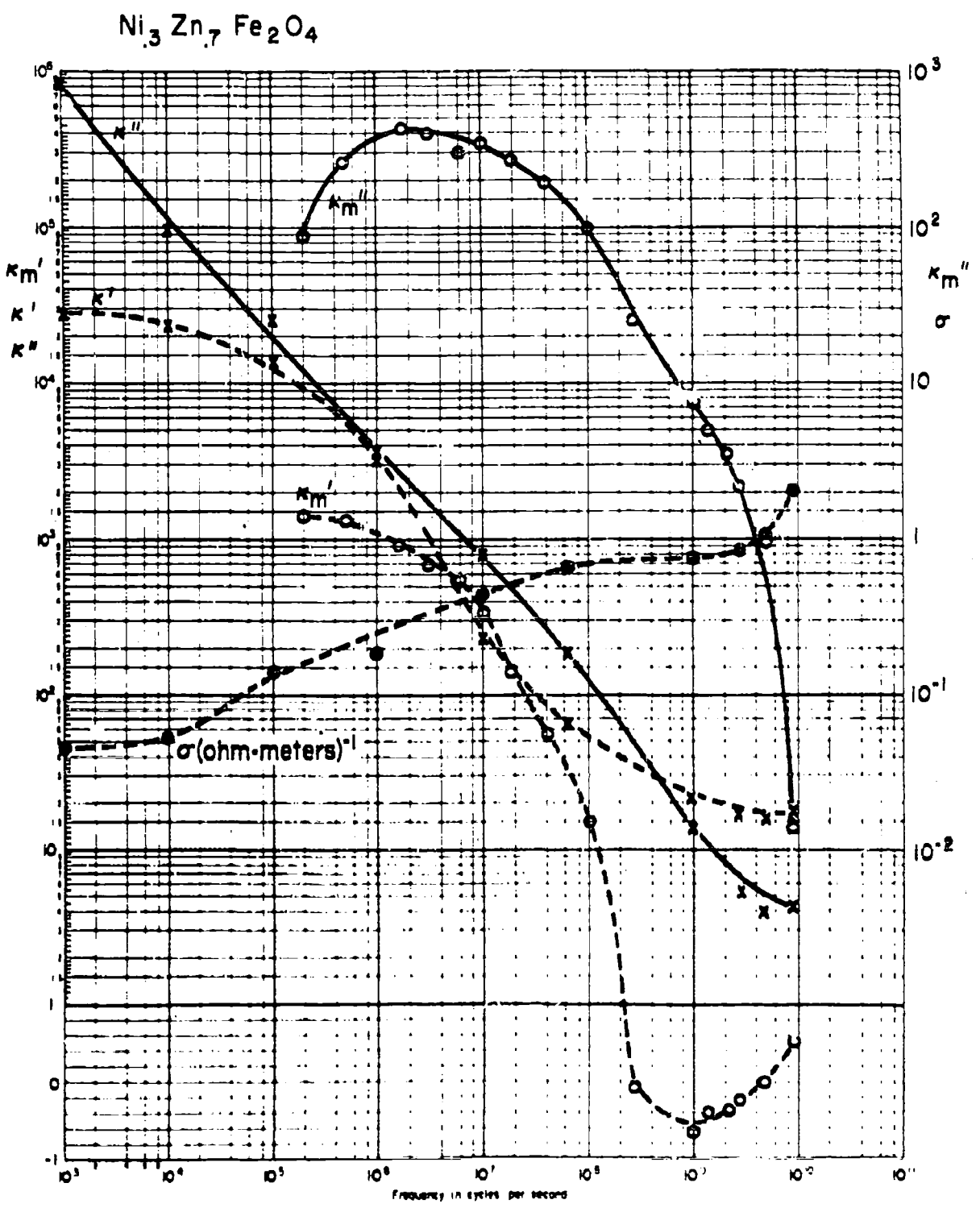

Fig. 14.6. Dielectric constant and loss, magnetic permeability and loss for $Ni_{0.3}Zn_{0.7}$.

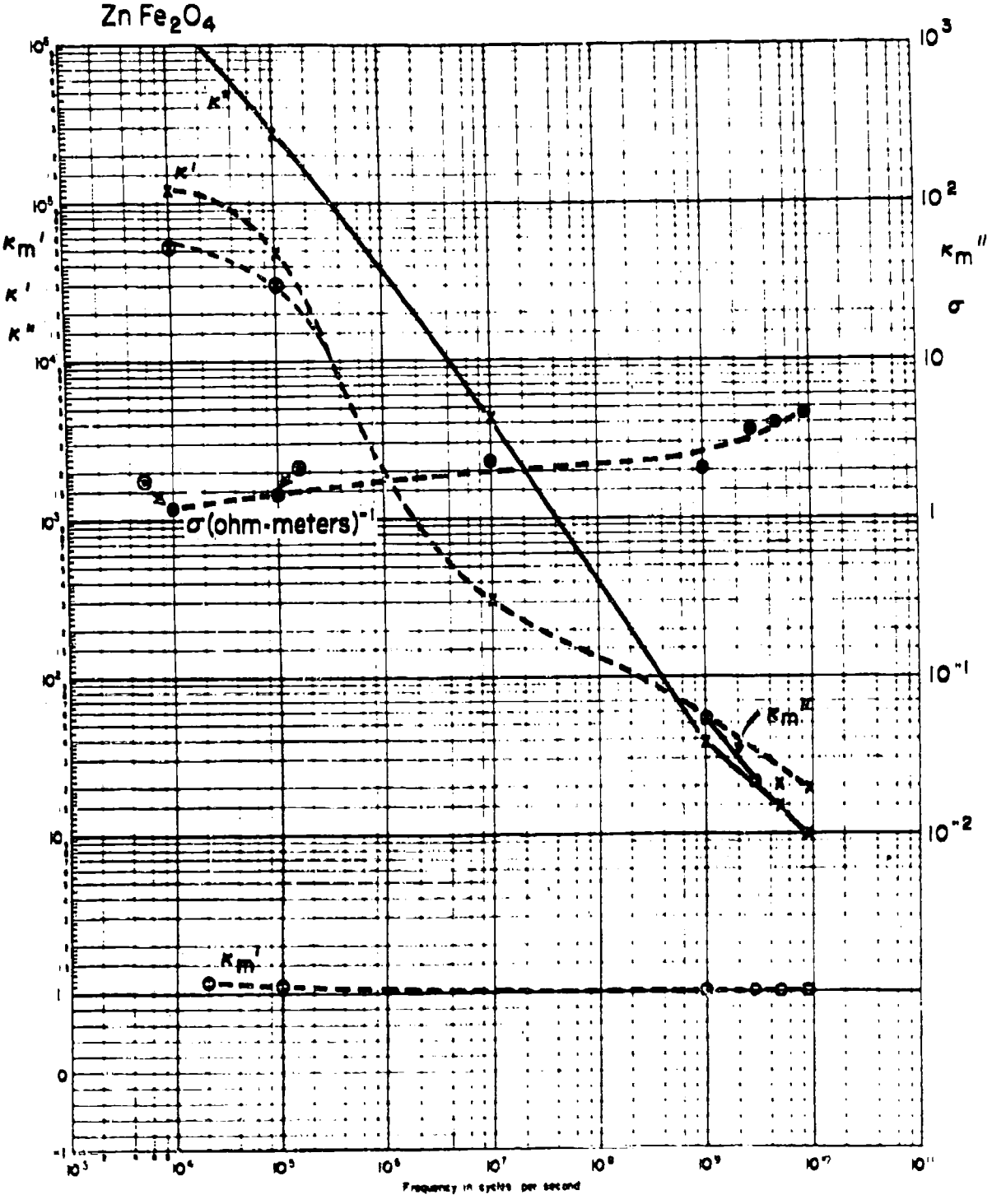

Fig. 14.9. Dielectric constant and loss, magnetic permeability and loss for $ZnFe_2O_4$.

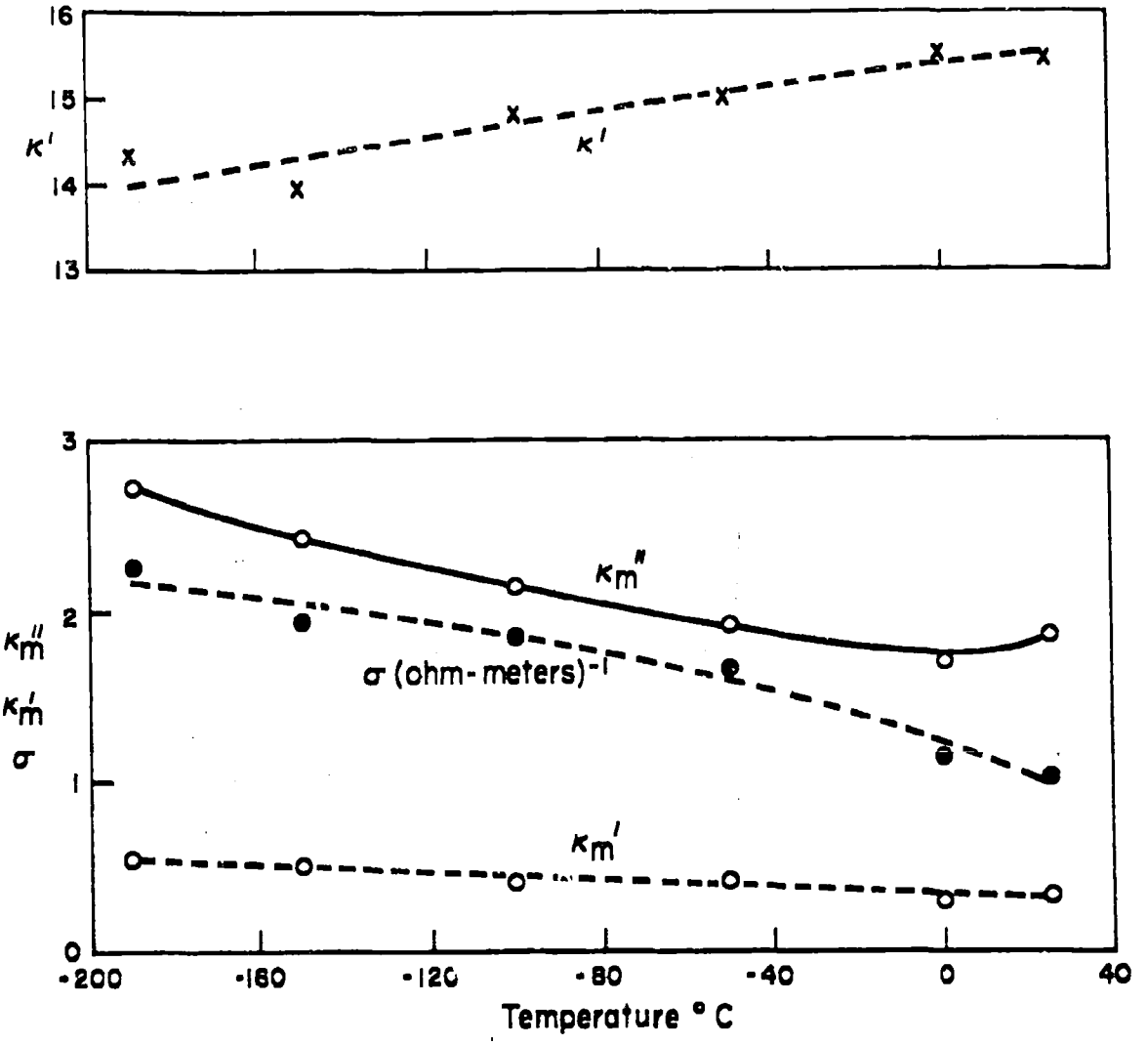

Fig. 14.10. Temperature dependence of microwave conductivity measurements on $Ni_{0.3}Zn_{0.7}Fe_2O_4$.

characteristic of semiconductors (cf. Fig. 15.3). It seems that an absorption spectrum, due perhaps to loosely bound charges, lies in the 10^{11} to 10^{12} cps range and moves towards the microwave region as the temperature decreases. Thus we should interpret only the flat region of the σ-characteristic as descriptive of the true conductivity of the ferrites, while the bulk of the electric losses at microwave frequencies stems from this incoming absorption spectrum.

Turning to the relaxation spectrum at low frequencies, we can match the

observed characteristics approximately by the equivalent circuit of the two-layer capacitor by adjusting the parameters a and b of Eq. (10.15). For magnesium ferrite-aluminates this has been done by Fairweather and Frost[37], but constants derived from 2-terminal measurements must be interpreted with caution. Our 2-terminal values showed some fluctuations at low frequencies and a field-strength dependence which varied with the type of electrode used. Four-terminal measurements at 10^4 and 10^5 cps gave values of κ' and σ which were appreciably different, as shown in Figs. 14.1 to 14.9 by crossed and dotted circles, respectively. The remaining field effect (Fig. 14.11) is not surprising since the field strength in the grain-boundary layers must reach very high values and result in localized field emission and breakdown.

Since the grain-boundary layers should be absent in single crystals, the parameters a and b and the intrinsic conductivity obtained by 4-terminal measurements, characterize the individual ceramic sample with all its fabrication variables. They will change within wide limits for a given composition depending on the handling procedures. It must be kept in mind that not only interface phenomena are responsible for such changes; variations in firing temperature, firing atmosphere and cooling may produce secondary phases and changes in the state of oxidation with striking influence on the electric and magnetic properties.

15. D-C Conductivity of Ferrites

On the basis of the two-layer model, the d-c conductivity is determined essentially by the across-grain contacts. Previous measurements on the more highly resistive ferrites[37] have shown an exponential temperature dependence at frequencies above and below the relaxation region, both governed by the same activation energy. This certifies that the boundary resistivities in these materials are caused essentially by a decrease in the area of perfect contact between grains,

37) A. Fairweather and E. J. Frost, Proc. Inst. Elec. Engrs. 100, Pt. IIA, 15 (1953).

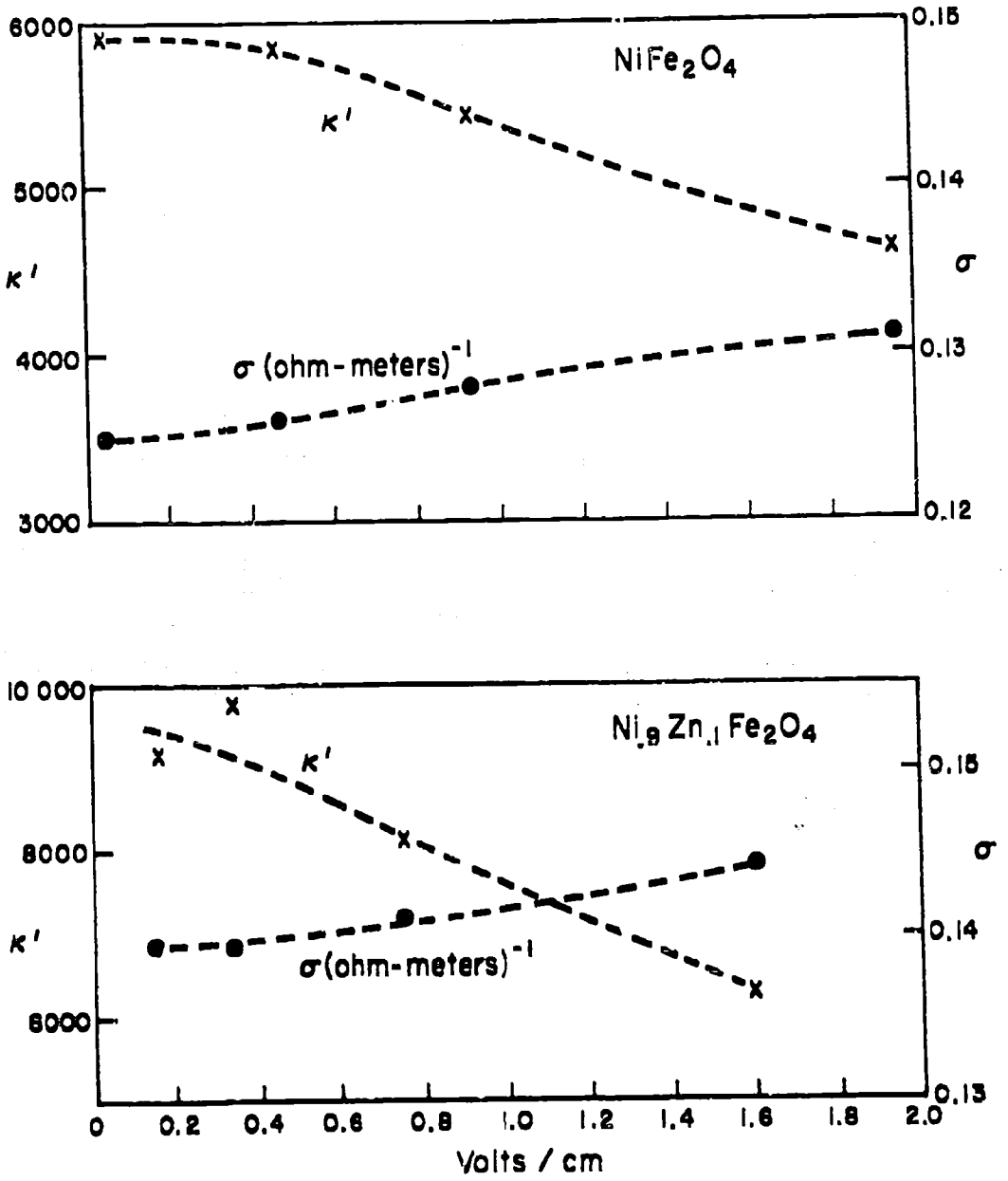

Fig. 14.11. Field-strength dependence of four-terminal a-c dielectric measurements at 10^4 cps.

and not by a boundary region with different intrinsic electrical properties. The latter possibility, however, can by no means be excluded in all cases, as evidenced by the highly resistive layers found on the outer surfaces of a sintered specimen of a manganese-zinc ferrite in the present work (Fig. 15.1).

Four-terminal d-c measurements show a field-strength dependence varying

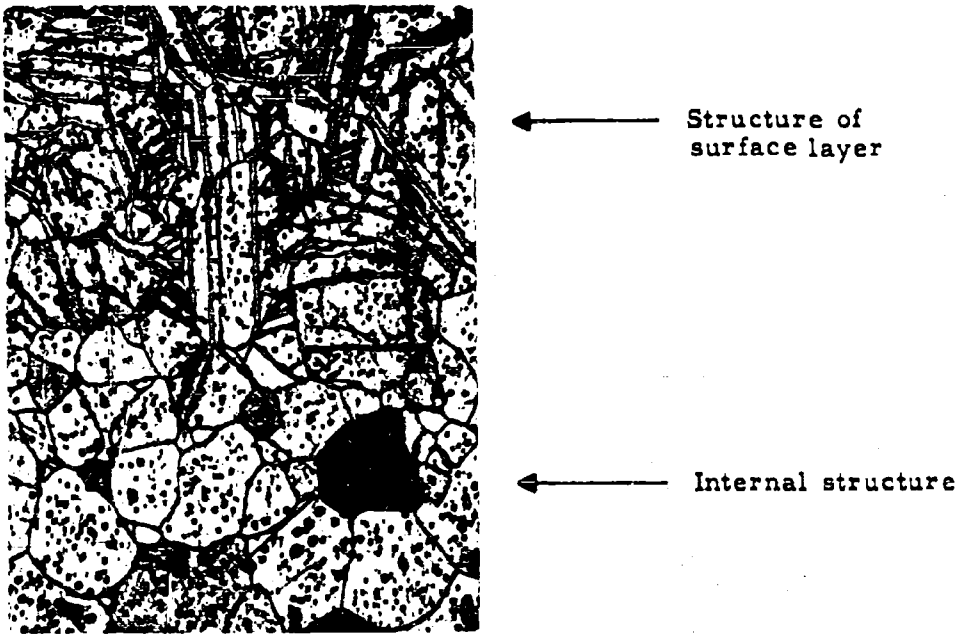

Fig. 15.1. Surface structure of a sintered Mn-Zn ferrite ceramic.

from ferrite to ferrite (Fig. 15.2), as well as between different specimens of the same ferrite. Limiting values of conductivity at low field strengths show the temperature dependence $\sigma = \sigma_o e^{-E/kT}$ (Fig. 15.3) with the activation energies E, as given in Table 15.1. Probably several conduction processes have to be considered. The work of Kamiyoshi[38] on nickel ferrite and cobalt ferrite indicates that activation energies may be decreased considerably by quenching from high temperatures. Wijn[23] has shown that an oxygen deficiency in a Ni-Zn ferrite can increase its conductivity from 10^{-5} to 10^{-6} $(\text{ohm-cm})^{-1}$ to 10^{-3} $(\text{ohm-cm})^{-1}$ while lowering the activation energy from 0.4 to 0.1 ev. This higher conductivity is attributed to the ferrous-ferric electron transfer process believed to be predominant in magnetite. However, our measurements on single-crystal specimens of magnetite (Fig. 15.4) show that we are not dealing with one simple activation process; mobility measurements are required before a unique interpretation is

38) K. Kamiyoshi, Sci. Rep. Res. Inst. Tohôku Univ. 3, 716 (1951).

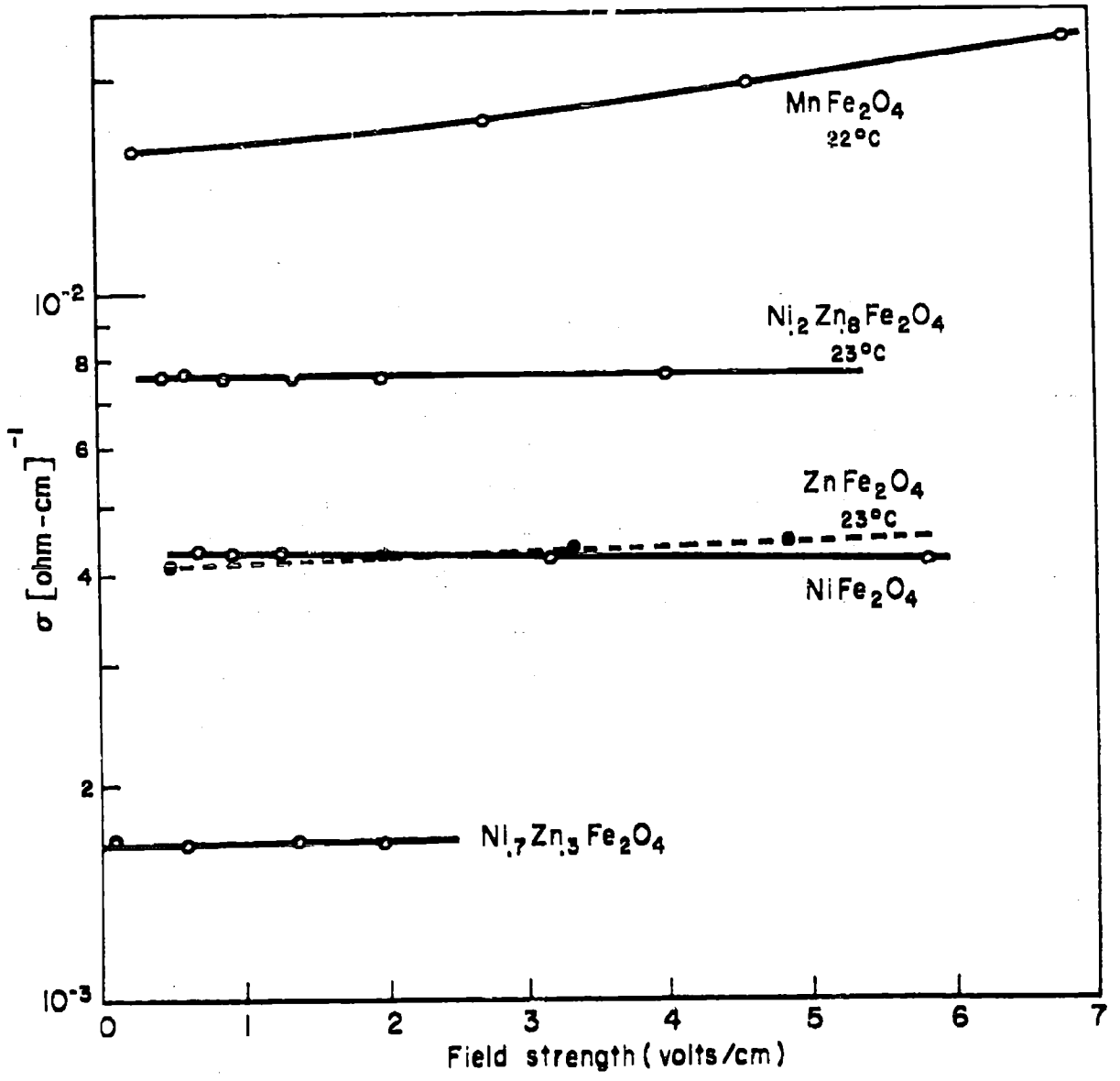

Fig. 15.2. Field-strength dependence of four-terminal d-c conductivity values for various ferrites.

feasible. At temperatures directly above the transition point of electronic ordering (-160°C) a slope corresponding to an energy of 0.05 ev is observed; just below this temperature a value of 0.1 ev is measured, decreasing to 0.03 ev at very low temperatures. The infrared absorption edge in magnetite occurs at about 0.15 ev at room temperature with a tail extending to much lower energies. At

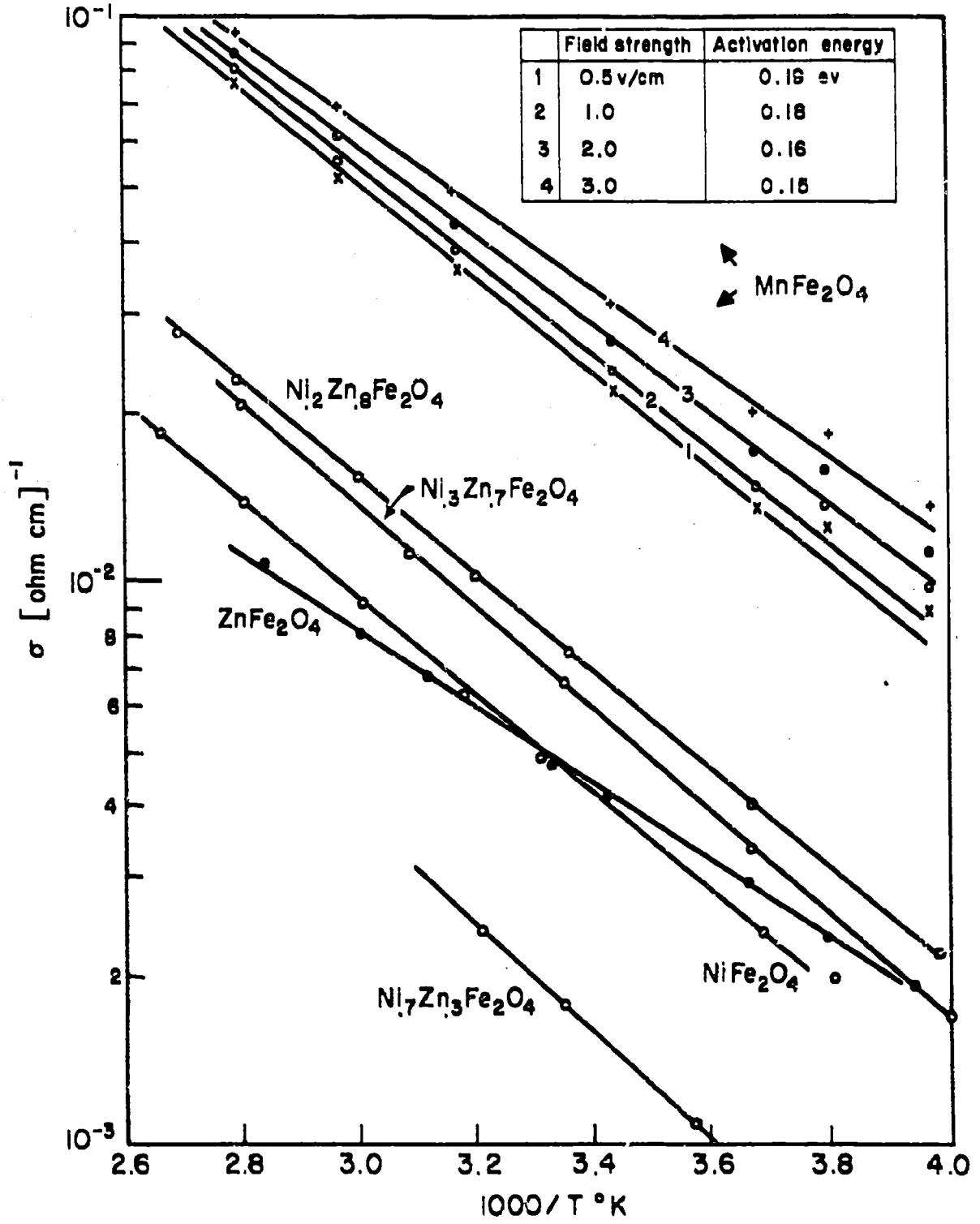

Fig. 15.3. Temperature dependence of four-terminal d-c conductivity values measured at low electric field strengths on various ferrites.

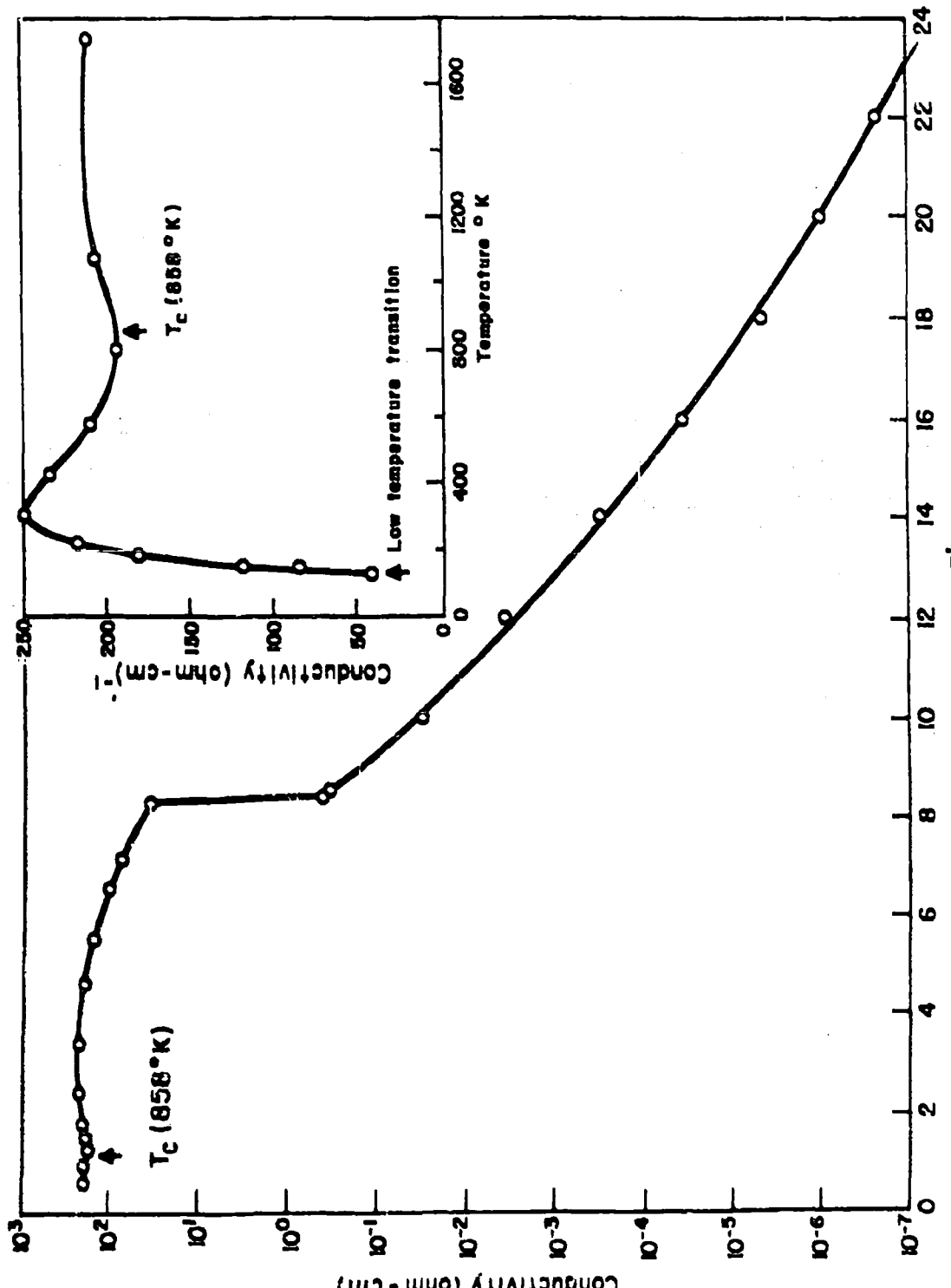

Fig. 15.4. Temperature dependence of d-c conductivity of magnetite.

Table 15.1. Activation energies deduced from d-c conductivity measurements.

Ferrite (M^{2+})	E ev	σ_o $(ohm-cm)^{-1}$
Mn	0.15 - 0.19 ± 0.02	-
Ni	0.17 ± 0.02	4 ± 2
$Ni_{0.7}Zn_{0.3}$	0.20 ± 0.02	5 ± 3
$Ni_{0.4}Zn_{0.6}$	0.18 ± 0.02	-
$Ni_{0.3}Zn_{0.7}$	0.18 ± 0.02	9 ± 4
$Ni_{0.2}Zn_{0.8}$	0.17 ± 0.02	7 ± 4
Zn	0.15 ± 0.02	2 ± 1

liquid nitrogen temperature, the edge has moved to about 0.17 ev.

In our experiments the level of conductivities in the nickel-zinc ferrites proved to be about three orders of magnitude greater than the values reported in the literature for similar compositions; our activation energies are all about 0.18 ev. This seems to indicate that the same conduction process is predominant in all members of our series. For nickel ferrite and zinc ferrite, the infrared absorption edge occurs at nearly twice the energy derived from the conductivity measurements. If this is not a coincidence, we seem to deal with some intrinsic conduction process.

Magnetization of Ferrites

16. Two Main Dispersion Regions

The initial permeability of ferrite ceramics is an effective scalar permeability averaging over the permeability matrices and interaction effects of the individual crystallites. Its frequency response characteristics show, in general, two main dispersion regions (cf. Figs. 14.1 to 14.9). The first, located

in the frequency range 1 to 500 Mc indicates frequently by the sharp rise of the loss curve κ''_m and sometimes by a maximum of κ'_m, that it is, at least in part, a resonance spectrum. The second dispersion, in the range 500 to 3000 Mc, clearly reveals a resonance phenomena by the minimum of the κ' curves.

The classical treatment of the gyroscopic effects given above leads to two types of resonances: spin resonance, caused by the Larmor precession of the magnetic moments (see Sec. 4); and domain-wall resonance, if the walls are bound quasi-elastically to equilibrium positions (see Sec. 5). It is natural, therefore, to ascribe the higher region to spin resonance and the lower frequency dispersion to domain-wall resonance. Rado and co-workers[39] especially have advanced this interpretation, while the scientists of the Philips Laboratories[22, 25] are inclined to attribute both resonance regions in cubic ferrites to spin resonance. An experimental decision is not easily made, as will become apparent.

In discussing the characteristics, we have two main pieces of experimental evidence: the static magnetic susceptibility $\chi_{ms} = \kappa'_{ms} - 1$, and the resonance frequency as characterized by a loss maximum. These quantities are related according to theory.

17. Domain Wall or Spin Resonance

a) Wall resonance

The resonance frequency of the domain wall in the case of low damping ($\beta << k$) is given by the frequency of the loss maximum as $\omega_o = \sqrt{k/m}$ (cf. Eq. 5.19), and the static susceptibility by $\chi_{ms} = \frac{4C\mu_o M^2}{k\ell}$, where C is a factor determined by the area and relative orientation of the walls present, and equals unity for a single wall parallel to the applied field and ℓ is the width of dispersion. Thus

39) G. T. Rado, Revs. Mod. Phys. 25, 81 (1953).

$$\omega_o^2 \chi_{ms} = \frac{4C\mu_o M^2}{m\ell} = \frac{4CM^2\gamma^2\mu_o^2 A^{1/2}}{\ell K_1^{1/2} \int_{\theta_1}^{\theta_2} \sqrt{\mathcal{E}(\theta)} \cdot d\theta} \quad . \tag{17.1}$$

For an overdamped wall motion, a loss peak will occur at $\omega_d \equiv \frac{1}{\tau} = \frac{k}{\beta}$ (cf. Eq. 5.21) and in this case

$$\omega_d \chi_{ms} = \frac{4C\mu_o M^2}{\beta\ell} = \frac{4CM^2\gamma^2\mu_o^2 A^{1/2}}{\lambda\ell K^{1/2} \int_{\theta_1}^{\theta_2} \sqrt{\mathcal{E}(\theta)} \cdot d\theta} \quad . \tag{17.2}$$

A ferrite with M = 250,000 amp./m (250 cgs units), a static susceptibility of 100 in a specimen 1 mm wide, due to the motion of a single 180° wall parallel to the apllied field, and a wall mass corresponding to that in nickel ferrite (9.4×10^{-10} kg/m^2), gives an undamped resonance frequency of 270 Mc/sec.

b) Spin resonance

The loss maximum associated with dipoles precessing under the action of an effective field H_{eff} occurs at $\omega_s = \sqrt{\gamma^2\mu_o^2 H_{eff}^2 + a^2}$, while the associated static susceptibility is given by $\chi_{ms} = \frac{C'M}{H_{eff}}$ (cf. Eq. 9.8), where C' is a constant determined by the spatial distribution of the spin directions (for completely random distribution, C' = 2/3). Thus

$$\omega_s \chi_{ms} = C'M\gamma\mu_o \sqrt{1 + \left(\frac{a}{\gamma\mu_o H_{eff}}\right)^2} \quad ; \qquad \simeq C'\gamma\mu_o M \quad \text{(for small a)} \; . \tag{17.3}$$

For an overdamped spin resonance ($a >> \omega_o$), the loss maximum occurs at $\omega_d' = a = \frac{\lambda H_{eff}}{M}$ (cf. Eq 10.8) and in this case,

$$\omega_d' \chi_{ms} = \frac{C'aM}{H_{eff}} = C'\lambda. \tag{17.4}$$

In a ferrite ceramic with M $\simeq$ 250 cgs units and a static susceptibility of 100 as above, but in this case due to spin orientation, the undamped spin resonance

loss maximum occurs at ca. 60 Mc/sec. The effective field causing this Larmor precession is ca. 1600 amp./m (20 oersteds).

The two examples show that both resonances can occur in the same frequency region; therefore, an a priori connection between the frequency location of the dispersion region and the mechanism cannot be postulated.

18. Evidence Found in the Nickel-Zinc Ferrite System

Of the various mixed ferrites, the nickel-zinc system has been investigated most extensively because of its early applications for high-frequency components. The loss peak of the lower dispersion region in this series is pronounced (cf. Figs. 14.1 to 14.9), hence offers a good chance of checking the relations between initial susceptibility and resonance frequency just derived. The saturation magnetization of these materials for room temperature is known (Fig. 18.1); to compare the susceptibilities, we have adjusted them to the identical saturation magnetization of M = 250 cgs units = 250,000 amp./m.

If this corrected initial susceptibility is plotted against the frequency of the loss peak maximum ω_L on a log-log scale, approximately a straight line with unit negative slope results (Fig. 18.2), that is,

$$\frac{\chi_{ms}}{M}\ \omega_L = \text{constant}. \qquad (18.1)$$

This agrees with the findings of previous workers[40] who have interpreted the result as confirmation of the spin resonance expression (cf. 17.3) $\frac{\chi_{ms}}{M}\ \omega_s = \frac{-2\gamma\mu_o}{3}$, shown as an unbroken line in Fig. 18.2. However, a similar straight line would result from a strongly damped domain-wall resonance (cf. Eq. 17.2) provided that the factor $\beta\ell/M$ is about constant throughout the series.

Further arguments for both points of view have been made. Domain arrangments should be sensitive to strain; the intial susceptibility and peak fre-

40) H. G. Beljers and J. L. Snoek, Philips Tech. Rev. 11, 313 (1949).

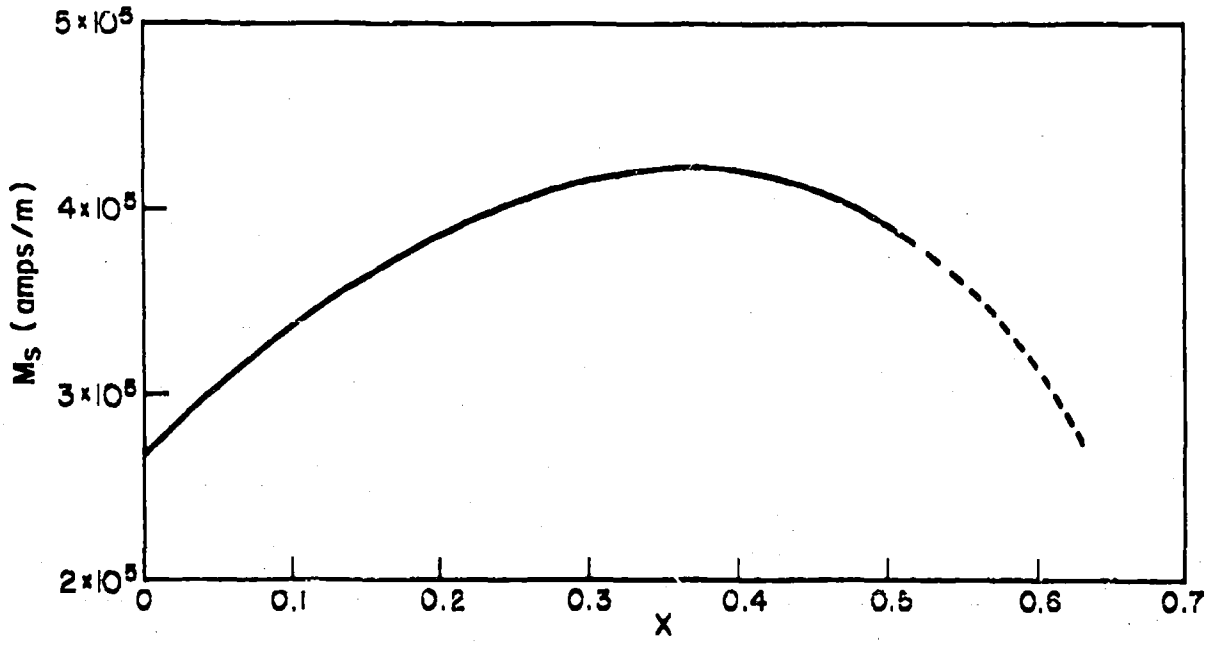

Fig. 18.1. Room temperature values of saturation magnetization for the nickel-zinc ferrites ($Ni_{1-x}Zn_xFe_2O_4$) calculated from data given by R. Pauthenet, Ann. phys. [12] 7, 714 (1952).

quency of these ferrites prove relatively insensitive to strain, a fact supporting the spin resonance interpretation.[22] On the other hand, as Rado[26] showed, when a nickel-zinc ferrite specimen is finely pulverized and reshaped with wax as a binder, the lower dispersion region has disappeared; this fact points to a domain-wall resonance, since the walls have presumably been taken out by the treatment.

Turning to the individual characterisitcs, we find for nickel ferrite (Fig. 14.1) that the steepness of the loss curve at the low-frequency side of the lower band indicates a resonance absorption of a halfwidth $2a \simeq 2\times10^8$ radians/sec., hence a Q of about 1. If the higher band is interpreted as a single damped spin resonance, which would require an effective internal field of about 240,000

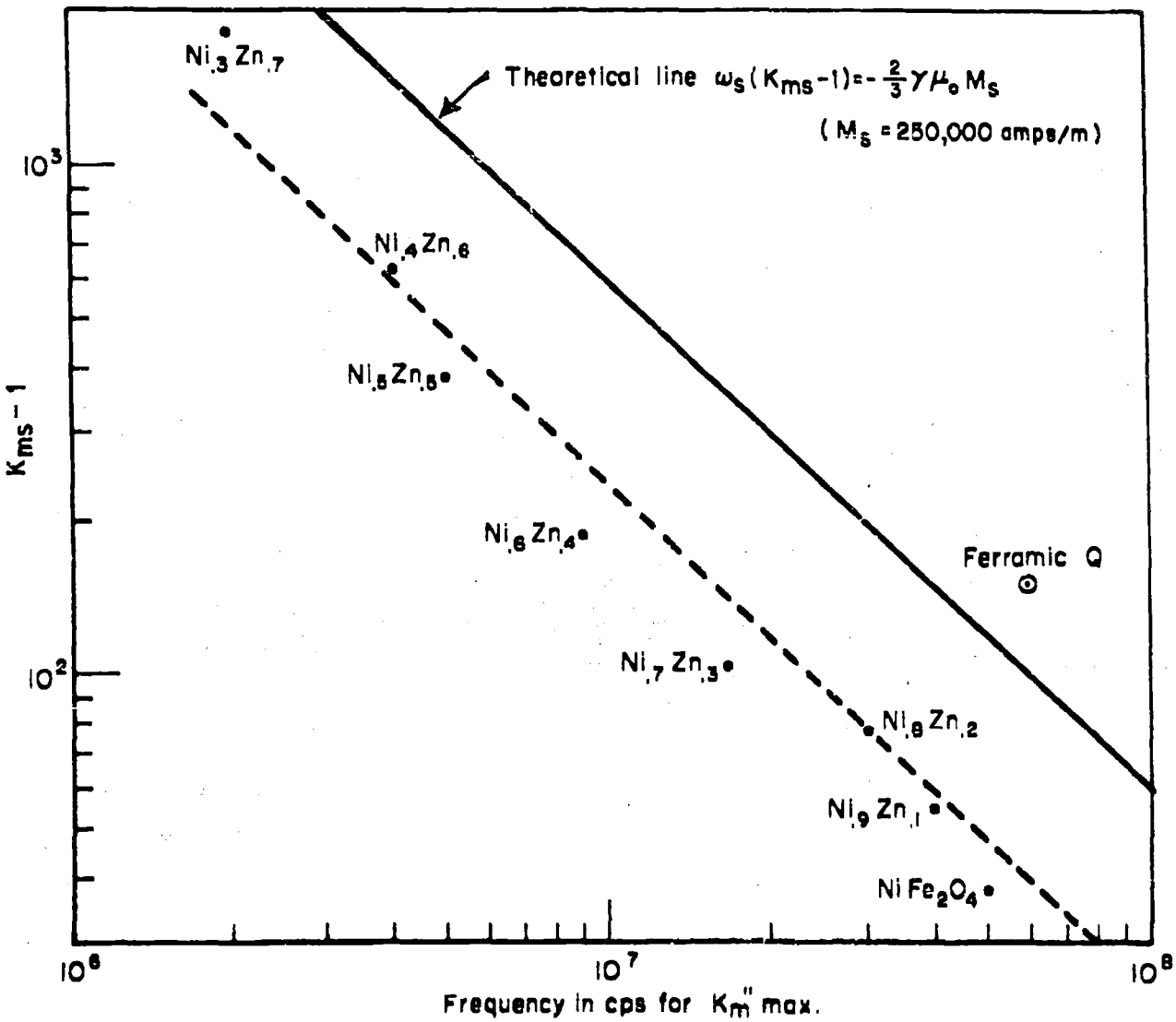

Fig. 18.2. Plot of $\kappa'_{ms} - 1$ vs. the frequency of the first loss peak for various ferrites.

amp./m, a halfwidth $2\alpha \simeq 2\times10^{10}$ is observed and the Q is again ca. 1. However, on single crystals of nickel ferrite, Yager et al.[41] observed $2\alpha \simeq 1\times10^{9}$, or a Q of about 100 for a spin resonance induced at 2.4×10^{10} cps (Fig. 18.3). Hence, the proper interpretation of the higher band might be that it consists of a sequence of narrow resonance lines.

41) W. A. Yager, J. K. Galt, F. R. Merrit and E. A. Wood, Phys. Rev. 80, 744 (1950).

The loss curve of $NiFe_2O_4$ ceramic between 10^6 and 10^{10} cps Fig. 14.1) might be roughly split into three resonance absorptions of $Q \simeq 1$, with maxima for κ''_m of about 17, 10, and 4 located at 50, 300, and 2000 Mc/sec. (Fig. 18.4). If these maxima are explained as spin resonances, the saturation moments responsible for them would amount to 25,000, 75,000 and 170,000 amp./m (cf. Eqs. 9.6 and 17.3). This totals up to a moment of 270,000 amp./m, while the saturation moment of nickel ferrite is 265,000 amp./m (see Fig. 18.1) and, in a ceramic of random crystallite orientation, only 2/3 of this amount or about 180,000 amp./m could be expected.

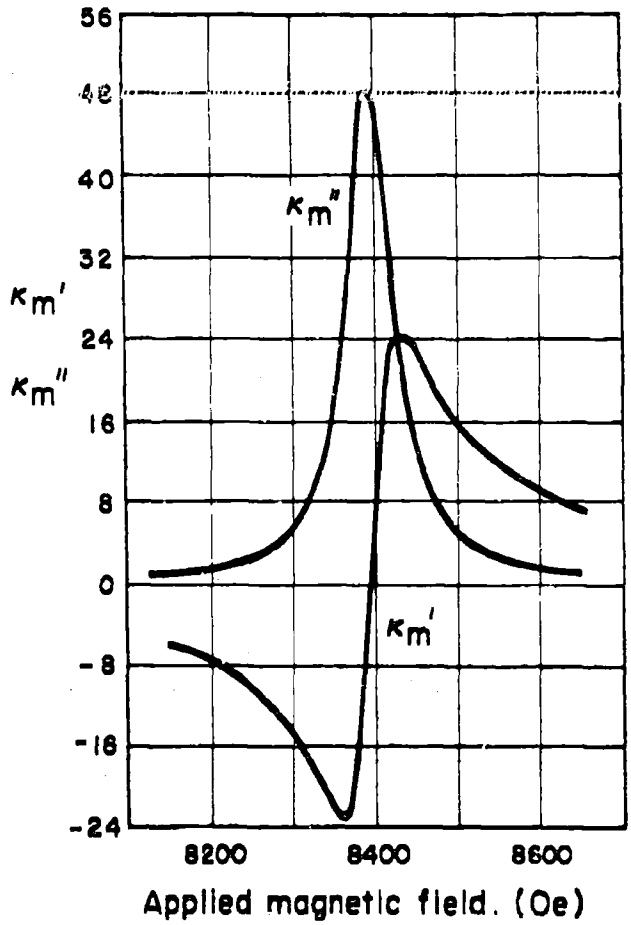

Fig. 18.3. Ferromagnetic resonance observed in a nickel-ferrite crystal.[41]

This discrepancy points to a contribution of domain-wall motions to the magnetic absorption. On the other hand, the difficulty might be removed by a different allocation of resonance peaks to the measured characteristic. Here obviously is a need for less arbitrary techniques of curve fitting. However this may be, the results show that the major part of the magnetic moments causes resonances in the high-frequency part of the spectrum and contributes therefore little to the static susceptibility. If these resonances could be shifted downwards, higher permeability bodies could be made with the same compositions. Ferramic

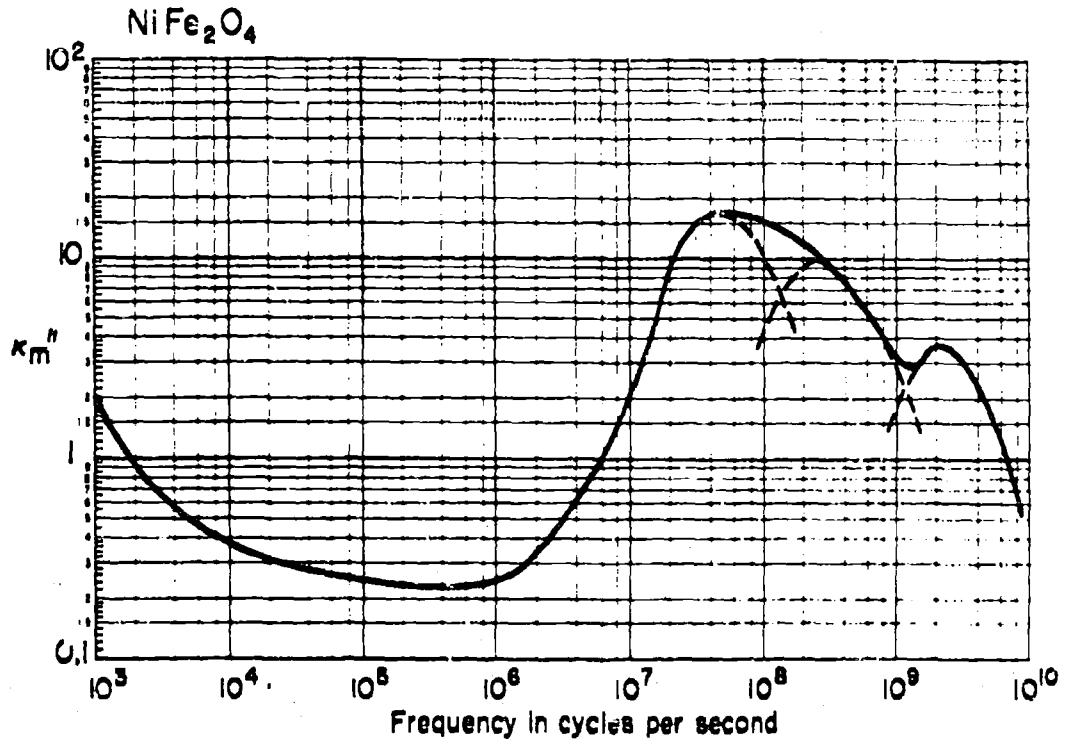

Fig. 18.4. The arbitrary division of the magnetic dispersion in nickel ferrite into three damped resonances.

Q (see Fig. 18.2) may represent this kind of improvement.

Additional evidence for the difficulty of explaining the whole absorption by spin resonances is found in the shift of the lowest resonance peak of the nickel-zinc ferrite series (see Fig. 18.2). The resonance of $NiFe_2O_4$ at 50 Mc/sec. moves down for $Ni_{0.3}Zn_{0.7}Fe_2O_4$ to about 3 Mc/sec. On the basis of spin resonance, we would have to assume that in the former case an internal magnetic field of 1600 amp./m acted, which has been lowered to about 80 amp./m. Such small fields can be visualized only as the difference between an anisotropy field and an opposing particle-shape field, – a somewhat improbable assumption.

Further information is obtained by observing, in our coaxial line equipment (see Fig. 2.12), the influence on the characteristics for $NiFe_2O_4$ of a biasing d-c magnetic field orientated parallel to the high-frequency field (Fig. 18.5). A field of 4000 amp./m cuts down both dispersion regions, but the lower one

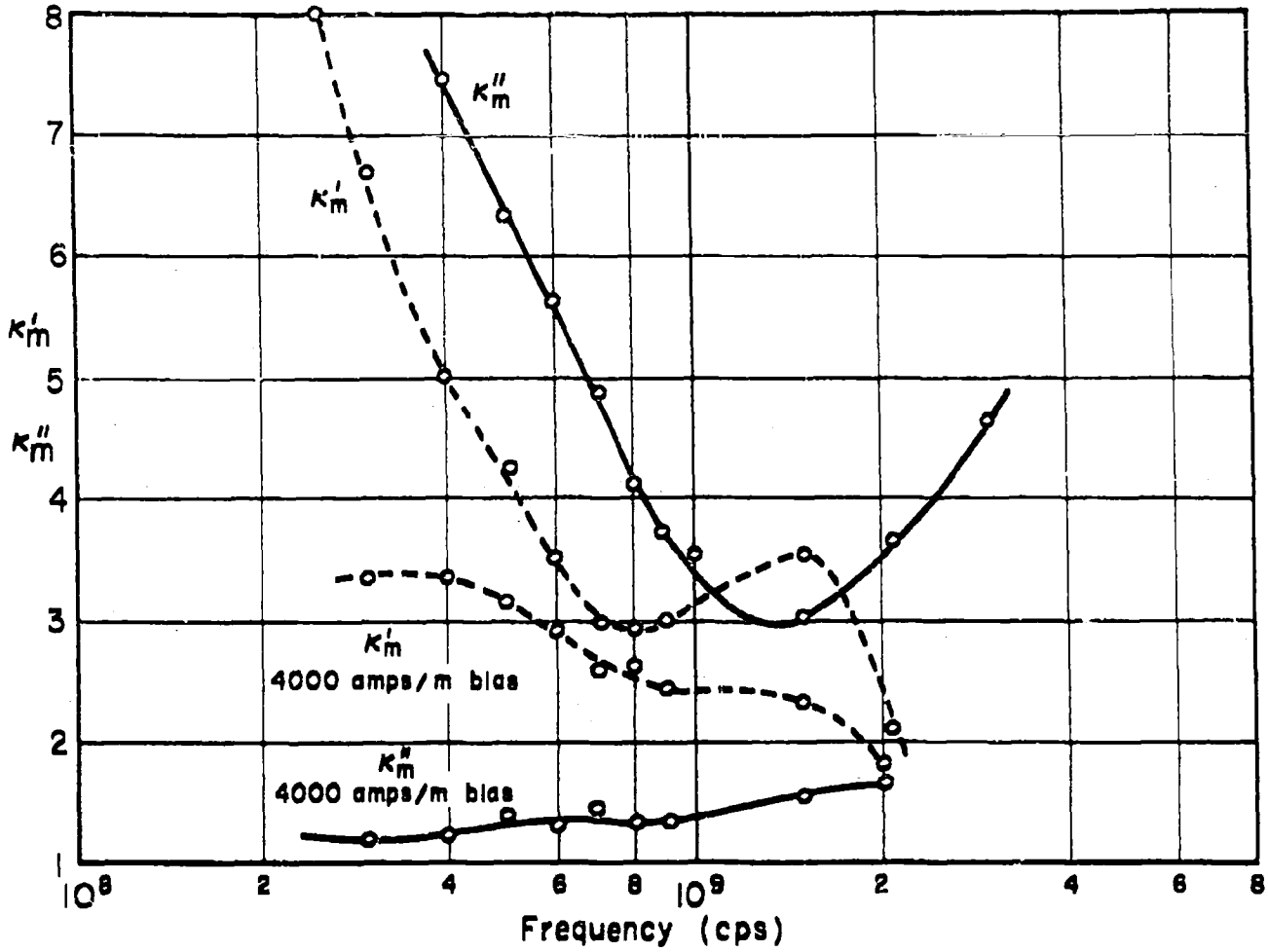

Fig. 18.5. Effect of magnetic bias on the microwave properties of $NiFe_2O_4$.

appreciably more. The pronounced permeability minimum near 800 Mc/sec. disappears, indicating that it is associated with the tail of the lower frequency band and does not represent the rapid rise of the permeability produced by the onset of the higher band. The narrow gap between the biased and unbiased μ' characteristic in this region is caused by the fact that now the positive contribution of the upper band comes into its own. This is even more evident in the case of a magnesium-manganese ferrite $\left[(MgO)_{0.58}(MnO)_{0.06}(Fe_2O_3)_{0.36}\right]$ (Fig. 18.6), where the permeability in this region actually increases on the application of the

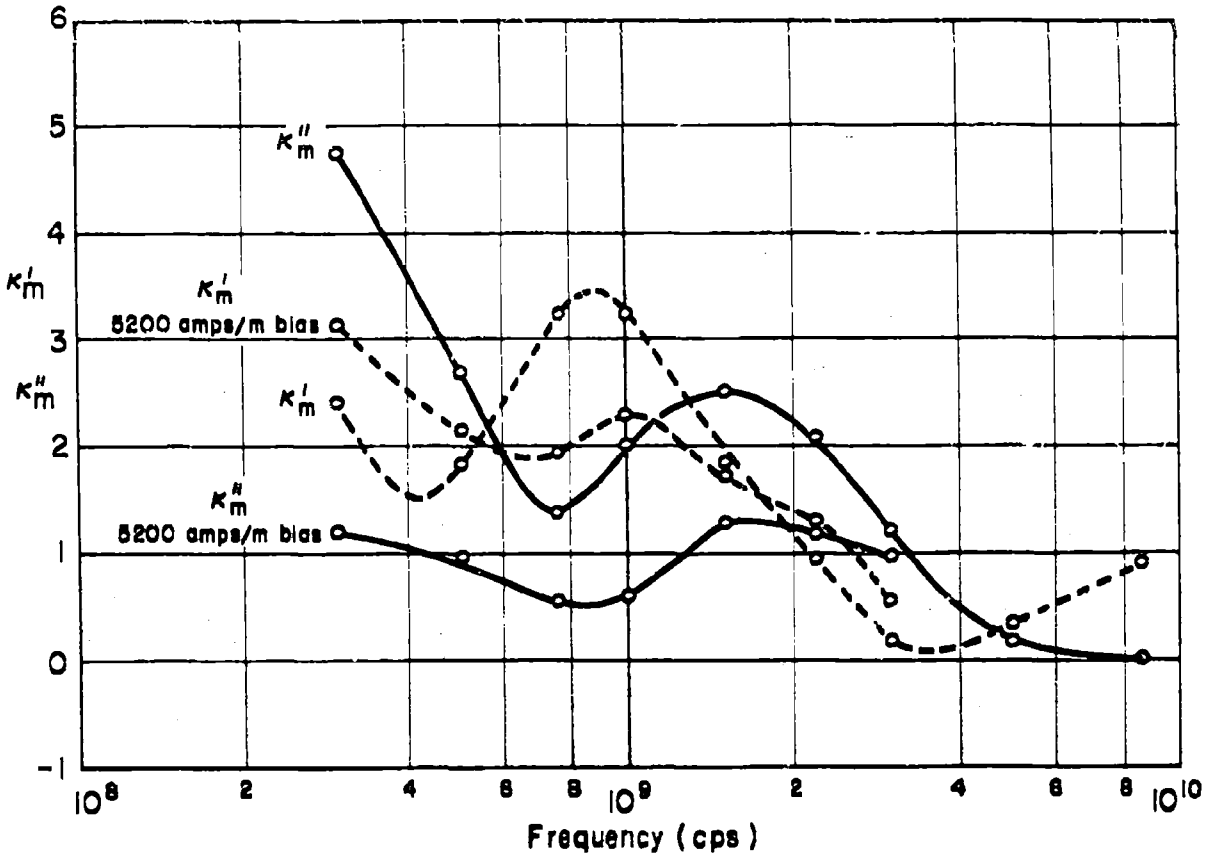

Fig. 18.6. Effect of magnetic bias on the microwave properties of $MgO_{0.58}MnO_{0.06}(Fe_2O_3)_{0.06}$.

biasing field.

We might have expected that the simplification of the domain pattern in the biased state would lead to a narrowing of the dispersion regions. This did not occur, indicating that the broadening of the resonance characteristic is caused mainly by magnetic anisotropy, crystallite interactions, or damping.

The randomizing influence of crystallite boundaries and crystallite orientation can be removed by switching from ceramics to single crystals. A single crystal of nickel ferrite (courtesy of the Linde Air Products Co.) was available, which we cut as a toroid orientated with the (110) plane parallel to the toroid plane (Fig. 18.7). The two [111] directions in this plane are the directions

of easy magnetization at room temperature; and, while in comparison to a true diamond-shaped sample a distorted domain pattern must be expected, this toroid is the best approximation to such a shape for measurements over a wide frequency range.

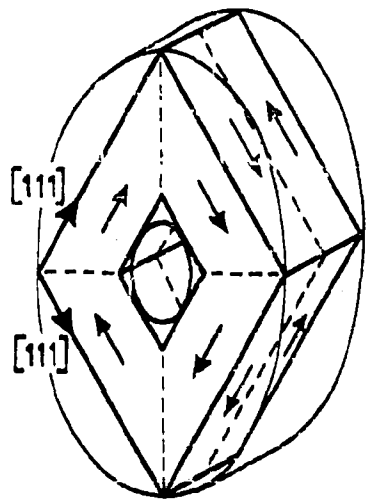

Fig. 18.7. Domain pattern found in nickel-ferrite diamond.

The low field-strength measurements of Fig. 18.8 show a general similarity to the ceramic characteristics of Fig. 14.1, but the loss peaks are higher and further separated. We obviously would describe the trend now as given by two dispersion regions located near 8 and 600 Mc/sec.

The behavior of the upper dispersion region corresponds to that of a spin resonance. That the Q of our single crystal appears to be no better than that of the ceramics (Q ca. 1) may not be significant; in these permeability measurements we see mainly the distorted part of the domain pattern of the toroid, where the magnetization is not parallel to the field.

Increasing a-c field strength leaves the high-frequency dispersion more or less unaffected, while the low-frequency region becomes completely altered. The loss maximum moves to low frequencies and flattens out, and the flat plateau of the low-frequency permeability is raised from 130 to about 1300 and greatly shortened.

A possible explanation is that the low-frequency, low-field strength dispersion stems from a reversible wall oscillation and that at higher field strengths the walls tear loose from their anchored positions and traverse the material in widening swings.

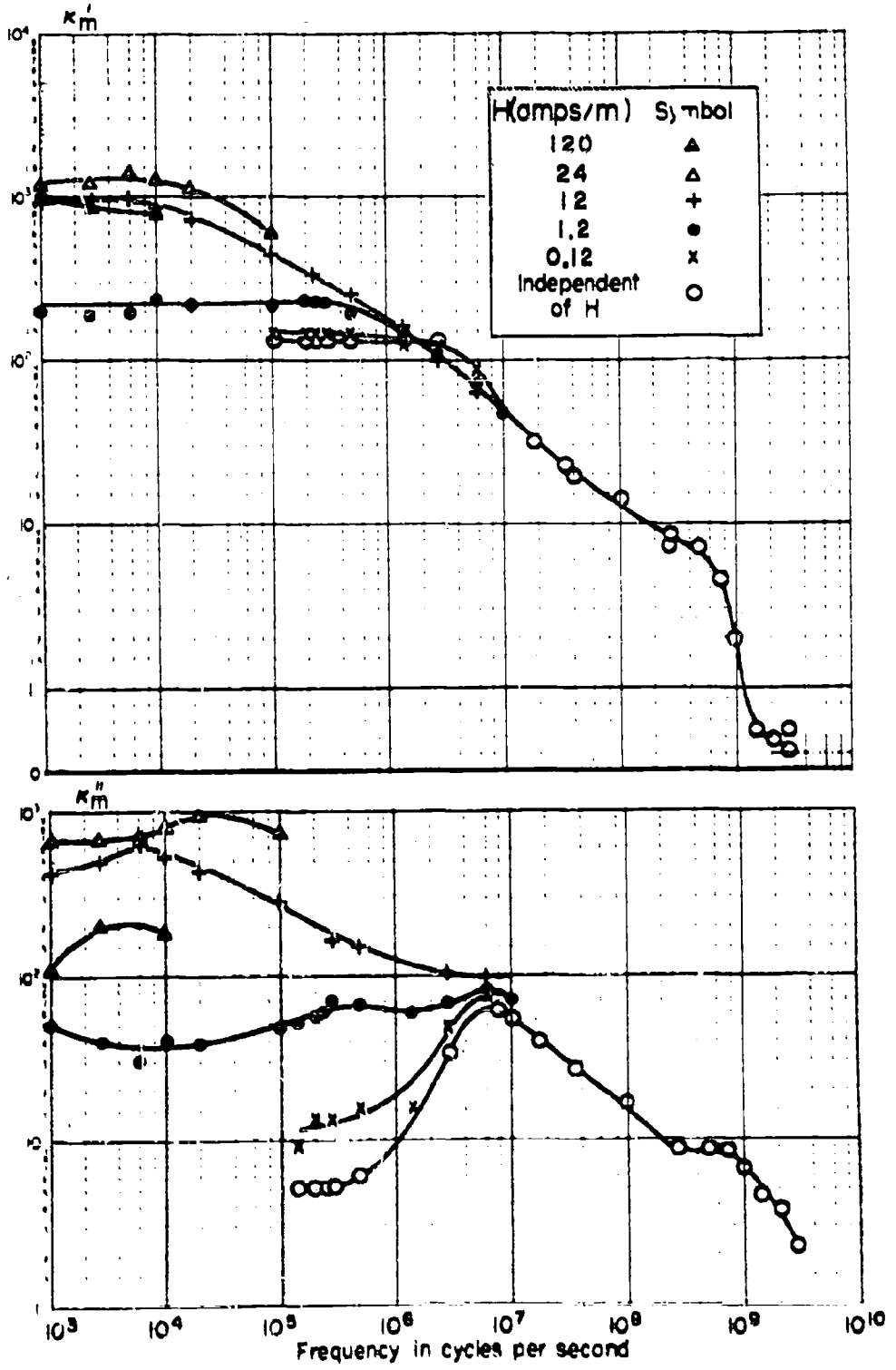

Fig. 18.8. Permeability measurements on a single-crystal toroid of nickel ferrite at room temperature.

19. Temperature and Time Effects

A change in the overall magnetization of a ferromagnetic may be achieved, as previously discussed, by two processes: reorientation of the magnetization vector within individual domains, and change of the domain pattern by wall movements. The former process depends on the internal magnetic field; the latter on wall stiffness and mass, and on the ease of wall generation. The acuteness of the frequency response is given by the damping attenuating these motions. The temperature and time dependence of the magnetization is therefore controlled by the temperature and time dependence of the phenomena which influence internal fields, wall properties, and damping processes.

Internal fields arise from magneto-crystalline anisotropy, from distortions caused by strain and imperfections, and from demagnetizing fields created by free poles at boundaries of domains, of crystallites and of the overall sample (shape effects). The wall stiffness reflects the fact that a domain wall is held in a potential well; a domain pattern represents a minimum energy constellation and, in addition, individual walls may be anchored in real crystals by lattice disturbances (impurities, defects and strain patterns).

At the present stage, the temperature dependence of anisotropy and magnetostriction can not be predicted except for the fact that both effects become very small as the Curie point is approached. Figure 19.1 shows the situation for magnetite. Since near the Curie point the anisotropy and stiffness are low, the initial permeability is high, as Fig. 19.2 demonstrates for the series of nickel-zinc ferrites. Magnetite has an isotropy point near -143°C, hence exhibits a peak of the initial permeability in this region, as well as near the Curie point (Fig. 19.3). The magnitude of the initial permeability of magnetite is much larger than rotation against the anisotropy would predict, hence domain-wall motion must play a major part in shaping this lower-frequency characteristic.

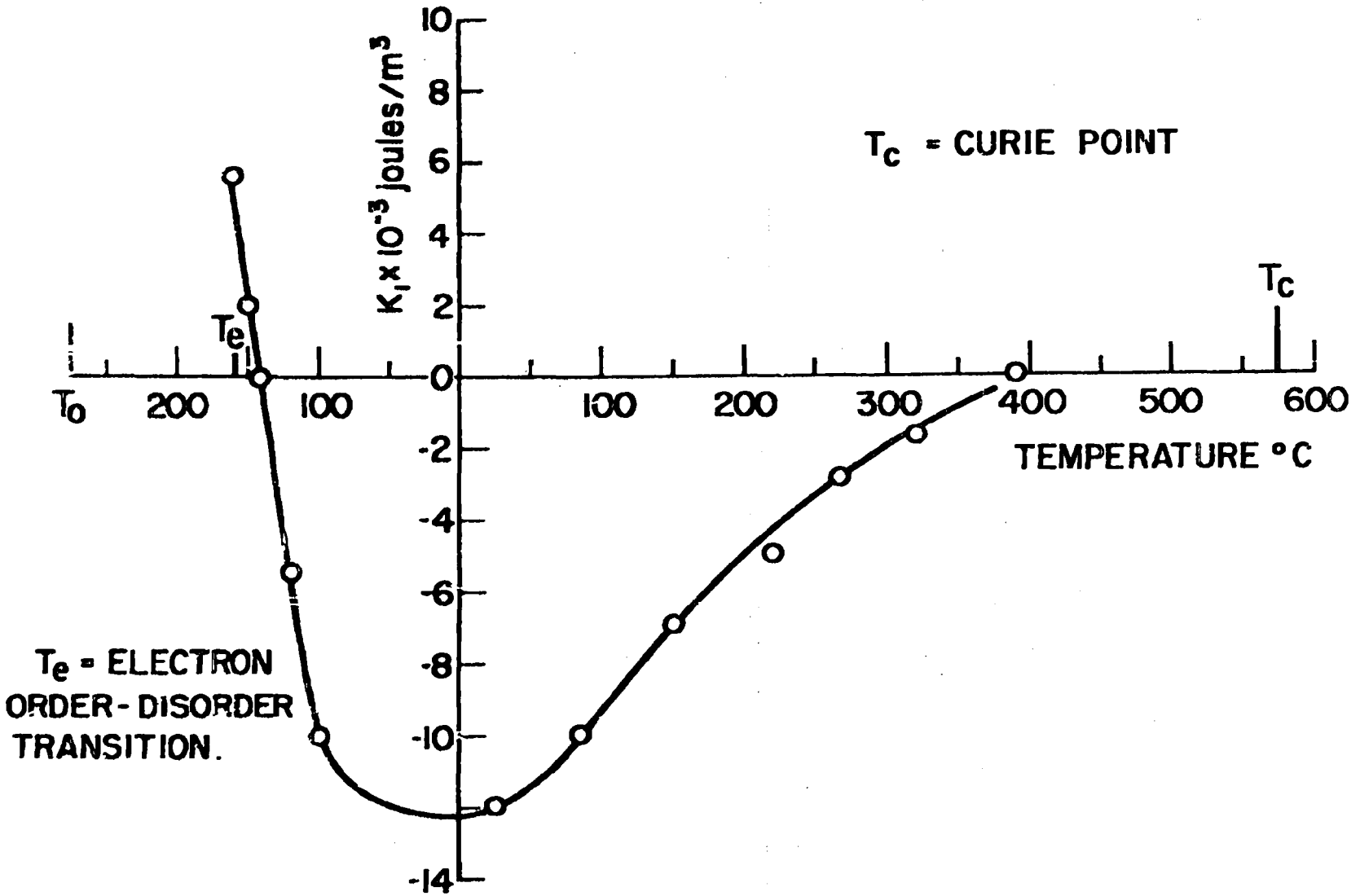

Fig. 19.1. The first-order anisotropy constant (K_1) in magnetite as a function of temperature.

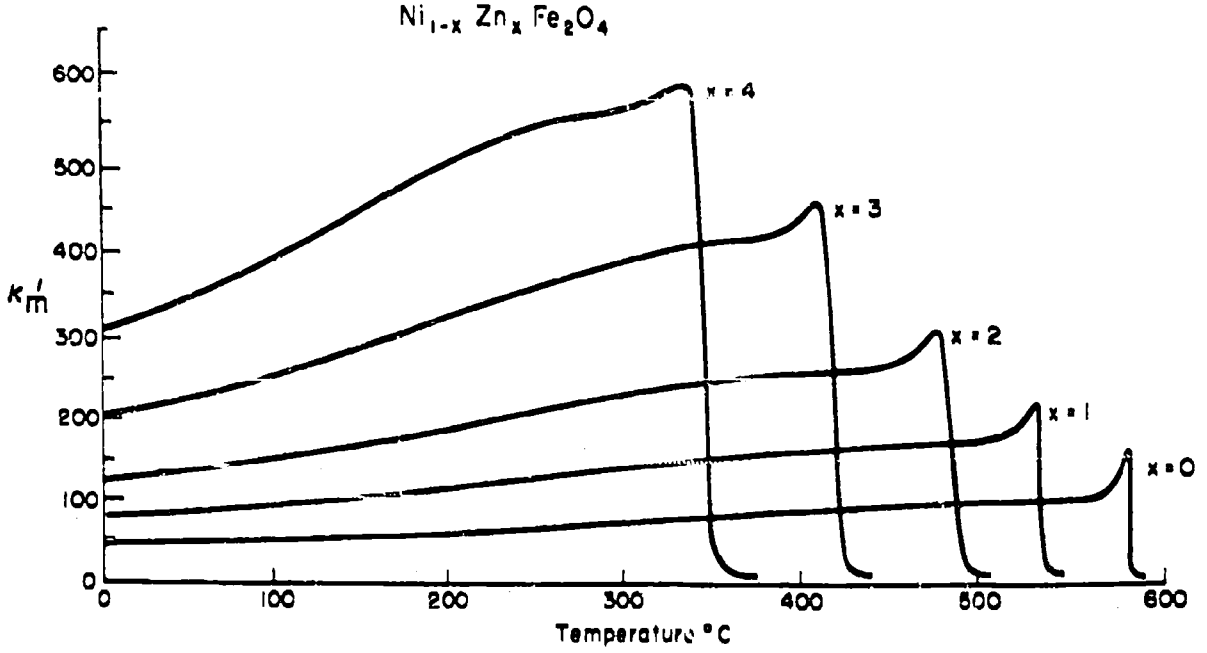

Fig. 19.2. Temperature dependence of initial permeability of the nickel-zinc ferrites measured at 10^3 cps.

The potential wells of domain walls may be changed and deepened by processes of diffusion which lower the potential energy of the system. Such diffusion processes depend on activation energies U and therefore exponentially on temperature with relaxation times

$$\tau = \tau_0\, e^{-U/kT} \quad . \tag{19.1}$$

For example, the diffusion of carbon or nitrogen atoms in the domain walls of iron may produce magnetic after-effects which decrease the intial permeability of a newly demagnetized specimen over minutes and even hours.[20] Electron diffusion can be observed most dramatically in magnetite, where below -160°C an ordered arrangement of Fe^{2+} and Fe^{3+} ions develops in the octahedral lattice sites (cf. Sec. 7). When a magnetite single crystal is cooled through this electronic order-disorder transition in a magnetic field, a magnetic axis is frozen in, orientated

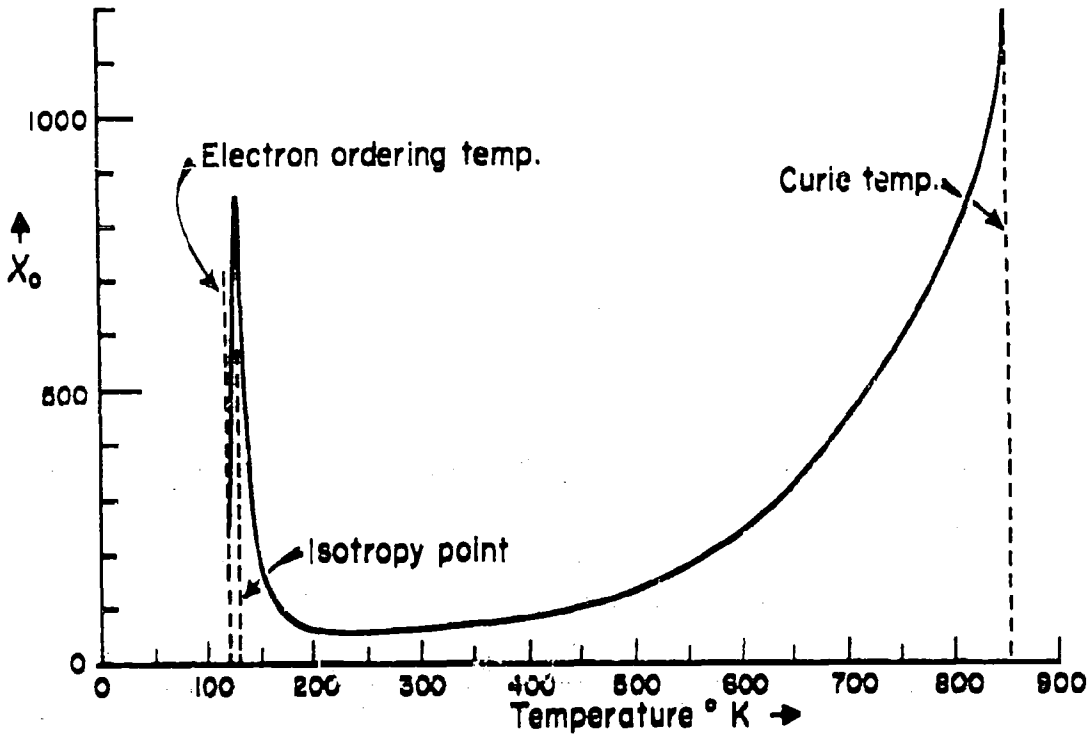

Fig. 19.3. Temperature dependence of the initial susceptibility of magnetite.

in the cube-edge direction closest to the external field direction. In this direction, remagnetization below the transition is easy; perpendicular to the axis, magnetization is difficult. But, if a sufficiently strong field is applied perpendicular to the frozen-in axis, this axis can be turned into the new direction, as Bickford[42] and Calhoun[43] showed in this laboratory in detailed experiments (Fig. 19.4). The activation energy for this process is ca. 0.03 ev and the same as that indicated by conductivity measurements at low temperature (cf. Fig. 15.4). By rearranging the checkerboard pattern of the Fe^{2+} -Fe^{3+} ion distribution, the magnetic moments have been turned in space.

42) L. R. Bickford, Jr., Phys. Rev. 78, 449 (1950).

43) B. A. Calhoun, Phys. Rev. 94, 1577 (1954).

(a)

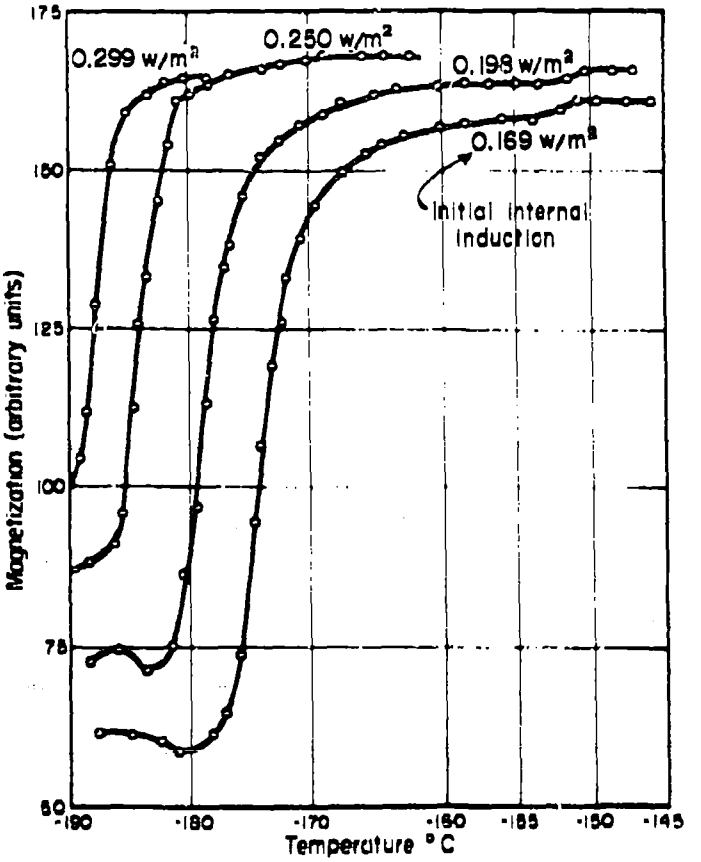

(b)

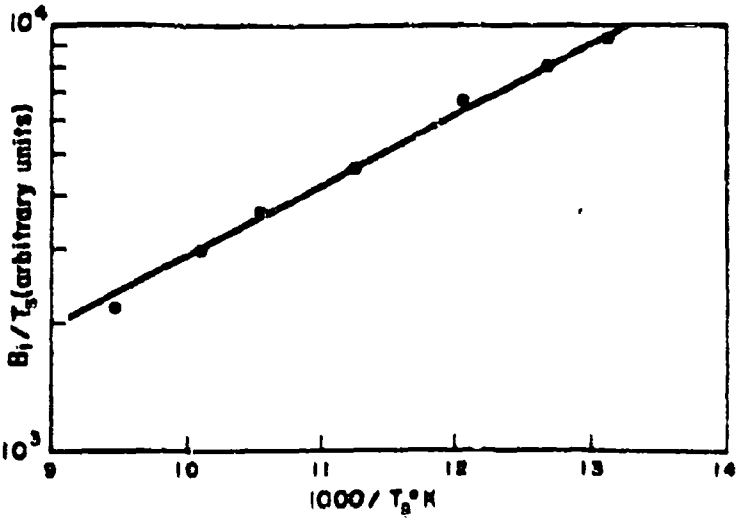

Fig. 19.4. (a) Thermal switching of the magnetic axis in the ordered state of magnetite from a premagnetized [100] direction to a [100] -direction parallel to a bias field; B_i is the internal induction prior to switching.

(b) A plot of log (B_i/T_s) vs. $1/T_s$ (T_s is the switching temperature) indicating an activation energy of 0.03 ev for the process.

Wijn and van der Heide[22, 44] have invoked this electron diffusion process to explain a low-frequency relaxation-type dispersion in iron-rich manganese-zinc and nickel-zinc ferrites; Galt[45] has associated it with the slowing down of the motion of a single domain wall in a nickel-iron ferrite single crystal at low temperature.

The frequency response characteristics of the nickel ferrite and nickel-zinc ferrite ceramics show drastic changes at low temperatures . Figure 19.5 shows the results for $Ni_{0.9}Zn_{0.1}Fe_2O_4$. The static permeability decreases; the lower dispersion region moves to lower frequencies and becomes very broad and diffuse; the absorption region near 10^8 cps becomes clearly separated; the high-frequency dispersion with its minimum between 10^9 and 10^{10} cycles seems to remain unaltered. The shift of the peak of the lower absorption region obeys the temperature dependence of a relaxation spectrum governed by an activation energy of ca. 0.13 ev.

The effect of lowering the temperature on the nickel ferrite single crystal is similarly striking. While down to about -80°C the situation appears practically unchanged, at liquid nitrogen temperature, the change corresponds to that described for the ceramics. The lower dispersion region is obviously due to wall motion and is greatly affected by an activation process. At -190°C this motion is very reduced in the kilocycle range and practically suppressed above 10^5 cps (Fig. 19.6). Figures 19.7 and 19.8 give a detailed representation of the temperature dependence for 10^3 and 3×10^5 cps with the a-c field strength as parameter.*

44) H. P. J. Wijn and H. van der Heide, Revs. Mod. Phys. 25, 98 (1953).

45) J. K. Galt, Bell System Tech. J. 33, 1023 (1954); 34, 439 (1955).

* The cross-over of the κ'_m curves for 1 kc is caused by the nonlinearity of the magnetization characteristic; the κ'_m data refer to the fundamental component of the magnetic response, and at 22 amp./m the amplitude is already reaching into the saturation region.

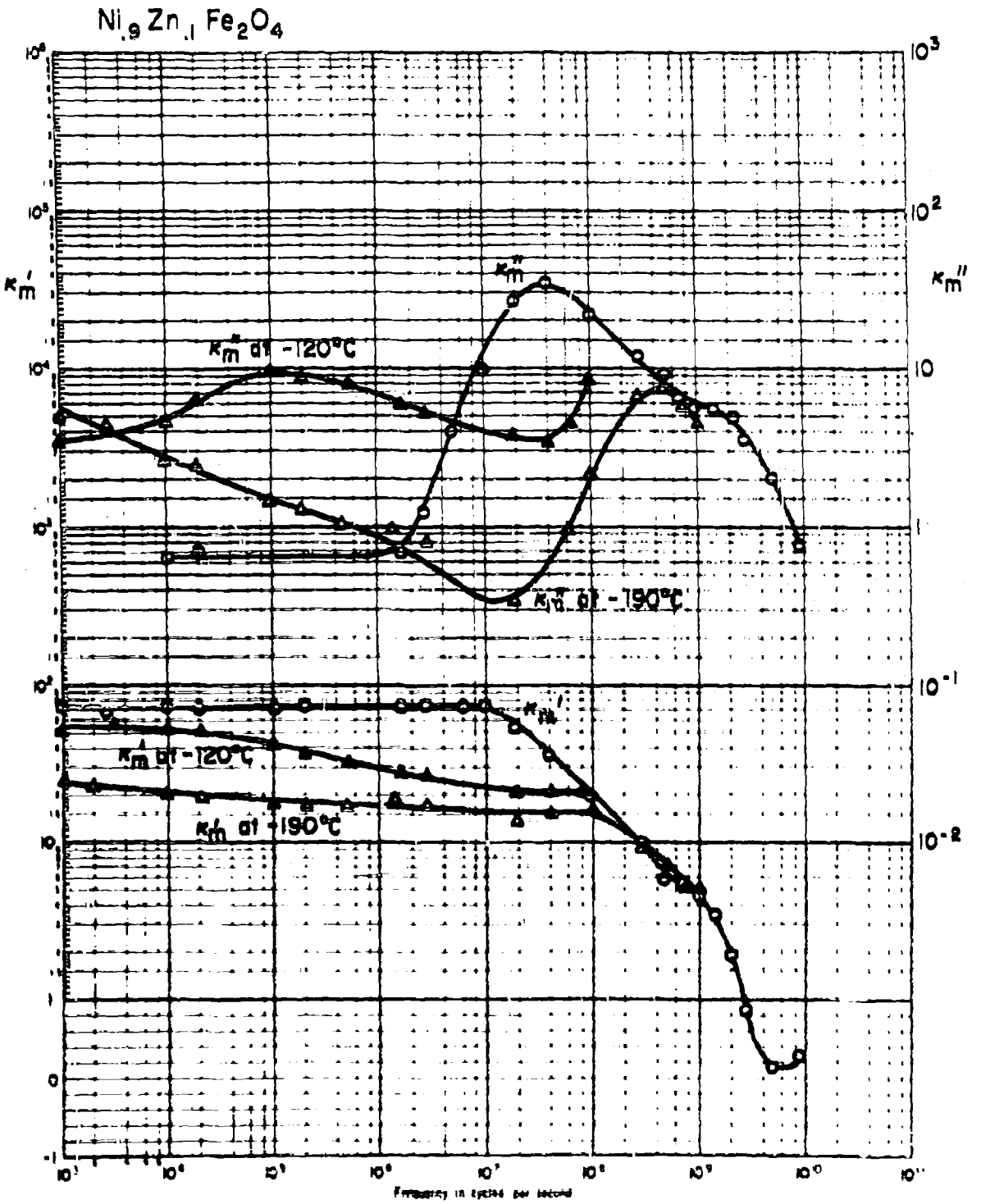

Fig. 19.5. Effect of temperature on the magnetic properties of $Ni_{0.9}Zn_{0.1}Fe_2O_4$.

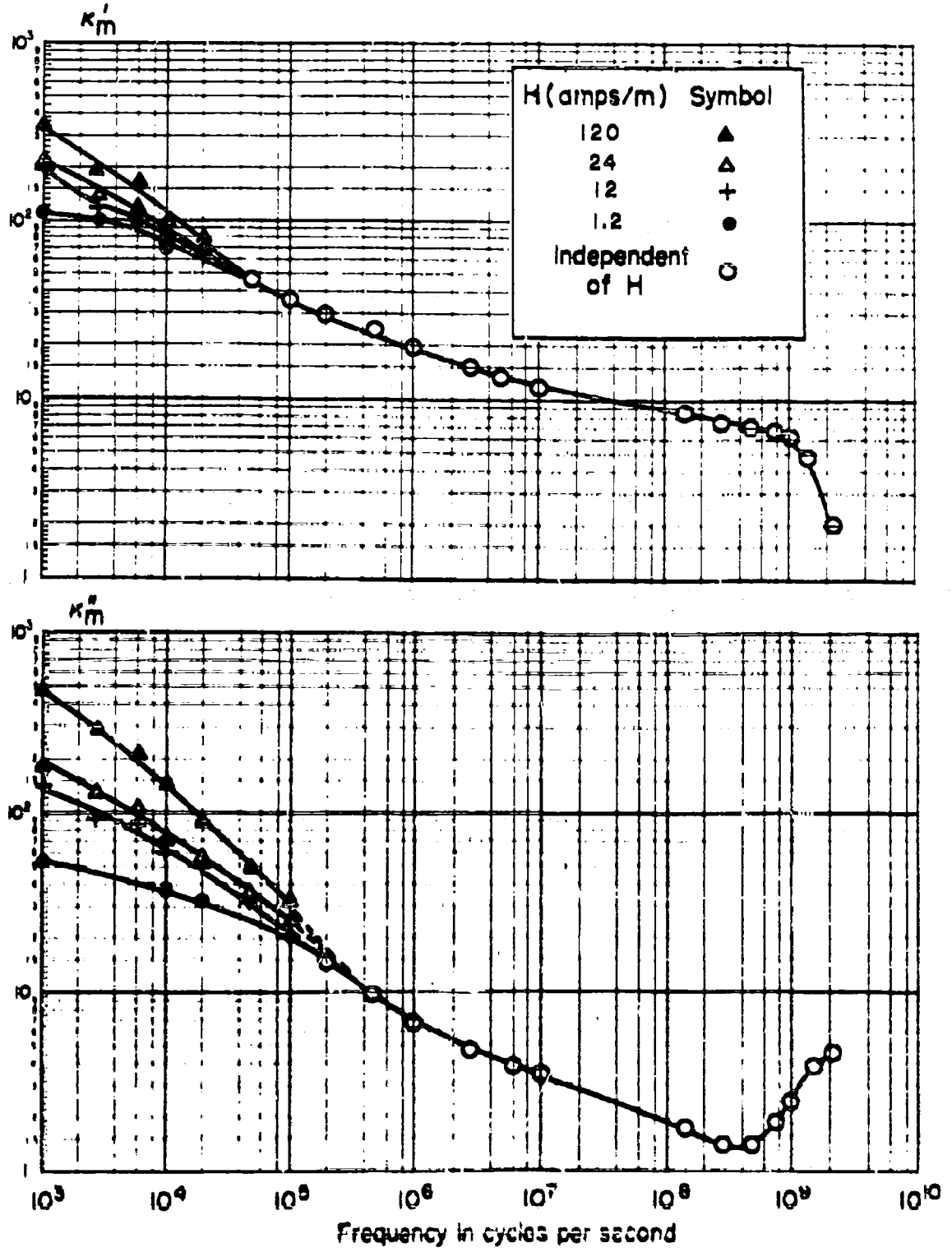

Fig. 19.6. Permeability measurements on a single-crystal toroid of nickel ferrite at -190°C.

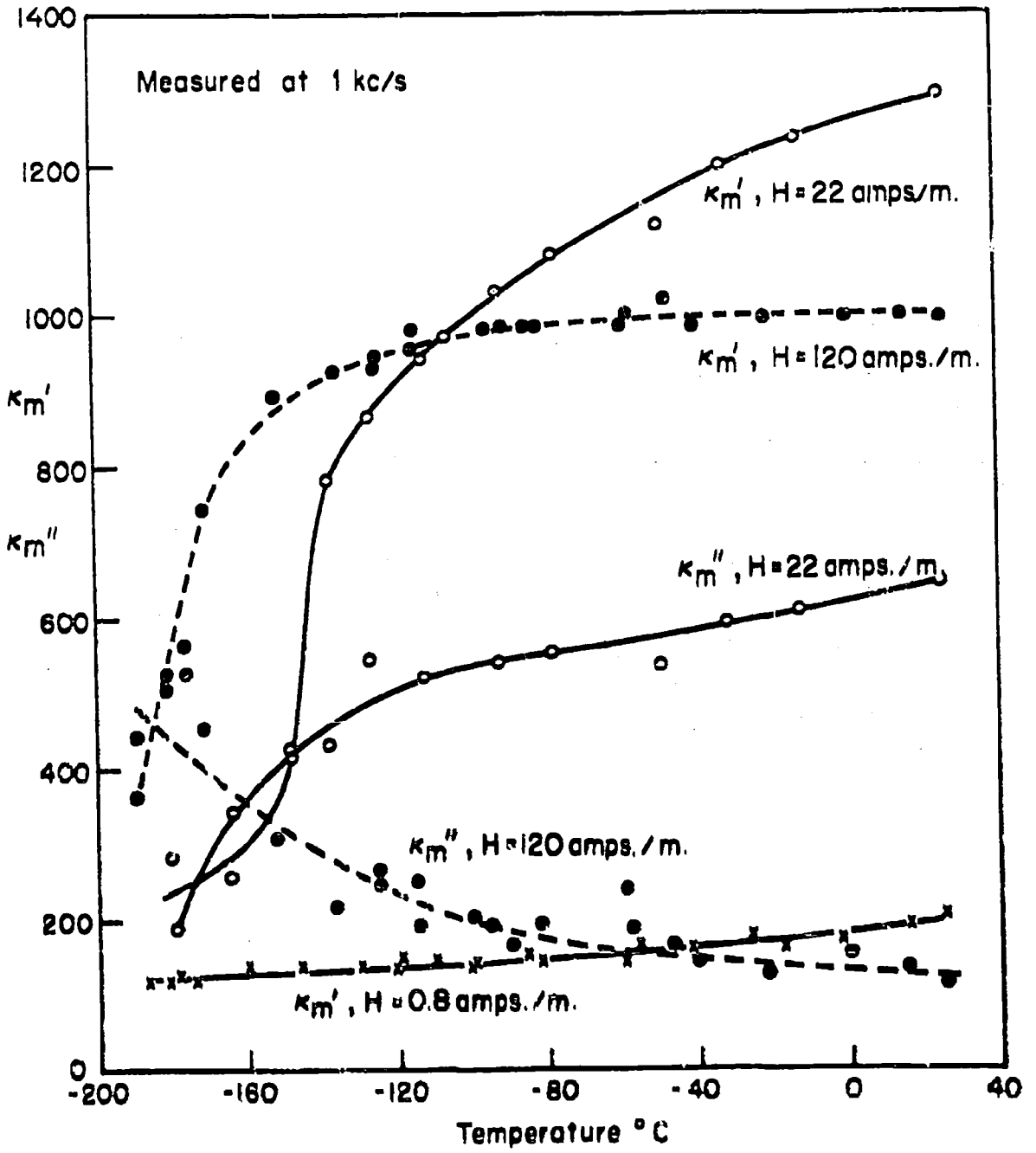

Fig. 19.7. Permeability measurements on a single-crystal toroid of nickel-ferrite, measured at 10^3 cps, as a function of temperature.

This temperature behavior in obviously related to the great increase in wall "damping" noted in nickel-iron ferrite by Galt.[45] The wall motion depends on a thermal activation process; the walls have to be unhooked in order for them to move. Whether this unhooking is done by direct thermal agitation of the lattice

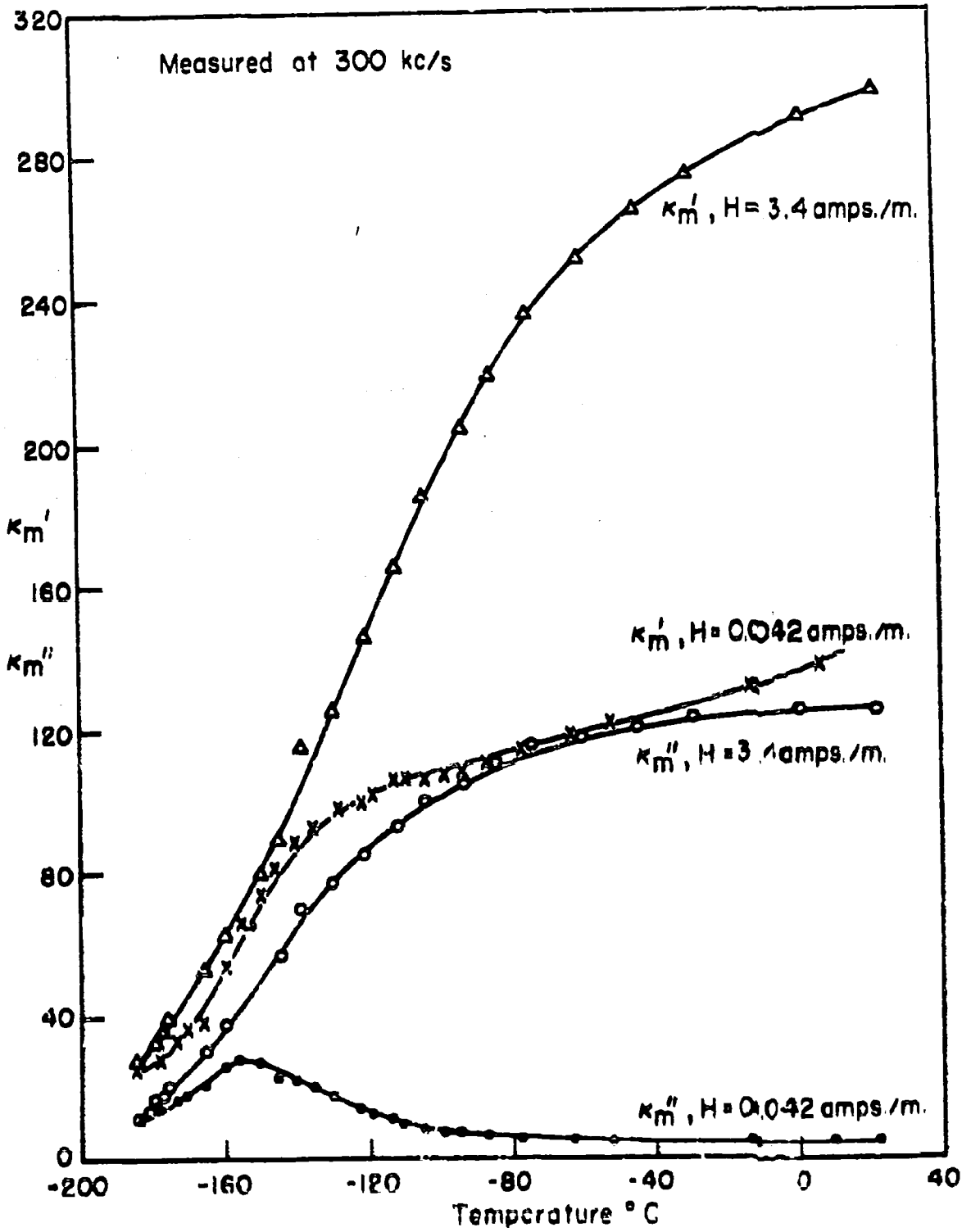

Fig. 19.8. Permeability measurements on a single-crystal toroid of nickel-ferrite, measured at 3×10^5 cps, as a function of temperature.

or by electron diffusion due to thermal activation, can not be decided offhand. Both cases probably occur.

20. Magnetostriction as a Cause of Dispersion and Absorption

The magnetic moments of the ferrites stem, as far as is known today, mainly from the spin moments of unpaired 3d electrons. Since these moments reside in individual ions, it is theoretically feasible, and has been assumed, that the spin system of the electrons can be turned without affecting the position of the nuclei. Thus one speaks about the energy and oscillations of this spin system as if the magnetic moments were assembled in free space. One admits, as a perturbation, a spin-lattice coupling that forces upon the spin array the crystal symmetry and is reflected in the magnetic anisotropy of the ferrite. As evidence that this coupling is only a secondary effect, the existence of isotropy regions is cited, wherein the effect of the lattice on the spin orientation disappears. In magnetite this occurs at about $-140^{\circ}C$ (see Fig. 19.1).

An isotropy region signifies that the magnetic energy is the same for magnetic moments aligned in the elementary directions. However, once a momentum axis is established in one of these directions, the cubic symmetry is actually destroyed. One may therefore observe magnetostriction even in isotropy regions.

If the spin system is always coupled to the lattice system in some degree, rapid changes in the magnetization direction tend to set up lattice vibrations. The spin system, graphically speaking, is coupled to a sound box, and a dispersion region will arise, determined by the sound velocity.

Previously, we have discussed the infrared vibrations of the lattice without reference to its ferromagnetic state (cf. Sec. 13). This was justified because the vibrations in molecular groups are dominated by strong electric bonds between the elementary particles. In ferromagnetism, the spontaneous alignment of magnetic spins in long dipole chains produces a long-range order with the ferromag-

netic domain as its elementary unit. This unit can adjust freely to orientation changes of the magnetization vector only when the magnetostrictive lattice distortion over the whole length of the domain is in phase. We may therefore expect a dispersion region characterizing the transition from a "free" to a "clamped" domain state. For a sound velocity of about 5×10^5 cm/sec. this dispersion region might lie between 10^6 and 10^{10} cps, depending on the domain size. If this effect is of importance, one would expect the anisotropy constants obtained from quasi-static measurements on single crystals to differ from those deduced from resonance experiments at microwave frequencies, where the lattice can be regarded as clamped. No reliable evidence on this point exists as yet.

21. The Dynamic Response of a Ferromagnetic Spin System

Let us visualize a ferromagnetic domain as a parallel array of elementary magnets held in a preferential orientation by the structure of a crystal lattice. The lowest energy state of such a system would be classically a rigid parallelism of all the spins; quantum-mechanically, a zero-point energy has to be provided. At higher temperature, a thermal agitation of the spin system occurs which corresponds to excitation of quantized states, each state corresponding to the reversal of a discrete number of spins. Since the spins are coupled by strong, short-range exchange forces, the flipping over of a spin to an antiparallel position may require the thermal activation energy kT_c ($\simeq 0.1$ ev) of the Curie temperature, and hence correspond to an excited state in the infrared. Less energetic ways of reducing the total magnetic moment exist. These are the so-called "spin-wave" states, which may be looked upon as the excitation of standing waves in the spin system, with each spin tilted by a small angle with respect to its neighbors in a periodic way, each mode being characterized by a wave number k.[46] The energy necessary to establish such a state in the presence of an external field H is given by

46) F. Keffer, H. Kaplan and V. Yafet, Am. J. Phys. 21, 250 (1953).

$E_s = 2\vec{m}\mu_o H + X\vec{k}^2$, where $\vec{m}$ is the elementary spin moment, and X is a factor proportional to the exchange energy and normally of the order of 10^{-16} ev cm^2. This expression is only applicable at very low temperatures where the spin system is almost completely aligned, but in general we may say that the permissible states of a ferromagnetic system extend on an energy scale from extremely low values to excited levels corresponding to energies of the order of 0.1 ev. With each of these states there is associated another set corresponding to the tipping of the total spin vector relative to an external field. These latter levels are separated, in the absence of anisotropic forces, by the energy difference $\hbar\omega \simeq \hbar\gamma\mu_o H$.

In the ferrites special resonance effects may arise due to the existence of magnetic sublattices.[47] It seems possible that the antiferromagnetic coupling produces an infrared mode which corresponds to an oscillation of the sublattice spin groups against each other. A calculation for nickel ferrite[48] leads to an expected absorption at about 40 μ. At still higher frequencies the dynamic response of the ferromagnetic state ceases; however, the existence of ferromagnetism is still felt in magneto-optical effects. For example, the rotation of the plane of polarization in the Faraday effect for ferromagnetics is greater by several orders of magnitude in comparison with paramagnetic and diamagnetic materials. This is due to the influence of the spin alignment in ferromagnetics on the energy of the electronic states and their transition probabilities.[49]

22. Bandwidth of Magnetic Resonance Spectra

Ferromagnetic resonance, described classically as a Larmor precession resonance (cf. Sec. 4), reduces the magnetization components in the direction

47) C. Kittel, Phys. Rev. 82, 565 (1951).

48) J. Kaplan and C. Kittel, J. Chem. Phys. 21, 760 (1953).

49) H. R. Hulme, Proc. Roy. Soc. (London) A135, 237 (1932); P. N. Argyres, Phys. Rev. 97, 334 (1955).

of the effective field by quantized amounts. The energy is absorbed in specific excited spin states and, if not re-radiated, goes over into the total spin system raising its temperature and then by spin-lattice coupling into the thermal agitation of the crystal as a whole. If this energy transfer did not take place, the excitation to a definite spin state would be observed as an absorption indicating by its half-width $\Delta\omega_h$ or Q the natural lifetime of the excited state[50]

$$\tau = \frac{1}{\Delta\omega_h} = \frac{Q}{\omega_o} \quad . \tag{22.1}$$

If the lifetime is decreased by energy transfer, the absorption broadens.

The experimentally observed line width of ferromagnetic resonance even in single crystals is very much larger than expected; the magnetic line width at constant frequency being of the order of 4,000 amp./m. This could be interpreted as indicating a lifetime of the order of 10^{-9} sec.

The theoretical difficulty is to arrive at a plausible model of coupling between the various spin-wave states. The normal exchange energy cannot be invoked, since it is isotropic, that is, does not depend on the magnetization direction. An anisotropy has to be introduced by binding the individual spin to the average direction of the spin array in its surroundings. This seems to be the meaning of the approach tried by Kittel and Abrahams[51], which couples the absorbing state to other spin wave states tightly enough to account for the observed line width. In the same model, the direct coupling between the absorbing state and the lattice would seem to be so weak that the line width due to it is about 10^7 times smaller than observed.

From an experimental standpoint, there is as yet no conclusive evidence that the low Q is really produced by a damping process. It is still quite possible that the ferromagnetic resonance as observed consists of many absorption states of narrow line width and is thus the envelope of these states just as a vibration

50) A. von Hippel, "Dielectrics and Waves," p. 166.

51) C. Kittel and E. Abrahams, Revs. Mod. Phys. 25, 233 (1953).

resonance is broad when not resolved into its rotation components.

23. Ferromagnetic Research and Dielectric Spectroscopy

A fundamental discussion of ferromagnetism begins with the origin of the magnetic moments and their distribution in space; with the mutual coupling of these moments by exchange forces leading to ferro- and antiferromagnetism; and with the coupling of the moments to the crystal lattice resulting in crystal anisotropy and magnetostriction. It advances to a comprehension of the ferromagnetic state as influenced by temperature, field strength, pressure and composition. The formation, shape and arrangement of domains, and the structure and dynamics of the domain walls emerge. The contrast becomes visible between the ideal structure and composition of single crystals and their real structure as influenced by the conditions of preparation and handling. The complications multiply as one proceeds from single crystals to the multicrystalline array of ceramics where structure, composition and properties are at the mercy of fabrication parameters. Finally, the insight gained should suffice for the tailoring to order of ferromagnetic materials of prescribed characteristics.

Obviously, we are still far away from such a thorough understanding of ferromagnetics. Many pieces of the puzzle, however, have been identified, and dielectric spectroscopy is one approach of assembling them in their proper perspective. We visualize the elementary spins, coupled by strong exchange forces and organized in parallel arrays, as domains separated by walls. The walls consist of transition layers of spins bridging between the orientations of the abutting domains. The original domain pattern corresponds to a minimum energy constellation in field-free space. When a magnetic field is applied, a more favorable domain constellation tends to develop by wall displacement, by the creation of new walls and the removal of existing ones. Simultaneously, the magnetization vectors of the individual domains tend to reduce their deviation from the field direction by

rotation.

All changes in spin direction proceed by attenuated gyroscopic motions. The spins of a domain act in the lower frequency range as a rigidly coupled unit. Its resultant magnetization vector precesses with a Larmor frequency prescribed by the effective magnetic field. This effective field stems from a variety of sources: the applied field, the magnetic anisotropy and magnetostrictive effect of strains of the material, the shape of the domains, fields created by surrounding domains and crystallite boundaries, and moments induced by the precession of the magnetization vectors. In consequence, each domain in its individual environment has its own ferromagnetic resonance frequency which depends also on the relative orientation between domain and applied field. A wide distribution of ferromagnetic resonance frequencies must therefore be expected, sensitive to and varying with the domain pattern, until a dominating external field enforces a single domain status. Even in this state, the broad frequency distribution of resonances does not coalesce into a single resonance response, unless we deal with a single crystal. In ceramics, a distribution remains, because the anisotropy axes of the crystallites are more or less randomly distributed and hence cause local variations in the internal fields of the order of $2K_1/\mu_o M$, in addition to inhomogeneous strain and shape effects.

The spins of a domain wall, in contrast to those of a domain, have a common orientation and precession frequency only in each layer parallel to the wall. As the wall moves, the angular spin velocity of each layer changes depending on its position and reaches a maximum when it finds itself in the middle of the wall. The layers are strongly coupled, hence no ferromagnetic resonance can develop, but only an erecting torque that pushes the wall along. Since the original domain pattern represents a minimum energy constellation, alternating fields of small amplitude will produce resonance or relaxation vibrations of the walls around this equilibrium state. The resonance frequency or relaxation time of each wall depends

on its particular surroundings, and these wall vibrations are coupled more or less strongly. In consequence, the reversible wall vibrations will contribute a broad spectrum of resonance and/or relaxation states.

Spin resonances and reversible harmonic wall vibrations produce a permeability that is independent of field strength. A B-H plot with the driving frequency as parameter shows Lissajou figures containing only the fundamental frequency. As the amplitude increases, the wall motion may still be reversible, but anharmonicity terms enter and add even harmonics. Finally, the walls will begin to break loose, new walls appear, old ones disappear, and the Lissajou figures change into hysteresis loops characterized by odd harmonics.

The remanent magnetic state of a material can be realized by a variety of domain patterns, each one of them representing some minimum constellation to which the sample returns according to its prehistory. Obviously, some of these arrangments correspond to lower energy states than others; hence there is a tendency to approach these by a long-time readjustment of structure and composition, that is, by "aging." In general, activation energies intervene and some premagnetized state remains.

The two dispersion regions caused by spin resonance and by domain-wall resonance and/or relaxation overlap and there is no a priori necessity that the ferromagnetic resonance will extend to higher and the domain-wall effects to lower frequency regions. Furthermore, we should expect that both spectra are modified by a dispersion phenomena which stems from the magneto-elastic coupling. As the frequency increases, magnetostrictive resonances of the whole sample, as well as of crystallites, should appear; the magnetization in the individual domains should change from the "free" to the "clamped" state; and, since the readjustment of the lattice cannot propagate faster than the velocity of sound, the domain-wall motion demanding such readjustment will be modified, if not wholly prevented

Sound velocity must create a dispersion at high frequencies for all magnetic phenomena influenced by the coupling between electron spins and lattice. A dispersion region must develop at low frequencies in which electron diffusion through the lattice, for example, from Fe^{3+} to Fe^{2+} or between Mn^{2+}, Mn^{3+} and Mn^{4+} cations alters the magnetic-spin arrangment to more favorable patterns, releases caught walls and leads to long-time readjustments. Obviously, here the interesting possibility exists of changing the magnetic state of a material with electric fields.

As far as we know today, these four effects: spin resonance; wall resonance and/or relaxation; coupling between magnetic and elastic spectrum; and their modification by electron diffusion, shape the magnetic spectra in the electrical range.

As we proceed towards the optical range, polarization spectra belonging to loosely bound charge carriers begin to announce themselves and spin-wave resonances may occur in a yet nearly inaccessible spectral range. Next the true lattice vibrations set in and promise some detailed information about the cation distribution. They are underlaid and followed by electronic absorption spectra, which give the optical binding energies of the electrons in the crystal structure. Here an intimate link exists to the thermal activation energies obtained by conduction measurements at low frequencies as well as to the cations and their distribution in the crystal lattices.

From infrared frequencies upwards the ferromagnetic state as such cannot respond to electromagnetic fields; it is "frozen in," but its existence may still be detected by Faraday-effect measurements. The Faraday effect in the microwave range informs on ferromagnetic resonances and the effective field; in the optical region it measures the influence of ferromagnetic coupling on the atomic and the electronic polarization.

Finally, X-ray spectroscopy terminates the electromagnetic spectrum and provides data on crystal structure and crystalline phases, electron density maps and information on the distribution of cations over the various lattice sites.

Acknowledgement

It is obvious that in a summarizing paper of this kind the experimental work and experience of a number of our co-workers has greatly contributed, as indicated in the text. In addition we want to thank Professor D. J. Epstein and Drs. F. E. Scarf and R. D. Waldron for helpful discussions.